Spontaneous symmetry breaking in rotating nuclei

Stefan Frauendorf

Department of Physics, University of Notre Dame, Notre Dame, Indiana 46556 and Institute for Nuclear and Hadronic Physics, Research Center Rossendorf, PB 51 01 19, D-01314 Dresden, Germany

(Published 13 June 2001)

The concept of spontaneous symmetry breaking is applied to the rotating mean field of nuclei. The description is based on the tilted-axis cranking model, which takes into account that the rotational axis can take any orientation with respect to the deformed density distribution. The appearance of rotational bands in nuclei is analyzed, focusing on weakly deformed nuclei at high angular momentum. The quantization of the angular momentum of the valence nucleons leads to new phenomena. Magnetic rotation represents the quantized rotation of the anisotropic current distribution in a near spherical nucleus. The restricted amount of angular momentum of the valence particles causes band termination. The discrete symmetries of the mean-field Hamiltonian provide a classification scheme of rotational bands. New symmetries result from the combination of the spatial symmetries of the density distribution with the vector of the angular momentum. The author discusses in detail which symmetries appear for a reflection-symmetric density distribution and how they show up in the properties of the rotational bands. In particular, the consequences of rotation about a nonprincipal axis and of breaking the chiral symmetry are analyzed. Also discussed are which symmetries and band structures appear for non-reflection-symmetric mean fields. The consequences of breaking the symmetry with respect to gauge and isospin rotations are sketched. Some analogies outside nuclear physics are mentioned. The application of symmetry-restoring methods to states with large angular momentum is reviewed.

CONTENTS

I. INTRODUCTION

A. Scope

Many nuclei possess energy levels which form rotational bands similar to the bands observed in molecules. However, in nuclei there is no molecular skeleton to

provide the inertia for the rotational motion. It is the nucleons themselves which generate it. As a consequence, nuclear rotation has features that are rather different from what we know about the rotation of molecules. For example, when we consider the rotation of a system composed of relatively few fermions at zero temperature, the moments of inertia deviate from the values for classically rotating solids or liquids. Atomic nuclei can be set into rapid rotation, such that the rotational frequency ω becomes comparable with the frequency of the nucleonic motion, which will then be substantially modified by inertial forces. The peculiarities of nuclear rotation become more evident in this high-spin regime. Rotational bands may terminate after a finite number of transitions. There may be uniform rotation about an axis, which is different from the principal axes of the density distribution. A nearly isotropic density distribution does not always prevent the appearance of rotational bands, which may be understood as the quantal rotation of a magnetic dipole. This review focuses on these features of rapidly rotating nuclei, which deepen our understanding of how microscopic objects rotate.

The experimental angular momentum reaches tens of units of $\hbar$. This permits a semiclassical treatment of the rotation and the application of the mean-field approximation. This approach, the *cranking model*, has turned out to be most useful in interpreting high-spin experiments. A new class of solutions has recently been found, which represent the uniform rotation about an axis that is tilted with respect to the principal axes of the density distribution. The present review will discuss this development, which has been called the *tilted-axis-cranking* (TAC) model. New types of discrete symmetries appear if the angular momentum vector is not constrained to be parallel to one of the principal axes of the nucleonic density. These symmetries and their manifestation as different types of rotational bands will be analyzed. Magnetic rotation and band termination, which are observed in weakly and moderately deformed nuclei, will be another important topic of the review. We shall also briefly discuss nonspatial symmetries. The common point of view of the discussion will be the spontaneous breaking of symmetries of the nuclear many-body Hamiltonian by the rotating mean field.

We are not going to review the whole field of high-spin nuclear physics. Concerning the early developments, the reader is referred to the review articles by Stephens (1975), de Voigt *et al.* (1983), Bengtsson and Garrett (1984), Garrett *et al.* (1986), and Åberg *et al.* (1990), as well as to the textbooks of Ring and Schuck (1980) and Szymanski (1983). The textbook of Nilsson and Ragnarsson (1995) covers some more recent developments. After their discovery by Twin *et al.* (1986), superdeformed bands became the subject of intensive study. These results have been reviewed by Nolan and Twin (1988) and Janssens and Khoo (1991). The review article of Butler and Nazarewicz (1996) contains a discussion of rotation in nuclei with an octupole deformation. When discussing pair correlations we shall focus on the symmetries. Shimizu *et al.* (1989) gave an overview of pair correlations at high spin. Goodman (1979) reviewed the early investigations of the proton-neutron pair field. The new experimental possibilities for studying medium-mass $N \approx Z$ nuclei have initiated numerous theoretical studies, which we cannot review. The papers of Dean *et al.* (1997), Terasaki *et al.* (1998), Kaneko *et al.* (1999), and Goodman (2000a) are good starting points if the reader is interested in these recent developments.

B. Rotational bands

The concept of rotational bands emerged in molecular physics. The anisotropic arrangement of the nuclei in the molecular skeleton specifies the orientation of the molecule. The classical expression for the rotational energy,

$$H = \sum_{i=1}^{3} \frac{R_i^2}{2\mathcal{J}_i}, \tag{1}$$

defines the rotor Hamiltonian, where R_i is the angular momentum generated by the motion of the nuclei. The moments of inertia $\mathcal{J}_i$ are given by the classical expression for point masses (the nuclei). The Hamiltonian is treated quantum mechanically. Its eigenvalues form regular sequences, the rotational bands. The quantum states of the electrons are almost the same for many levels of the band, because the rotational frequency ω is much lower than the typical frequencies of electronic motion (Born-Oppenheimer approximation). Different electronic states define different rotational bands. The different energy scales permit a clear distinction between ''intrinsic'' electronic excitation and the rotational excitations ($\omega_R \ll \omega_i$). Rotation about the symmetry axis of a linear molecule is not possible, because the orientation angle is not specified. Likewise, certain point-group symmetries of the molecule restrict the domain of the orientation, imposing restrictions on the rotational spectrum. A comprehensive presentation of molecular rotational bands is given in the textbooks by Herzberg (1945, 1950, 1966).

Bohr and Mottelson (1975) adapted this concept of ''quantal rotation'' very successfully to nuclei and discussed it thoroughly in their textbook. The view of nuclear rotation presented there and in other textbooks on nuclear physics, like those of deShalit and Feshbach (1974) and Krane (1988), is the following: The nucleus is considered as a droplet of a quantum liquid, which may take a nonspherical shape as a consequence of the shell structure. Since the deformed nuclear surface specifies an orientation in space it can execute quantal rotation. That is, a rotor Hamiltonian of type (1) describes this excitation mode, which carries the ''collective'' angular momentum $\vec{R}$. Its sequences of eigenstates are the rotational bands. The different quantal states of the nucleons moving in the deformed potential define the different bands. Spherical nuclei do not show bands, and there is no quantal rotation about the symmetry axis of a deformed nucleus.

Although this concept is quite similar to that in molecular physics, there is a fundamental difference. In molecules the rotational degrees of freedom are directly given by the positions of the nuclei. Since the nucleons are not fixed, there is no simple relation between the positions of the nucleons and the rotation of the nucleus as a whole. Accordingly, the moment of inertia remains a free parameter. Simple macroscopic assumptions like rigid rotation or irrotational flow do not account for the experimental moments of inertia. Only microscopic theories, of which the cranking model has turned out to be most successful, achieve quantitative agreement. For low spin, the cranking calculations give very small moments of inertia when the deformation of the mean field becomes small. These results are considered as the microscopic justification of the common view that the nucleus must have a substantial deformation for rotational bands to emerge and that nuclear quantal rotation is a collective phenomenon.

There is no natural difference in the time scales of intrinsic and rotational motion in nuclei, because all constituents have the same mass. Only at low angular momentum is ω_R smaller than ω_i because many nucleons contribute to the collective angular momentum R. In this low-spin region of a few $\hbar$ the concept of combining the ''collective'' rotational excitations with the ''intrinsic'' excitations of the nucleons in the deformed potential is very successful. Bohr and Mottelson (1975) discussed this *unified model* thoroughly in their textbook.

C. High spin

The nuclear energy levels are labeled by the quantum number I of the total angular momentum, which is conserved. For each I there is a state with minimal energy. The sequence of these states is called the *yrast line*. The level density above the yrast line is low enough that the discrete quantal levels may be studied. We are going to restrict ourselves to this yrast region, where the nucleus represents a finite fermion system at zero temperature. The present experimental techniques combining reactions between heavy ions with large arrays of γ-ray detectors permit the study of discrete quantum states up to $I \approx 80\hbar$. Depending on the symmetry, the levels arrange into rotational bands or are distributed with irregular spacings (see Sec. II.F).

In this high-spin region the time scales of the rotational and intrinsic motion are comparable, $\omega_R \sim \omega_i$. A situation quite different from that in molecular physics is encountered. The rotational and intrinsic degrees of freedom are intimately interlaced. On the one hand, strong inertial forces modify the nucleonic motion substantially. On the other hand, the quantal nature of the nucleonic motion affects the rotational motion itself. Phenomena unknown to molecular physics appear, which lead us to readdress the question of when rotational degrees of freedom appear in a finite fermion system.

Figure 1 shows an example of a high-spin level scheme. The transition energies among the members of a band are comparable with the energy differences between the bands, which are given by the distances between levels of the same spin. Thus differences in the energy scales cannot be used to group the levels into bands. The experimentalists arrange the measured γ lines into a rotational spectrum like Fig. 1 as follows:

(1) The states of a band are connected by fast electromagnetic transitions of low multipolarity ($E2$, $M1$, $E1$, $E3$).
(2) The transition energy grows with the angular momentum I in a smooth way.
(3) The transition matrix elements connecting the states gradually change with I.

These criteria are quite handy tools for systematizing the data. However they also reflect those features of bands that remain valid at high spin. The first criterion states that the nucleus has electromagnetic multipole moments, which are carried along with the rotation. They are the source of the radiation, which manifests itself as a cascade of sequential fast transitions. The multicoincidence γ-detector arrays are very good filters for such cascades, examples of which are shown in Figs. 2 and 3. The second and third criteria state that the intrinsic nuclear structure changes only gradually along a band. The regularity of the transition energies is a very obvious feature of the measured spectra, as demonstrated by the ''picket fence.'' The traditional view is that these criteria are met only if the nuclear density has a substantial deformation, which specifies the orientation. Figure 2 presents evidence for this view, whereas Fig. 3 demonstrates that this is too narrow a perspective. The Dy spectrum consists of $E2$ transitions, which indicate a strong quadrupole moment of the charge distribution, whereas the picket fence in Pb is made of $M1$ transitions. The physics of the latter will be discussed in Sec. IV. In Appendix A, where we shall readdress the question of what should be called a rotational band on a more theoretical foundation, the criteria will emerge as a natural consequence of the breaking of rotational symmetry by the mean field.

D. Rotational frequency

When the angular momentum is large it behaves almost like a classical quantity. As a consequence, the angular frequency ω also becomes a well defined observable. This presumes that we can construct a wave packet out of states with different I that have otherwise similar structure, i.e., out of the members of a rotational band. At high spin it is often preferable to choose the angular frequency as the parameter that changes along the band and not the angular momentum. Modifications of the nucleonic motion are directly controlled by ω, because the inertial forces depend on the angular velocity. The central role of the angular frequency in the analysis of the experimental spectra was appreciated by Bengtsson

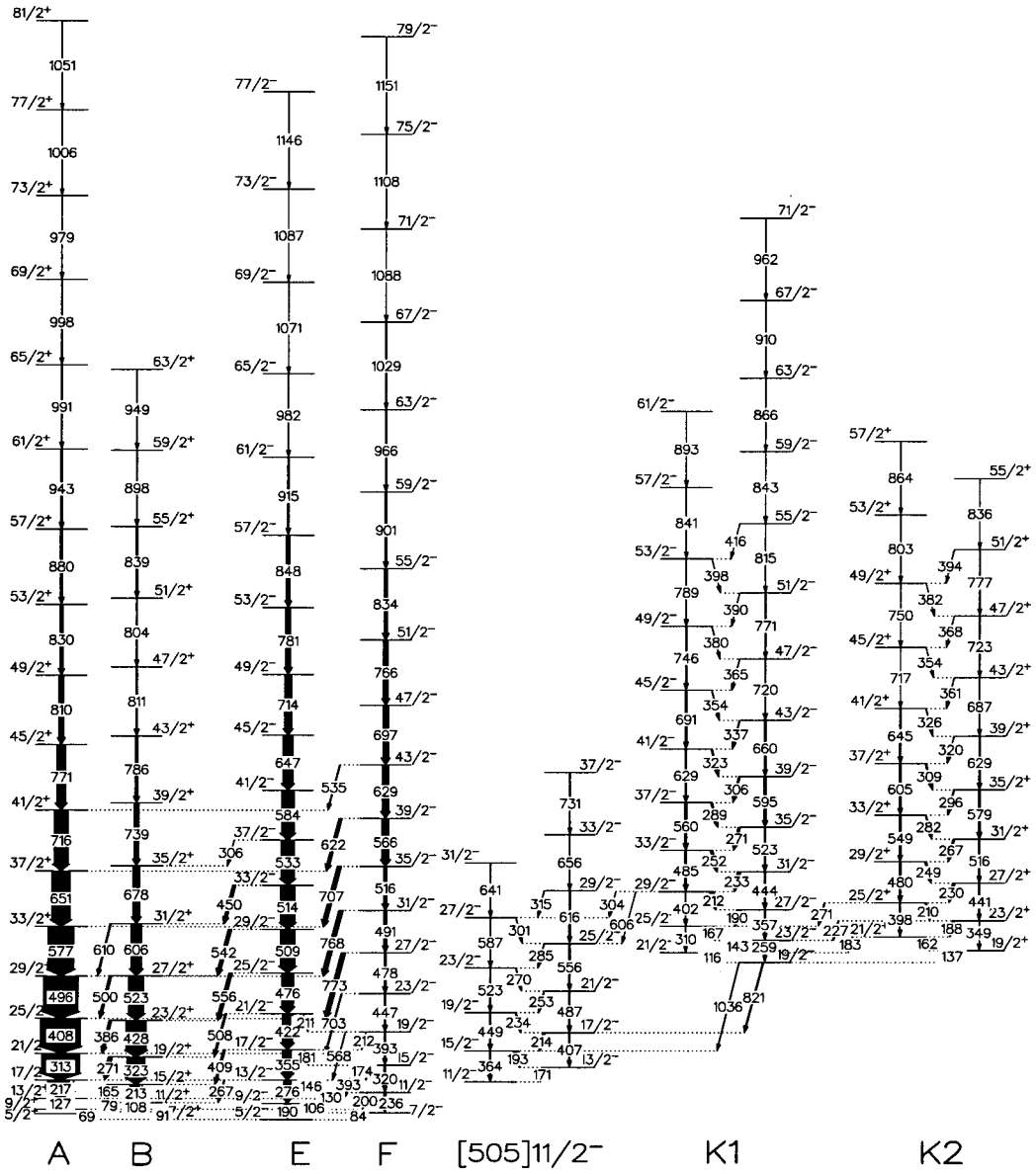

FIG. 1. Partial level scheme of the nucleus ^{163}Er. The new γ-ray multidetector arrays permit identifying up to about 30 individual bands, which comprise the full scheme presented by Hagemann *et al.* (1997). The energies are given in keV. Each level is labeled by the spin and parity I^{π}. The bands are denoted by the quasiparticle configurations, which are discussed in Secs. III.A and III.B.4.

and Frauendorf (1979b). They introduced the experimental Routhian $E'(\omega)$, which is energy in the rotating frame of reference. It is the appropriate quantity to consider when referring to the frequency ω. According to the correspondence with classical electrodynamics, ω is given by the frequency of the electromagnetic radiation. One may define E' and ω on the basis of the stretched quadrupole ($\Delta I=2$) or dipole ($\Delta I=1$) transitions. The choice depends on the symmetry (see Sec. II.F).

If states differing by one unit of angular momentum arrange into a "$\Delta I=1$ band" (e.g., the band K1 in Fig. 1), one can use

$$J=I, \quad \omega=E(I)-E(I-1), \tag{2}$$

$$E'=\frac{1}{2}[E(I)+E(I-1)]-\omega J. \tag{3}$$

Here we introduced the "classical value" of angular momentum J, which can be directly compared with the results of the mean-field theory.

Due to the leading-order quantal correction (see Sec. VIII.C) one must associate the classical angular momentum J with the quantal value $I+\frac{1}{2}$. The rotational frequency ω, which is defined by a transition between two rotational levels, is assigned to the mean value of J for the two levels.

If states differing by two units of angular momentum arrange into a "$\Delta I=2$ band" (e.g., band A in Fig. 1) one must use

$$J=I-\frac{1}{2}, \quad \omega=\frac{1}{2}[E(I)-E(I-2)], \tag{4}$$

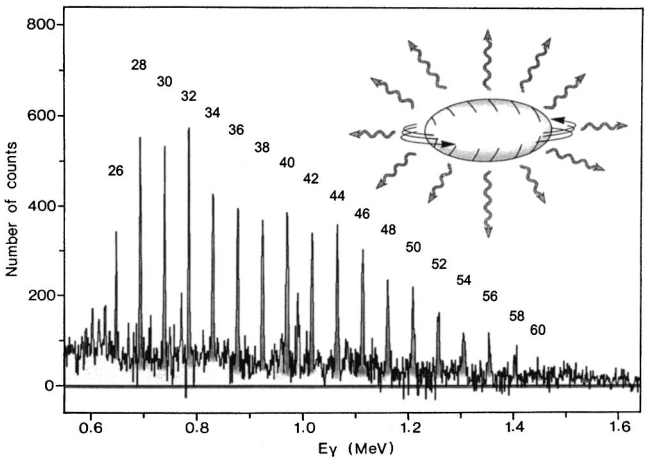

FIG. 2. The spectrum of electric quadrupole transitions within the yrast band of the superdeformed nucleus ^{152}Dy. From Clark and Wadsworth, 1998.

$$E' = \frac{1}{2}[E(I) + E(I-2)] - \omega J. \tag{5}$$

Figure 4 shows the experimental Routhians derived from the spectrum in Fig. 1.

Since ω changes in many small steps along a band, it is a convenient measure for studying the reaction of the nucleonic motion to the inertial forces. This is almost like studying the response of electrons confined by a potential to an external magnetic field (see Sec. IX.) The frequency is a more direct experimental observable than the angular momentum, which must be constructed from the multipolarities of all the γ transitions that form the cascade. If a certain sequence of coincident transitions is not connected with the rest of the spectrum, then one knows the frequency ω but the angular momentum only up to a constant. Choosing the rotational frequency as the band parameter facilitates a comparison with the cranking mean-field theory because the latter is formulated for a given frequency, which can be identified with the experimental frequency. Taken at a given ω, the bands above the yrast line may be interpreted as the particle-hole or quasiparticle excitations defined by the Hamiltonian of the rotating mean field (cf. Fig. 4).

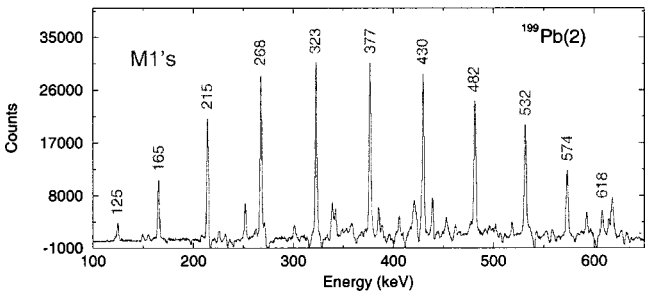

FIG. 3. The spectrum of magnetic dipole transitions within the shears band 2 of the near spherical nucleus ^{199}Pb. From Clark and Wadsworth, 1998.

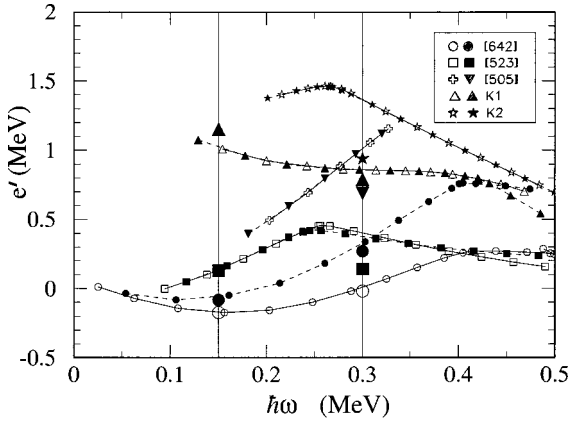

FIG. 4. Experimental Routhians of the rotational bands in ^{163}Er. The bands are labeled by the Nilsson quantum numbers. In Fig. 1, [642] is labeled by A and B and [523] by E and F. The tilted-axis cranking-model Routhians are shown as the large symbols on the two vertical lines where the calculations have been carried out. The same symbols are used for the experiment and calculations. A rigid-rotor reference Routhian $-\omega^2 \times 31.7\,\mathrm{MeV}^{-1}$ is subtracted. From Frauendorf *et al.*, 1994, after Brockstedt *et al.*, 1994.

II. THE ROTATING MEAN FIELD

The cranking model was introduced by Inglis (1954a, 1954b) for calculating the magnetic moments of rotating molecules. It has turned out to be a very successful microscopic approach to rapidly rotating nuclei. The model approximates the eigenstates of the Hamiltonian $H = T + v$ by a Slater determinant (or a more sophisticated mean-field state) $|\rangle$, which rotates uniformly about the z axis. That is, $|t\rangle = e^{-\omega \hat{J}_z t}|\rangle$, where $|\rangle$ is time independent and $\hat{J}_z$ is the total angular momentum. Substituting this ansatz into the time-dependent Schrödinger equation, one immediately sees that $|\rangle$ must be an approximate eigenstate of the Routhian operator

$$H' = H - \omega \hat{J}_z . \tag{6}$$

The familiar steps of the Hartree-Fock approximation lead to the mean-field Routhian

$$h' = T + V - \omega \hat{J}_z , \quad V = \mathrm{tr}[v(1,2)\rho(2)], \tag{7}$$

to which $|\rangle$ is an eigenfunction. The average potential V is calculated in the standard way from the two-body interaction $v(1,2)$ and single-particle density matrix $\rho(2)$ belonging to $|\rangle$. Following Ring and Schuck (1980), we shall refer to this problem as the *self-consistent cranking (SCC) model*. One readily recognizes Eq. (7) as the Hamiltonian in the rotating frame. This is why Neergard *et al.* (1976) invoked the terminology of classical mechanics by calling it "Routhian." We shall refer to V also as the *rotating mean field*, because it rotates uniformly in the laboratory system. The large value of the angular momentum permits the classical treatment of rotational motion and makes the semiclassical quantization very accurate.

One may arrive at the SCC equations in other ways. The rotating state $|t\rangle$ is a solution of the time-dependent

Hartree-Fock (TDHF) scheme, which will be discussed in Sec. VIII.D. Yet another possibility is to consider the Hartree-Fock scheme as a variational method to find the best Slater determinant. The SCC model is obtained when the variation is carried out under the constraint that the angular momentum expectation value $\langle|J_z|\rangle$ is fixed and finite. This amounts to applying the ordinary Hartree-Fock scheme to the two-body Routhian (6), which contains the Lagrangian multiplier ωJ_z. This point of view will be most useful for discussion of the symmetries in Sec. II.F. More detailed derivations of the SCC equations can be found in the textbooks by Ring and Schuck (1980), Szymanski (1983), and Blaizot and Ripka (1986).

A. Effective interactions

Since the self-consistent cranking model has been reviewed several times before (Ring and Schuck, 1980; de Voigt *et al.*, 1983; Szymanski, 1983; Bengtsson and Garrett, 1984; Nilsson and Ragnarsson, 1995), we mention here only a few publications that highlight the important steps in its application to high-spin problems. The nonperturbative treatment of the cranking term $\omega\hat{J}_z$ is essential for the proper description of nucleonic motion in a rapidly rotating potential. Banerjee *et al.* (1973) found the first exact solutions of the SCC problem with the pairing-plus-quadrupole model interaction. Neergard *et al.* (1976) and Andersson *et al.*, (1976) generalized Strutinsky's shell correction method (see Brack *et al.*, 1972) to the cranking problem (7), making possible the study of large deformations which resulted in the prediction of the superdeformed bands, which were discovered ten years later by Twin *et al.* (1986). These calculations assume that the rotating potential is the same as the nonrotating one, except that its shape may change. Goodman *et al.* (1976) used a realistic G matrix for $v(1,2)$. Fleckner *et al.* (1979) applied the Skyrme interaction (a zero-range density-dependent force), which became popular for the SCC model after work by Bonche *et al.* (1987). Egido and Robledo (1993) introduced the finite-range Gogny interaction to self-consistent cranking. In these calculations one no longer has to make assumptions about the radial profile of the density distribution. In addition, new, time-odd terms appear in the potential V, which reflect the presence of currents in the rotating nucleus. Koepf and Ring (1989) introduced the relativistic mean-field version of the SCC equations. The effective two-body interaction v is expressed in terms of meson exchange. The resulting constraints on the parameters of v are important for rotating nuclei, because those parts of the interaction that generate the time-odd components of the mean field are not well known. The pair correlations are taken into account by means of the Hartree-Fock-Bogoliubov version of the SCC equations (see Ring and Schuck, 1980).

B. The pairing-plus-quadrupole model

Most of the issues addressed in this review can already be understood in the framework of the SCC model using the pairing-plus-quadrupole interaction. In order to keep the presentation simple we shall mostly stay within this frame. The pairing-plus-quadrupole model is described in the textbook by Ring and Schuck (1980), to which the reader is referred for further details. The two-body Routhian has the form

$$H' = H_{sph} - \frac{\chi}{2}\sum_{\mu=-2}^{2} Q_\mu^+ Q_\mu - GP^+P - \lambda\hat{N} - \omega\hat{J}_z . \tag{8}$$

This model incorporates three important aspects of the nuclear many-body system.

The nucleons move in a spherical potential with a strong spin-orbit term. The average potential is not derived from the interaction but simply given by the energies e_k of the levels labeled by k. In second quantization this reads

$$H_{sph} = \sum_k e_k c_k^+ c_k . \tag{9}$$

The long-range particle-hole correlations are taken into account by the second term, the quadrupole interaction, which is assumed to be a product of the quadrupole operators,[1]

$$Q_\mu = \sum_{kk'} \sqrt{\frac{4\pi}{5}} \langle k|r^2 Y_{2\mu}|k'\rangle c_k^+ c_{k'} . \tag{10}$$

This part of the interaction is responsible for the quadrupole deformation of the mean field.

The short-range particle-particle pair correlations are taken into account by the third term, the pairing interaction. It is a product of the operators of the monopole pair field,

$$P^+ = \sum_{k>0} c_k^+ c_{\bar{k}}^+ , \tag{11}$$

where $\bar{k}$ is the time-reversed state of k. The monopole pair field consists of Cooper pairs of protons or neutrons coupled to zero angular momentum.

The term $-\lambda\hat{N}$ controls the particle number N. To simplify the notation, the Routhian (8) is written only for one kind of particle. The terms h_{sph}, Q_μ, and $\hat{J}_z$ must be understood as sums of a proton and a neutron part, and there are terms $-GP^+P$ and $-\lambda\hat{N}$ for both protons and neutrons.

The Hartree-Fock-Bogoliubov approximation is used for the state vector $|\rangle$, which is an eigenstate of the mean-field Routhian h'. Neglecting exchange terms, the latter is given by

$$h' = h_{sph} - \sum_{\mu=-2}^{2} q_\mu Q_\mu^+ - \Delta(P^+ + P) - \lambda\hat{N} - \omega\hat{J}_z . \tag{12}$$

[1]This definition of the quadrupole operators corresponds to $Q_0 = r^2 P_2(\cos\vartheta)$, with P_2 being the Legendre polynomial.

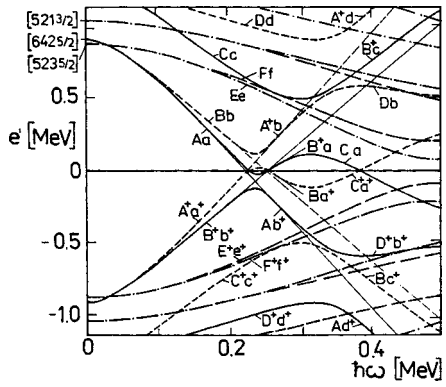

FIG. 5. Quasineutron Routhians for $N\approx 96$. The rotational axis lies perpendicular to the symmetry axis. Parity and signature (π, α) are indicated by the line type: solid line $(+, 1/2)$; short-dashed line $(+, -1/2)$; dash-dotted line $(-, 1/2)$; long-dashed line $(-, -1/2)$. The adiabatic trajectories are labeled with lower-case letters, the diabatic trajectories with upper-case letters. The diabatic trajectories are extended through the quasicrossings only for the levels A, B, A^+, and B^+. The parameters are $\varepsilon=0.246$, $\gamma=0°$, $\varepsilon_4=0.004$, $\Delta=0.86$ MeV, $\vartheta=90°$, $\varphi=0°$. From Bengtsson *et al.*, 1986.

The self-consistency equations determine the deformed part of the potential,

$$q_\mu=\chi\langle Q_\mu\rangle, \tag{13}$$

the pair potential,

$$\Delta=G\langle P\rangle, \tag{14}$$

and implicitly the chemical potential λ by

$$N=\langle\hat{N}\rangle. \tag{15}$$

The quasiparticle operators

$$\alpha_i^+=\sum_k U_{ki}c_k^+ + V_{ki}c_k \tag{16}$$

obey the equations of motion

$$[h',\alpha_i^+]=e_i'\alpha_i^+ \tag{17}$$

which define the eigenvalue equations for the quasiparticle amplitudes U_{ki} and V_{ki}. The explicit form of these Hartree-Fock-Bogoliubov equations can be found in the textbooks by Ring and Schuck (1980) and Szymanski (1983). The eigenvalues e_i' are called *quasiparticle Routhians*; examples are shown in Fig. 5.

The quasiparticle operators refer to the vacuum state $|0\rangle$,

$$\alpha_i|0\rangle=0\forall i, \tag{18}$$

and define the excited quasiparticle configurations

$$|i_1,i_2,\ldots\rangle=\alpha_{i_1}^+\alpha_{i_2}^+\cdots|0\rangle. \tag{19}$$

The construction of a configuration for a sequence of ω values, which represents a rotational band, will be discussed in Sec. III.A.2.

The set of Hartree-Fock-Bogoliubov equations (12)–(19) can be solved for any configuration $|\rangle=|i_1,i_2,\ldots\rangle$. For such a self-consistent solution, the total Routhian

$$E'=\langle H'\rangle \tag{20}$$

has an extremum

$$\left.\frac{\partial E'}{\partial q_\mu}\right|_\omega=0, \quad \left.\frac{\partial E'}{\partial\Delta}\right|_\omega=0. \tag{21}$$

The total energy as a function of the angular momentum is given by

$$E(J)=E'(\omega)+\omega J(\omega), \tag{22}$$

$$J(\omega)=\langle\hat{J}_z\rangle, \tag{23}$$

where Eq. (23) implicitly determines $\omega(J)$. The total energy is extremal for a fixed value of J,

$$\left.\frac{\partial E}{\partial q_\mu}\right|_J=0, \quad \left.\frac{\partial E}{\partial\Delta}\right|_J=0. \tag{24}$$

For a family of self-consistent solutions $|\omega\rangle$ found for different values of ω, the following canonical relations hold:

$$\frac{dE'}{d\omega}=-J, \tag{25}$$

$$\frac{dE}{dJ}=\omega. \tag{26}$$

The *dynamic* moment of inertia is defined by

$$\mathcal{J}^{(2)}=\frac{dJ}{d\omega}, \tag{27}$$

which generally differs from the *kinematic* one, $\mathcal{J}^{(1)}=J/\omega$.

Kerman and Onishi (1981) showed that for a self-consistent solution the vector of the angular velocity

$$\vec{\omega}=(\omega_x,\omega_y,\omega_z)=(0,0,\omega) \tag{28}$$

and the vector of the expectation values of the angular momentum components

$$\vec{J}=(\langle\hat{J}_x\rangle,\langle\hat{J}_y\rangle,\langle\hat{J}_z\rangle) \tag{29}$$

must be parallel. Since the interaction is rotational by invariant, one has

$$\langle[H',\hat{J}_x]\rangle=i\omega\langle\hat{J}_y\rangle, \tag{30}$$

$$\langle[H',\hat{J}_y]\rangle=-i\omega\langle\hat{J}_x\rangle. \tag{31}$$

The left-hand sides are small variations of E', the stationarity of which implies

$$\langle\hat{J}_x\rangle=\langle\hat{J}_y\rangle=0, \tag{32}$$

i.e.,

$$\vec{\omega}\|\vec{J}, \tag{33}$$

Q.E.D.

The reduced probabilities for electromagnetic transitions are given by the semiclassical expressions (see, for example, Bohr and Mottelson 1975)

$$B(E2,I\to I-2)=\frac{5}{4\pi}|\langle Q_{22}\rangle|^2, \tag{34}$$

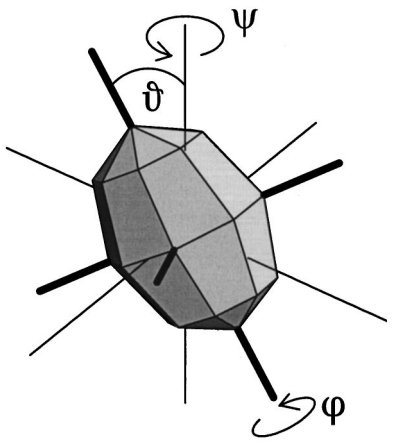

FIG. 6. Euler angles specifying the orientation of the triaxial reflection-symmetric density distribution.

$$B(E2,I\rightarrow I-1)=\frac{5}{4\pi}|\langle Q_{21}\rangle|^2, \tag{35}$$

$$B(M1,I\rightarrow I-1)=\frac{3}{4\pi}|\langle \mu_{11}\rangle|^2. \tag{36}$$

The static electromagnetic moments are equal to their expectation values. The matrix elements $\langle Q_{2\nu}\rangle$ are the components of the charge quadrupole moment and $\langle \mu_{1\nu}\rangle$ the components of the magnetic dipole moment, both of which refer to the laboratory axis z. They are related intrinsically to the components by a rotation which is discussed in Sec. II.C. If one uses the high-spin approximation for the Clebsch-Gordan coefficients (Edmonds, 1957) in the unified model, one obtains the semiclassical form of Eqs. (34)–(36). Dönau and Frauendorf (1983) applied the semiclassical expressions to the rotating mean field.

C. Intrinsic frame of reference

In the pairing-plus-quadrupole model the anisotropy of the average potential is described by the quadrupole tensor q_μ. Let us now introduce the intrinsic frame of reference. It is the frame of principal axes within which the quadrupole tensor takes the simple form $q'_{-1}=q'_1=0$ and $q'_{-2}=q'_2$. The principal axes are denoted by 1, 2, and 3. Their orientation with respect to the laboratory frame is fixed by the three Euler angles ψ, ϑ, and φ. Figure 6 illustrates the definition of these angles. In our convention, $\psi(=\omega t)$ is the angle that grows as the nucleus rotates uniformly about the z axis. The angles ϑ and φ are the orientation angles of $\vec{J}$ (i.e., of the z axis) with respect to the intrinsic frame of reference. This convention has been used in the tilted-axis cranking literature. We retain it but point out that the meaning of the angles ψ and φ is reversed as compared to the convention of Bohr and Mottelson (1975). The two ''intrinsic'' quadrupole moments q'_0 and q'_2 specify the deformation of the potential. The quadrupole moments in the laboratory frame are related to them by

$$q_\mu=D^2_{\mu 0}(\psi,\vartheta,\varphi)q'_0 + [D^2_{\mu 2}(\psi,\vartheta,\varphi)+D^2_{\mu -2}(\psi,\vartheta,\varphi)]q'_2, \tag{37}$$

where $D^2_{\nu\mu}(\psi,\vartheta,\varphi)$ are the Wigner D functions.[2]

The two intrinsic quadrupole moments are expressed by the standard deformation parameters (the Lund convention)

$$q'_0=K\beta\cos\gamma, \quad q'_2=-K\beta\sin\gamma/\sqrt{2}, \tag{38}$$

where K sets the energy scale for the deformed potential. The parameter β measures the deviation of the shape from a sphere. Often the parameter ε is used, which is $\varepsilon=0.95\beta$ for not too large deformation. The parameter γ measures the deviation from axial shape. It changes from 0° (prolate shape) to 60° (oblate shape).

The calculations are most conveniently carried out in the intrinsic frame, where the mean-field Routhian is fixed by the two deformation parameters β and γ and the two angles ϑ and φ, which determine the orientation of $\vec{\omega}$ with respect to the principal axes (see Fig. 6). The mean-field Routhian reads

$$h'=h_{sph}-q'_0Q'_0-q'_2(Q'_2+Q'_{-2})-\Delta(P^+ +P)-\lambda\hat{N} - (\omega_1\hat{J}_1+\omega_2\hat{J}_2+\omega_3\hat{J}_3), \tag{39}$$

where Eq. (37) relates the intrinsic quadrupole moments Q'_μ to the Q_μ in the laboratory frame. The vector $\vec{\omega}$ refers to the principal axes, i.e.,

$$\vec{\omega}=(\omega_1,\ \omega_2,\ \omega_3) =\omega(\sin\vartheta\cos\varphi,\ \sin\vartheta\sin\varphi,\ \cos\vartheta). \tag{40}$$

The five self-consistency equations (13) are reduced to two,

$$q'_0=\kappa\langle Q'_0\rangle, \quad q'_2=\kappa\langle Q'_2\rangle, \tag{41}$$

which determine β and γ. They are complemented by the condition (33) that $\vec{J}$ must be parallel to $\vec{\omega}$ at the point of self-consistency, which is used to determine the angles ϑ and φ. The Routhian $E'(\vartheta,\varphi)$ has an extremum for this orientation. Since we are going to use diagrams showing $e'_i(\vartheta)$ and $E'(\vartheta)$ for fixed deformation, it should be emphasized that the deformation parameters and the orientation angles influence each other, and Eqs. (41) and (33) must be solved as a coupled system of equations.

If the rotational axis agrees with one of the principal axes, the convention has been adopted of choosing 1 as the axis of rotation ($\vartheta=90°$, $\varphi=0$) and of considering the deformation parameter γ to be in the extended range of 180°. The two additional sectors repeat the family of shapes such that the axis of rotation coincides with one of the other two principal axes. Frauendorf (2000) extended this practical convention to the case in which the axis of rotation lies in one of the principal planes of the triaxial potential. He assumes that the ro-

[2]We use the definition of the D functions by Bohr and Mottelson (1975).

TABLE I. Association of the principal axes of the triaxial potential with the axes 1 and 3. The asterisk indicates a symmetry axis.

γ	shape	1 axis	3 axis
$-270°$	prolate	short	short
	triaxial	intermediate	short
$-180°$	oblate	long	short*
	triaxial	long	short
$-120°$	prolate	long*	short
	triaxial	long	intermediate
$-60°$	oblate	long	long
	triaxial	intermediate	long
$0°$	prolate	short	long*
	triaxial	short	long
$60°$	oblate	short*	long
	triaxial	short	intermediate
$120°$	prolate	short	short

tational axis lies in the 1-3 plane ($\varphi=0$) and selects the desired plane of the potential by letting γ vary in the range of 180°. Table I shows which of the principal axes correspond to 1 and 3 in the different sectors of the $\beta-\gamma$ plane. Choosing the 1-3 plane has the technical advantage that the matrix of the quasiparticle Routhian (39) remains real with the standard choice of phases for the angular momentum eigenfunctions. The reader may find more details about the deformation parameters in the textbooks by Szymanski (1983) and Nilsson and Ragnarsson (1995).

Figures 5 and 7 show the quasiparticle Routhians e_i' as functions of the frequency ω and the tilt angle ϑ, where all the other parameters of the mean field are kept fixed. Such quasiparticle diagrams, which are dubbed "spaghetti plots," are indispensable for constructing the quasiparticle configurations representing rotational bands. The slopes of the trajectories contain information about the expectation value of the angular momentum,

$$\vec{j}_i=(j_{1,i},\ j_{2,i},\ j_{3,i}), \tag{42}$$

for the quasiparticle i, the components of which are also called the quasiparticle alignments. The slope with respect to ω is $-(\vec{\omega}/\omega)\cdot\vec{j}$. The slopes with respect to the tilt angles ϑ and φ are $-(\partial\vec{\omega}/\partial\vartheta)\cdot\vec{j}_i$ and $-(\partial\vec{\omega}/\partial\varphi)\cdot\vec{j}_i$, respectively. For the important case $\varphi=0°$ one has

$$\frac{\partial e_i'(\omega,\vartheta)}{\partial\omega}=-(j_{1,i}\sin\vartheta+j_{3,i}\cos\vartheta) \tag{43}$$

and

$$\frac{\partial e_i'(\omega,\vartheta)}{\partial\vartheta}=-\omega(j_{1,i}\cos\vartheta-j_{3,i}\sin\vartheta). \tag{44}$$

In Fig. 5 ($\vartheta=90°$), the slope is $-j_{1,i}$.

The components of the electromagnetic moments in the laboratory frame, which appear in Eqs. (34)–(36), are obtained from components with respect to the principal axes by means of Eq. (37) and the corresponding transformation for the dipole moments. The explicit equations are given by Frauendorf (1997, 2000) for axial deformation and by Frauendorf and Meng (1997b) for triaxial deformation. The evaluation of the intrinsic components of the magnetic moment $\langle\mu_\nu'\rangle$ and of the charge quadrupole moment $\langle Q_{2\mu}'\rangle$ is described by Frauendorf (2000). There, the reader can also find the details of the tilted-axis cranking calculations within the frame of the pairing-plus-quadrupole model and the shell correction version, as well as a collection of TAC formulas.

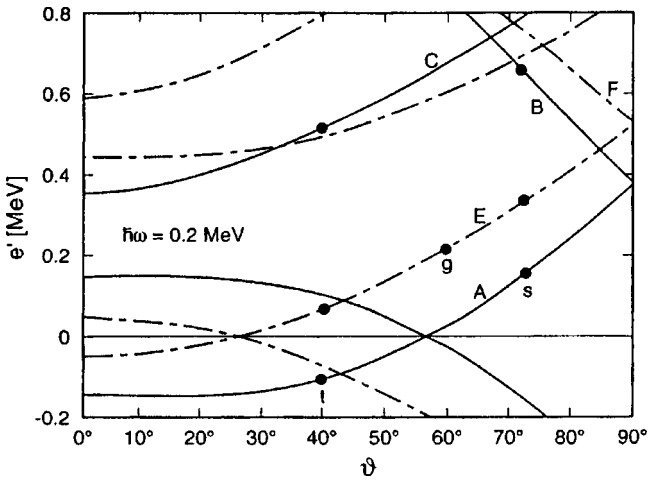

FIG. 7. Quasineutron Routhians for $N\approx105$ as functions of the tilt angle ϑ: solid lines, positive parity; dash-dotted lines, negative parity. The dots indicate the occupation of the levels. They are located at the equilibrium angle of each configuration. The parameters are $\varepsilon=0.26$, $\gamma=0°$, $\varepsilon_4=0$, $\Delta_n=0.65$ MeV, $\omega=0.2$ MeV, $\varphi=0°$. From Frauendorf, 1993a.

D. Coupling of the quasiparticles to the deformed potential

Let us consider some general features of the quasiparticle response to rotation. How do these show up in the spaghetti diagrams, which look rather erratic at a first glance? The high-j intruder orbitals $g_{9/2}$, $h_{11/2}$, $i_{13/2}$, and $j_{15/2}$ determine the physics of many phenomena to be discussed. For moderate deformation of the potential, to which we restrict our considerations, their total angular momentum is still approximately equal to the quantal value in the spherical potential, because large spin-orbit splitting prevents substantial mixing with orbitals of lower j. Hence the state is described by the orientation of the angular momentum vector $\vec{J}$. The nucleon moves on a circular orbit in the plane perpendicular to $\vec{J}$. Its density distribution looks like a doughnut.

Consider the important case of an axial prolate potential. The particle angular momentum will orient perpendicular to the symmetry axis, to be definite $\vec{j}=(j_1,0,0)$. This direction corresponds to a maximal overlap of the doughnut with the attractive potential, i.e., to minimal energy. Its Routhian is $e'(\vartheta)\approx e'(0)-\omega j_1\sin\vartheta$. The

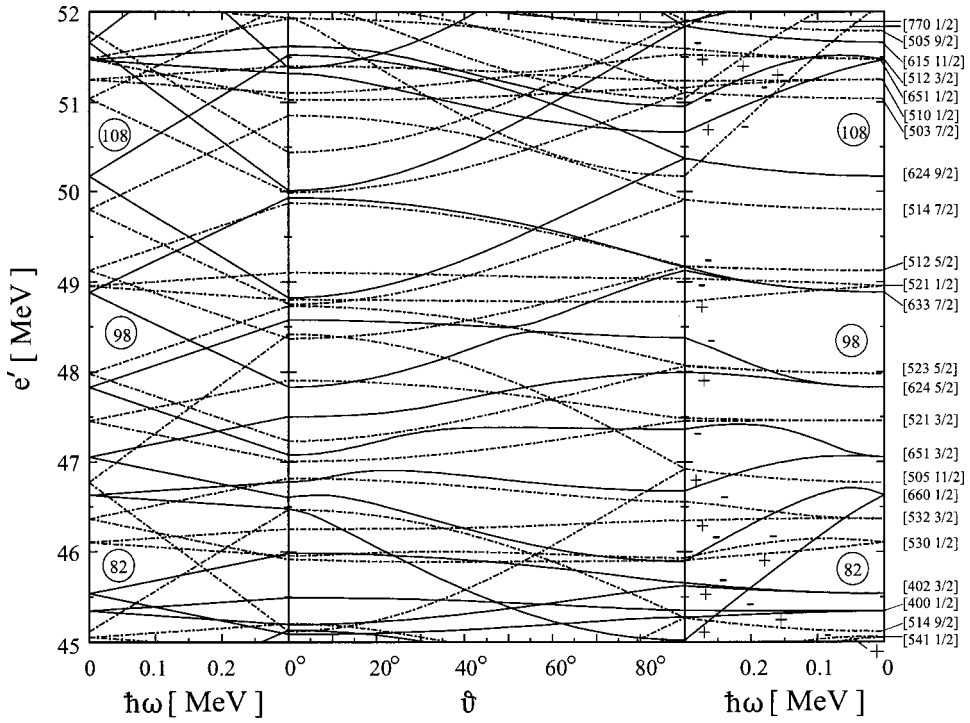

FIG. 8. Single-neutron energies for $\varepsilon=0.24$, $\varepsilon_4=0$: solid lines, positive parity; dash-dotted lines, negative parity. For $\vartheta=90°$ the signature is indicated by $\pm$ standing for $\alpha=\pm 1/2$. From Frauendorf, 2000.

next particle in the j shell cannot have the same direction as the first one, because this is forbidden by the Pauli principle. Still, its angular momentum tends to orient perpendicular to the symmetry axis. It has the same ϑ dependence with a smaller value of j_1. Examples are the two lowest $i_{13/2}$ trajectories in Fig. 8, which emanate from the $[660]1/2^+$ Nilsson state. Conventionally, such orbitals are called "decoupled" because they do not participate in the rotational motion if the rotational axis has the direction of the 1 axis. They just contribute a constant value of j_1 to the total angular momentum. However, if the rotational axis is tilted away from the principal axis 1 they are no longer decoupled.

The angular momentum of a hole in a full j shell will orient parallel to the symmetry axis, because it experiences the potential as repulsive, i.e., $\vec{j}=(0,0,j_3=K)$. This direction corresponds to minimal overlap of the doughnutlike wave function with the potential. Equivalently, one may consider a full j shell with one particle taken out. This system has a dumbbell-like density distribution (sphere minus doughnut), in which all particles feel an attractive potential. The preferred orientation of $\vec{j}$ is parallel to the symmetry axis, which maximizes the overlap of the dumbbell with the potential. The Routhian will be $e'(\vartheta)\approx e'(0)-\omega j_3\cos\vartheta$. Examples are the two $i_{13/2}$ trajectories in Fig. 8, which emanate from the $[624]9/2^+$ Nilsson state. These orbitals are also called *strongly coupled* because $\vec{j}$ follows the symmetry axis, being carried around by the rotation.

In the case of an oblate axial potential the roles of the particle and hole are exchanged. If the potential is triaxial, $\vec{j}$ of the hole will align with the long axis and $\vec{j}$ of the particle with the short axis. These orientations correspond, respectively, to minimal and maximal overlap of the density distributions with the triaxial potential. Bengtsson *et al.* (1987) studied in detail the response of a high-j quasiparticle in a triaxial potential to a change in the orientation of the rotational axis. A systematic semiclassical analysis of all quantal states (not only the lowest and highest ones) of a high-j particle in a deformed potential was carried out by Bohr and Mottelson (1980), Frauendorf (1982), Mottelson (1983), and Vigezzi *et al.* (1988).

Frauendorf (2000) also analyzed how the other normal-parity quasiparticles couple to a deformed rotating potential. Let us continue with the case of a prolate axial deformation. Orbitals with a large projection j_3 are strongly coupled to the deformed potential. They have the same $\pm K\omega\cos\vartheta$ dependence discussed above for the hole-type high-j orbitals. An example is $[512]5/2^-$ in Fig. 8. The states originating from low-K Nilsson levels show a complex behavior, which cannot be explained in a simple way. An exception are the pseudo spin singlets. The pair of parallel trajectories emanating from the Nilsson state $[521]1/2^-$ is an example. Their Routhian does not change with ϑ and their distance is equal to ω. They behave in this way because their angular momentum is approximately equal to the pseudo spin, which is decoupled from the deformed field. It takes the direction of $\vec{\omega}$ or opposite to it, corresponding to a Routhian $e'(\vec{\omega})\approx e(\omega=0)\pm\omega/2$. The concept of pseudospin and the reason for the decoupling are explained in Sec. VII.D.

E. Approximate solutions—The cranked shell model

Bands with a finite angular momentum projection J_3 on the symmetry axis were first described by means of the unified model (Bohr and Mottelson 1975), which treats angular momentum quantum mechanically. The

central approximation is the *strong-coupling limit*, which assumes that $J_3=K$ is conserved. Tilted-axis cranking treats the angular momentum semiclassically. In the strong-coupling limit, the total angular momentum is composed only of the collective part $J_1=R$ and $J_3=K$, which is constant. The energy

$$E=\frac{R^2}{2\mathcal{J}}=\frac{J^2-K^2}{2\mathcal{J}} \tag{45}$$

is the same as in the unified model. The tilt angle is given by

$$\cos\vartheta=\frac{K}{J}. \tag{46}$$

For this value of ϑ, the TAC expressions (34)–(36) agree with the transitions probabilities in the unified model when the Clebsch-Gordan coefficients are approximated by their high-spin asymptotic values.

Bengtsson and Frauendorf (1979b) suggested a less stringent approximation. The assumption that $J_3=K$ is kept, but J_1 is calculated by means of the principal-axis cranking model at the frequency $\omega_1=\omega\sin\vartheta$, where ϑ is given by Eq. (46). This approach has become known as the *cranked shell model* (CSM). It amounts to neglecting the term $-\omega\hat{J}_3\cos\vartheta$ in the mean-field Routhian. If J_3 is not too large, the band starts at a relatively low frequency and ϑ changes rapidly from 0° to 90°. The neglected term is not too important if the coupling of the quasiparticle orbital to the deformed potential is much stronger than $-\omega\hat{J}_3\cos\vartheta$. Then it is a good approximation to take only $-\omega\hat{J}_1\sin\vartheta$ into account. This is not the case for weakly coupled orbitals or small deformation. Of course, the CSM approximation becomes better and better as ϑ approaches 90°.

Dönau and Frauendorf (1983) worked out the transition probabilities for the CSM approximation. These probabilities agree with Eqs. (34), (35), and (36) if the strong-coupling limit (46) is used for ϑ in the transformation from the intrinsic to the laboratory components. The intrinsic components of the magnetic moments of the excited quasiparticles i are calculated by means of the relations

$$\mu_\nu=\sum_i g_{K,i}j_{\nu,i}, \quad \nu=1,2,3. \tag{47}$$

The collective part, which accounts for the rest, is

$$\mu_1^c=g_R\left(J_1-\sum_i j_{1,i}\right). \tag{48}$$

The gyromagnetic ratios $g_{K,i}$ and g_R are either taken from experiment or calculated from the mean-field solutions at $\omega_1=0$. The components $j_{3,i}$ are set equal to the angular momentum projection K_i at $\omega_1=0$. The aligned angular momenta $j_{1,i}$ are either calculated by means of the cranked shell model or extracted from the differences between the experimental functions $J_1(\omega_1)$ with and without the quasiparticle i present. Dönau (1987) introduced a term that permits the calculation of the signature dependence (see Sec. III.A) of the $B(M1)$ values. He demonstrated its validity for the case when the J_3 component is generated by only one quasiparticle. It is not expected that his expression will also hold when J_3 is generated by many quasiparticles. The original expressions without the signature term also apply to this important case. This calculation scheme for transition probabilities is referred to as the semiclassical vector model or Dönau-Frauendorf model. It seems more appropriate to call it a cranked shell model as well, because it extends the CSM concept from the energies to the transition matrix elements. The possibility of extracting the aligned angular momenta and the g-factors from experiment substantially improves the accuracy of the calculation.

What are the merits and limitations of the CSM and tilted-axis cranking Frauendorf and Meng (1997a) and Frauendorf (2000) compared the two models? On the one hand, the CSM is quite commonly used because of its simplicity. The spectrum of rotational bands can be constructed by occupying the quasiparticle levels in a single spaghetti diagram like Fig. 5. It does not have the unpleasant discontinuities caused by the change of symmetry with frequency, which we shall discuss in Sec. III.B. On the other hand, the CSM must be seen as an approximation to TAC, which is the best possible mean-field solution. The CSM amounts to extrapolating the TAC quasiparticle Routhians from the values calculated at $\vartheta=90^\circ$ by means of the expression

$$e_i'(\omega,\vartheta)=e_i'(\omega,90^\circ)-\omega[j_{1,i}(\sin\vartheta-1)+K_i\cos\vartheta]. \tag{49}$$

As can be seen in Fig. 12, below this is a quite decent approximation for a number of quasiparticles. But it certainly fails to account for the complex behavior of the $i_{13/2}$ quasineutrons as functions of ϑ, which leads to the coexistence of the t and s bands discussed in Sec. III.B.4. The fixed-K approximation becomes particularly bad for the weakly deformed nuclei discussed in Sec. IV, because the almost spherical potential cannot keep the orientation of the high-j orbitals. Calculations of the $B(M1)$ values which demonstrate this failure can be found in the articles of Neffgen *et al.* (1995), Clark *et al.* (1998), and Jenkins *et al.* (1998).

F. Symmetries

The symmetries of the two-body Routhian (6) and of the mean-field Routhian (7) play a central role in the interpretation of the rotating mean-field solutions. The symmetries are not necessarily the same. If the mean-field Routhian has a lower symmetry one speaks of *spontaneous symmetry breaking*. The concept of spontaneous symmetry breaking is discussed in the textbooks on many-body theory of finite quantum systems by Ring and Schuck (1980) and Blaizot and Ripka (1986). It was conceived for infinite systems, where it applies to the exact many-body solution. For finite systems the exact solutions are the eigenstates of the two-body Routhian, which have the same symmetry. Only approximate solutions may have a lower symmetry. Classifying the mean-

field solutions according to their symmetry is a fruitful concept, because the different symmetries manifest themselves clearly as different types of rotational bands. As discussed by Ring and Schuck (1980) and Blaizot and Ripka (1986), breaking of rotational symmetry with respect to the angular momentum axis leads to the appearance of a rotational band. The breaking of a discrete twofold symmetry results in the appearance of pairs of degenerate states.

It seems useful to invoke the concept of an order parameter, which is used for the description of phase transitions in infinite systems. An order parameter is some physical quantity that is zero in one phase, which has a certain symmetry, and finite in the other phase, which does not have the symmetry.[3] Spontaneous magnetization is an example. It is finite for a ferromagnet, which is anisotropic. It becomes zero when the temperature exceeds the critical value, where the phase transition into the isotropic nonferromagnetic state takes place. For finite systems we call an order parameter a quantity that becomes large compared with a typical single-particle matrix element when the mean field breaks a symmetry.

Bohr and Mottelson (1975) analyzed the spatial symmetries of the intrinsic wave function and their consequences for nuclear rotational spectra in the frame of their unified model. Goodman (1976) investigated the symmetries of the mean-field Routhian in a systematic way, but did not consider the consequences for rotational spectra. Further work will be cited when discussing the concrete symmetries. We are now going to discuss the different symmetries in detail.

The two-body Routhian (6) is invariant with respect to

(1) $\mathcal{R}_z(\psi)$, rotation about the z axis,
(2) $\mathcal{P}$, space inversion,
(3) $\mathcal{R}_z(\pi)$, rotation about the z axis by an angle of π,
(4) $\mathcal{T}R_y(\pi)$, rotation about the x axis by an angle of π combined with the time reversal $\mathcal{T}$.

The symmetry (4) is a consequence of $\vec{J}$'s being odd under the time-reversal operation $\mathcal{T}$. We assume that 1 is broken. The symmetry operations (2)–(4) are twofold and commute. Table II lists the different combinations by which the rotating mean field can break the three symmetries.

The two-body Routhian also conserves the particle number $\hat{N}$, i.e., it is invariant with respect to the transformation $e^{-i\chi\hat{N}}$, which is called a rotation in gauge space. If the electromagnetic interaction is neglected the isospin is conserved. Then the two-body Routhian is invariant with respect to rotations in isospace. There is an approximate symmetry of the mean field, which leads to the appearance of pseudo-spin. The implications of these nonspatial symmetries are not the focus of this review. They will be briefly discussed in Sec. VII.

[3]The reader may find a more extended discussion in the textbook of Landau and Lifshitz (1985).

TABLE II. Discrete symmetries of the rotating mean field. Columns 1–3 list the results of the symmetry operation. D(ifferent) means the mean field has changed and S(ame) it has not. An operation as entry means it is identical with that of the column. Column 4 shows the spin and parity I^π of the rotational states, where $I^\pm$ means that there are two degenerate states of opposite parity (parity doubling). The 2 indicates that there are two degenerate states with the same I^π (chiral doubling) and $2I^\pm$ means that there are four degenerate states, two with I^+ and two with I^- (parity and chiral doubling). For I-V $\pi=-$ also appears, although it is not explicitly indicated.

$\mathcal{P}$	$\mathcal{R}_z(\pi)$	$\mathcal{T}\mathcal{R}_y(\pi)$	level sequence
S	S	S	$I^+,(I+2)^+,(I+4)^+,\ \ldots$
S	D	S	$I^+,(I+1)^+,(I+2)^+,\ \ldots$
S	D	D	$2I^+,2(I+1)^+,2(I+2)^+,\ \ldots$
S	S	D	$2I^+,2(I+2)^+,2(I+4)^+,\ \ldots$
S	D	$\mathcal{R}_z(\pi)$	$I^+,(I+1)^+,(I+2)^+,\ \ldots$
D	S	S	$I^\pm,(I+2)^\pm,(I+4)^\pm,\ \ldots$
D	D	S	$I^\pm,(I+1)^\pm,(I+2)^\pm,\ \ldots$
D	S	D	$2I^\pm,2(I+2)^\pm,2(I+4)^\pm,\ \ldots$
D	D	$\mathcal{R}_z(\pi)$	$I^\pm,(I+1)^\pm,(I+2)^\pm,\ \ldots$
$\mathcal{R}_z(\pi)$	D	S	$I^+,(I+1)^-,(I+2)^+,\ \ldots$
$\mathcal{R}_z(\pi)$	D	D	$2I^+,2(I+1)^-,2(I+2)^+,\ \ldots$
$\mathcal{T}\mathcal{R}_y(\pi)$	S	D	$I^\pm,(I+2)^\pm,(I+4)^\pm,\ \ldots$
$\mathcal{T}\mathcal{R}_y(\pi)$	D	D	$I^\pm,(I+1)^\pm,(I+2)^\pm,\ \ldots$
$\mathcal{R}_z(\pi)$	D	$\mathcal{R}_z(\pi)$	$I^+,(I+1)^-,(I+2)^+,\ \ldots$
D	D	D	$2I^\pm,2(I+1)^\pm,2(I+2)^\pm,\ \ldots$

Dobaczewski *et al.* (2000) recently classified the mean-field solutions according to the discrete symmetries which arise from the combination of $\mathcal{R}_x(\pi)$, $\mathcal{R}_y(\pi)$, $\mathcal{R}_z(\pi)$, $\mathcal{T}R_x(\pi)$, $\mathcal{T}R_y(\pi)$, $\mathcal{T}R_z(\pi)$, and $\mathcal{T}$. The symmetries, which are listed in Table II, are special cases of their scheme. Since their remaining symmetries do not leave the two-body Routhian invariant, they are not relevant for a discussion of spontaneous symmetry breaking within the self-consistent cranking model.

1. Symmetry with respect to the angular momentum vector

Breaking of the symmetry with respect to a rotation about the z axis (direction of angular momentum) is the prerequisite for the appearance of rotational bands. If $\mathcal{R}_z(\psi)$ is a symmetry of the mean field, the high-spin spectra show characteristic irregular spacings with increasing I. Isomers (yrast traps) frequently appear. This regime is not the subject of the present article. It is discussed in the review by de Voigt *et al.* (1983), and the textbooks of Szymanski (1983) and Nilsson and Ragnarsson (1995). Walker and Dracoulis (1999) give a short overview with a broad perspective.

The relation between the violation of rotational symmetry and the appearance of rotational bands is discussed in the textbooks by Ring and Schuck (1980) and Blaizot and Ripka (1986). Let us review the most important points. Breaking of the $\mathcal{R}_z(\psi)$ symmetry ensures the existence of an angle degree of freedom, whose quantized motion represents quantal rotation. The

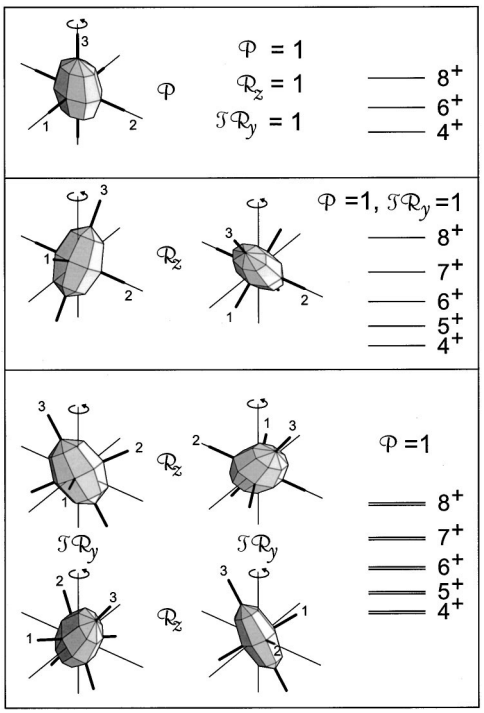

FIG. 9. Discrete symmetries of the mean field of a rotating triaxial reflection-symmetric nucleus (three symmetry planes). The mean field is represented by its density distribution. A polyhedron is used to make the symmetries better visible. The axis of rotation (z) is marked by the circular arrow. It coincides with the angular momentum $\vec{J}$. The figure illustrates the reorientation of the density distribution under the three symmetry operations that leave the two-body Routhian invariant. The structure of the rotational bands associated with each symmetry type is illustrated on the right side.

mean-field state $|\rangle$ is not invariant with respect to the rotation $\mathcal{R}_z(\psi)$ about the z axis, which is the direction of the angular momentum $\vec{J}=\langle\vec{J}\rangle$. The overlap $\langle\mathcal{R}_z(\psi)\rangle$ measures how strongly $\mathcal{R}_z(\psi)|\rangle$ differs from $|\rangle$, i.e., how well the state $|\rangle$ is oriented. Since H' is invariant with respect to $\mathcal{R}_z(\psi)$, all states $\mathcal{R}_z(\psi)|\rangle$ are degenerate solutions of the self-consistent cranking problem. The uniformly rotating wave packet $\mathcal{R}_z(\omega t)|\rangle$ is a solution of the corresponding time-dependent Hartree-Fock problem (see Sec. VIII.D). As in the case of a molecule, this classical motion can be quantized if $|\rangle$ is sufficiently well oriented, i.e., if the overlap $|\langle\mathcal{R}_z(\Delta\psi)\rangle|\ll 1$ for $\Delta\psi \ll 2\pi$. Semiclassical quantization of the rotational motion amounts to restricting the classical angular momentum J of the mean field to the discrete values $I+1/2$, where I is an integer or half integer for even or odd particle number, respectively (see Sec. VIII.C). Once the connection between the quantum number I and the mean-field value J is established, the interpretation of the experiment is straightforward. The canonical relations (25) between frequency and angular momentum are directly translated into Eqs. (2) and (4) for the experimental frequency and Routhian, which are discussed in Sec. I.D.

The heuristic concept of quantizing the classical rotational motion of the mean field has been justified in the framework of various many-body methods, a review of which can be found in the textbook by Blaizot and Ripka (1986), pp. 400 and 401. We shall return to it in Sec. VIII and Appendix A. Frauendorf and Meng (1997a) found for the model case of two particles coupled to an axial rotor that the semiclassical approximation works rather well.

2. Space inversion

For the main part of this review we shall assume that the mean field is reflection symmetric. Since the mean-field Routhian (12) is invariant with respect to space inversion (indicated by $\mathcal{P}=1$), the parity π is a good quantum number of the mean-field solutions,

$$\mathcal{P}|\rangle=\pi|\rangle. \tag{50}$$

Hence the rotational bands are characterized by a fixed parity π.

As indicated in Table II, there are five symmetry types. Three can be constructed by combining the angular momentum vector $\vec{J}$ with the deformed density distribution, which is reflection symmetric with respect to the three planes spanned by the principal axes. Figure 9 illustrates this case for the pairing-plus-quadrupole Routhian (8) the principal axes of the density distribution are those of the quadrupole tensor, which are introduced in Sec. II.C. Of course, the following discussion of the symmetries is not restricted to quadrupole deformations. It is valid for all shapes that have three symmetry planes (D_{2h} symmetry). We refer to them as the principal planes and to their intersections as the principal axes.

The symmetry operations $\mathcal{R}_z(\pi)$ and $\mathcal{TR}_y(\pi)$ are twofold. If the mean field is not symmetric with respect to one of them, there is for each self-consistent solution another one with the same energy, which is generated by the symmetry operation. This follows from the invariance of the two-body Routhian with respect to the symmetry operation. As a consequence, there will be two rotational bands with the same energy representing the linear combinations of the two mean-field solutions, which restore the broken symmetry.

3. Axis of rotation as a principal axis

The upper panel of Fig. 9 shows the case in which $\vec{J}$ has the direction of one of the principal axes. The mean-field Routhian h' is invariant with respect to $\mathcal{R}_z(\pi)$ and, as a consequence,

$$\mathcal{R}_z(\pi)|\rangle=e^{-i\alpha\pi}|\rangle, \tag{51}$$

where α is the signature exponent.[4] Since $\mathcal{R}_z(\pi)$ is a

[4]We use the notation introduced by Bengtsson and Frauendorf (1979b). Another convention, which follows Bohr and Mottelson (1975), uses the signature quantum number $r=e^{-i\alpha\pi}$. In order to avoid long-winded formulations we shall adopt the somewhat loose but common terminology calling α simply signature.

subgroup of the full rotational group, invariance of h' with respect to it leads to a selection rule for the total angular momentum,

$$I=\alpha+2n, \quad n=0,\pm1,\pm2,\ldots. \tag{52}$$

The relation between the total angular momentum and α follows directly from the decomposition of $|\rangle$ into states of good angular momentum $|I,M=I\rangle$

$$\mathcal{R}_z(\pi)|\rangle=\sum C_I\mathcal{R}_z(\pi)|I,M=I\rangle=e^{-iI\pi}|\rangle, \tag{53}$$

which implies by virtue of Eq. (51) that the sum contains only those values of I that obey the condition (52). Naturally such a wave packet is associated with a $\Delta I=2$ band according the selection rule (52).

Each quasiparticle configuration corresponds to a band of given parity and signature (π,α), i.e., to a sequence of states of given parity π and angular momentum I that changes in steps of 2, in accordance with Eq. (52). The configurations with different signatures have different energy. This is seen best if one connects the $\Delta I=2$ sequences of data points in a smooth way. As examples, Fig. 4 shows the two bands with $(\pi,\alpha)=(+,1/2)$ and $(+,-1/2)$, which originate from the Nilsson state [642][5] at $\omega=0$. In Fig. 5, they correspond to the configurations [A] and [B] with one quasineutron on the trajectories A or B.

The members of these $\Delta I=2$ bands are interconnected by fast $E2$ transitions. The γ lines in Fig. 2 and bands A and B in Fig. 1 are examples. The transitional quadrupole moment Q_{22}, which measures the asymmetry of the density distribution with respect to the rotational axis $\vec{J}$, can be considered as the order parameter. The large reduced transition probabilities $B(E2)$ between the members of $\Delta I=2$ sequences in well deformed nuclei are the direct experimental evidence for strong symmetry breaking of the considered type.

4. Axis of rotation in a principal plane

The middle panel of Fig. 9 shows the case in which the rotational axis $\vec{J}$ is tilted away from the principal axes but still lies in one of the three principal planes. This is always the case for axial shape. The mean-field Routhian is no longer invariant with respect to the rotation $\mathcal{R}_z(\pi)$. Since

$$\mathcal{R}_z(\pi)|\rangle\neq e^{-i\alpha\pi}|\rangle, \tag{54}$$

there is no restriction of I. The rotational bands correspond to sequences of states of all possible values of I and fixed parity π. If one plots experimental energies or Routhians of the states with $I=I_o+2n$ and $I=I_o+1+2n$ and connects them smoothly, the two $\Delta I=2$ sequences which combine to the $\Delta I=1$ band are degenerate. In this way, the expected doubling of the number of states due to the breaking of the $\mathcal{R}_z(\pi)$ symmetry shows up. The bands K1 and K2 in Figs. 1 and 4 are examples of this symmetry type. They should be compared with the bands A and B, for which the signature is conserved and the two $\Delta I=2$ sequences are well separated.

The members of the $\Delta I=1$ bands are linked by strong $E2$ transitions between the states I and $I-2$ as well as by $M1$ and $E2$ transitions between the states I and $I-1$. The latter are caused by the finite transitional magnetic moment μ_{11} and transitional quadrupole moment Q_{21}. Since both are equal to zero for $\mathcal{R}_z(\pi)$ symmetry, they may be considered as order parameters, measuring the tilt of the rotational axis or, equivalently, how strongly the $\mathcal{R}_z(\pi)$ symmetry is broken. Frauendorf (1993a) suggested calling the rotating mean-field solutions without $\mathcal{R}_z(\pi)$ symmetry ''tilted-axis cranking'' (TAC) states and the solutions with $\mathcal{R}_z(\pi)$ symmetry ''principal-axis cranking'' (PAC) states. Frauendorf and Meng (1997b), specified the notation by calling the symmetry type discussed in this subsection a ''planar'' TAC solution, because $\vec{J}$ and two principal axes lie in one of the principal planes.

5. Axis of rotation out of the principal planes

The lower panel of Fig. 9 displays the aplanar case when $\vec{J}$ does not lie in one of the principal planes. Then the mean-field Routhian h' is no longer invariant with respect to $\mathcal{T}R_y(\pi)$, because this operation leads to a new combination of $\vec{J}$ with the system of principal axes. The two combinations have opposite chirality. To see this, we first note that the angular momentum vector $\vec{J}$ selects three principal half axes (the ones with a positive projection on $\vec{J}$). Looking from the arrow head of $\vec{J}$ into this octant, we call the principal axes system right-handed if the short (1), intermediate (2), and long (3) axes are ordered counterclockwise (upper pair in Fig. 9) and left-handed if they are ordered clockwise (lower pair in Fig. 9). It is not possible to change the chirality by a rotation. Only the combination $\mathcal{T}R_y(\pi)$, which includes the time-reversal operation $\mathcal{T}$, reverses the chirality.

The breaking of the $\mathcal{T}R_y(\pi)$ symmetry causes a doubling of the rotational levels. There are two identical $\Delta I=1$ sequences with the same parity, which are the even and odd linear combinations of the left- and right-handed mean-field solutions. These linear combinations restore the broken $\mathcal{T}R_y(\pi)$ symmetry. The members of each band are connected by enhanced $E2$ and $M1$ transitions like the planar TAC solutions. The strength of the interband transitions is determined by the difference of the $M1$ and $E2$ matrix elements between the left- and right handed solutions (see Sec. III.C). Frauendorf and Meng (1997b) suggested calling solutions of this symmetry type either aplanar TAC solutions or simply chiral solutions.

[5]The labeling of the Nilsson states in a deformed axial potential is explained in standard textbooks like those of Bohr and Mottelson (1975) or Ring and Schuck (1980).

6. Other

Table II lists two more symmetries of the reflection-symmetric mean field, $\mathcal{R}_z(\pi)=1$ and $\mathcal{T}R_y(\pi)\neq 1$ and $\mathcal{R}_z(\pi)=\mathcal{T}R_y(\pi)\neq 1$. The first symmetry would show up as two identical $\Delta I=2$ bands of given parity and signature and the second as a $\Delta I=1$ band of given parity. Since we are not aware of any detailed study of these cases, we can make only a general remark. They cannot appear for a purely time-even mean field, like the density distribution in Fig. 9. An example of a mean-field component with the first mentioned symmetry is zp_z+p_zz, whereas xp_z+p_zx has the symmetry mentioned second.

III. COLLECTIVE ROTATION

In this section we shall discuss the familiar case of a nucleus with a substantial deformation. The anisotropy of the density distribution specifies the orientation of the nucleus and thus the rotational degree of freedom. A large part of the angular momentum is generated from small contributions of many particles, i.e., the rotation is collective. These statements will be quantified in Appendix A. The low-spin features of collective rotation are covered in nuclear physics textbooks, like those of Bohr and Mottelson (1975), and deShalit and Feshbach (1974).

A. Rotation about a principal axis

Let us start by assuming that the rotational axis coincides with one of the principal axes of the deformed density distribution. As discussed in Sec. II.F, the $\mathcal{R}_z(\pi)$ symmetry of these principal-axis cranking solutions implies that the signature α is a good quantum number. The signature quantum number was introduced in the textbook of Bohr and Mottelson (1975) in the context of the unified model. The $\mathcal{R}_z(\pi)$ symmetry was already pointed out in the first nonperturbative application of the self-consistent cranking model by Banerjee *et al.* (1973) and used to reduce the dimension of the eigenvalue problem (17). It is one of the cases Goodman (1975) treated in his systematic discussion of the symmetries of the rotating mean field. The selection rule (52) was first applied by Ring and Mang (1974) for cases with $\alpha\neq 0$ and discussed in a systematic way by Bengtsson and Frauendorf (1979b). Since this symmetry type has been covered in a number of reviews[6] we restrict ourselves to one illustrative example. We use the bands in ^{163}Er in order to explain some general features of the mean-field solutions, which we shall need later.

1. Bands as quasiparticle configurations

Figure 5 shows the quasineutron Routhians for $N\approx 96$. A collection of such quasiparticle diagrams for the rare-earth region can be found in Bengtsson *et al.* (1986).

The quasiparticle trajectories are classified by means of the parity and signature (π,α). The different rotational bands correspond to the various possibilities for occupying the quasiparticle levels. For a discussion of the high-spin case the double-dimensional occupation scheme is particularly instructive; this is explained in detail by Bengtsson and Frauendorf (1979b) and Bengtsson *et al.* (1986). In essence, when a quasiparticle level is occupied its conjugate partner must be free. The conjugate levels, which are labeled by crosses, are obtained by reflection on the line $E'=0$.

The vacuum configuration [0] has $(\pi,\alpha)=(0,0)$. It is the even-I ground-state rotational band of $^{164}_{66}\mathrm{Er}_{98}$. Exciting one quasineutron to the levels A or B generates the configurations [A] and [B] with $(\pi,\alpha)=(+,1/2)$ and $(+,-1/2)$, respectively, which represent bands with $I=1/2+2n$ and $I=-1/2+2n$ in $^{163}_{66}\mathrm{Er}_{97}$. In Figs. 1 and 4 they are denoted by A and B and by [642], respectively. The excitation of quasineutrons to the levels E and F generates the negative parity bands [523]. They are unstable against tilting the rotational axis and will be discussed below.

2. Band crossings

At $\omega=0.23$ MeV, the levels A and B^+ "quasicross," i.e., they exchange characters in the narrow region where they repel each other. The yrast configuration changes its character from the vacuum [0] to what was the two-quasineutron configuration [AB] before the quasicrossing. Such a rapid structural change is in conflict with the concept of a band. The appropriate point of view is to consider both configurations [0] and [AB] as two bands, which cross each other (an AB crossing). They are called the g and s bands.[7] The crossing is observed as a "back bending" (S shape) of the function $J(\omega)$ constructed from the yrast levels (Banerjee *et al.* 1973). The back bend is caused by the sudden alignment of the angular momentum of the two quasiparticles A and B with the 1 axis (Stephens and Simon, 1972). At given I, the frequency in the g band, $\omega=(I+1/2)/\mathcal{J}$, is larger than in the s band, $\omega=(I+1/2-j_{1,A}-j_{1,B})/\mathcal{J}$. This results in the the decrease of ω when the yrast levels change from the g to the s band.

The AB crossing appears in yrast lines of the even-N nuclei ^{162,164}Er. In Fig. 4, it is seen at the same frequency as the sudden increase in the negative slope of the bands [523] in ^{163}Er. The quasineutrons E and F are just spectators of the reaction of A and B to the inertial forces.

[6]See for example, Stephens, 1975; de Voigt *et al.*, 1983; Szymanski, 1983; Bengtsson and Garrett, 1984; Garrett *et al.*, 1986; Åberg *et al.*, 1990; Nilsson and Ragnarsson, 1995.

[7]The first acronym stands for ground-state band. When the back bending irregularity was discovered its nature was unclear, and the vague name superband was coined, which became s band with frequent use.

The configuration [A] is not disturbed by the AB crossing. It is "blocked" because both A and B^+ are occupied. The same holds for [B]. Bengtsson and Frauendorf (1997b) pointed out the appearance of characteristic frequencies of band crossings, which belong to one and the same crossing between two quasiparticle trajectories.

For a quantitative analysis of the band crossing it is useful to construct "diabatic" trajectories. These are the thin lines in Fig. 5 obtained by "switching off" the interaction, which causes the repulsion between A and B^+ near the crossing. In this way the problems near the crossing point are avoided. The SCC becomes a poor approximation there because the basic presumption that the dispersion in angular momentum (cf. Appendix A) depends weakly on ω is violated (Hamamoto, 1976; Marshalek and Goodman, 1978). Bengtsson and Frauendorf (1979a) suggested an analysis of experimental data based on the picture of two crossing bands. They relate the observed degree of band mixing with the calculated mixing between the quasiparticle configurations.

Let us return to Fig. 5. Instead of the well-pronounced AB crossing, only a very smooth up bending of the a and b trajectories occurs for other neutron numbers. The nuclei around $N=108$, which have recently been studied by Lee *et al.* (1997), are an example. In such a case it is more appropriate to interpret the bands as configurations of "adiabatic" trajectories, which are the quasiparticle Routhians $e_i'(\omega)$ in energetic order. The configuration [0] is the (perturbed) yrast band in the even-N system and [a] the yrast band in the odd-N neighbor. The structural changes become evident when the difference between the Routhians of the two neighbors is taken. This difference is given by the trajectory $e_a'(\omega)$. In the region where a and b are bending up, most of the angular momentum in [0] is generated by the alignment of the two quasineutrons (a^+ and b^+).

The AB crossing is just an example for the many quasicrossings between the quasiparticle Routhians $e_i'(\omega)$, for which either the diabatic or the adiabatic interpretation is more appropriate. Of course, there are intermediate cases where both the diabatic and adiabatic pictures are equally well (or badly) suited.

The shape of rapidly rotating nuclei is studied by mapping the total Routhian $E'(\beta,\gamma,\omega)$. Usually the cranked shell correction method is used to generate these maps. But the other versions of the SCC constraining the shape are also suited. The quasiparticle Routhians $e_i'(\beta,\gamma,\omega)$ cross each other as functions of the deformation parameters β and γ too. As with ω, there is a choice between adiabatic and diabatic configurations.

Following a configuration adiabatically generates the *total Routhian surface*, which represents the lowest value of $E'(\beta,\gamma,\omega)$ for a given combination of parity and signature (π,α). It is useful for a global survey of the shapes expected near the yrast line. Total Routhian surfaces have become quite popular for the interpretation of high-spin data. They can easily be generated by means of a public-domain computer code (Wyss, 1999). Calculating both $E'(\beta,\gamma,\omega)$ and $J(\beta,\gamma,\omega)$, the energy $E(\beta,\gamma,J)$ can be generated by interpolation. Extended collections of such total energy surfaces have been published by Werner and Dudek (1992, 1995). Figure 10 shows as an example $^{174}_{72}\mathrm{Hf}_{102}$ at $J=20$.

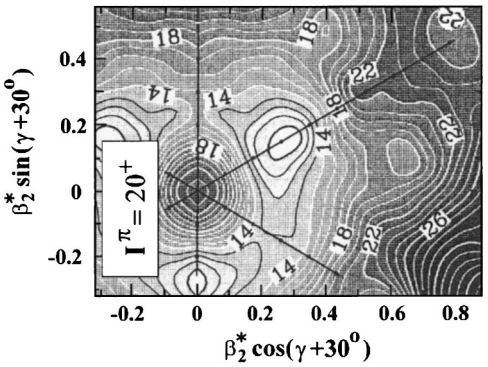

FIG. 10. Energy of $^{174}_{72}\mathrm{Hf}_{102}$ at $J=20$ as a function of the deformation parameters $\beta=\beta_2$ and γ. The y axis corresponds to $\gamma=60°$ and the x axis to $\gamma=-30°$. Axial shapes lie on the lines. They alternate between oblate and prolate, where the upper y axis is oblate. The three sectors in the β-γ plane represent the same sequence of shapes, where the upper sector corresponds to rotation about the short axis, the middle sector about the intermediate axis, and the lower sector about the long axis of the triaxial nucleus (cf. Table I). From Werner and Dudek, 1992.

If one wants to follow a band through crossings one must construct a diabatic quasiparticle configuration. Bengtsson and Ragnarsson (1985), Bengtsson *et al.* (1986), and Bengtsson (1989) described various methods. Bengtsson and Ragnarsson (1983,1985) and Afanasjev *et al.* (1999) implemented the interpolation technique into the cranked shell correction approach for principal-axis cranking solutions. They call this the *configuration-dependent cranked Nilsson-Strutinsky approach*. It has turned out to be particularly useful for the study of terminating bands in weakly deformed nuclei, which will be discussed in Sec. V. A public-domain computer code (ULTIMATE CRANKER) based on the techniques suggested by Bengtsson (1989) is available (Bengtsson and Bengtsson, 1999). The construction of diabatic trajectories has also turned out to be essential in the case of broken $\mathcal{R}_z(\pi)$ symmetry, to be discussed next (Frauendorf, 2000).

B. Rotation about a tilted axis

1. Appearance of tilted solutions

Conventionally it has been assumed that the axis of rotation coincides with a principal axis of the density distribution of the nucleus. Such a choice is consistent with the well-known result of classical mechanics that a rigid body rotates uniformly only about the long or short principal axis. In quantum mechanics this is reflected by the fact that the yrast states of a triaxial rigid quantal rotor correspond to rotation about the axis with the maximal moment of inertia. There is a zero-point precessional motion of the principal axes, whose amplitude decreases with the angular momentum (Bohr and Mot-

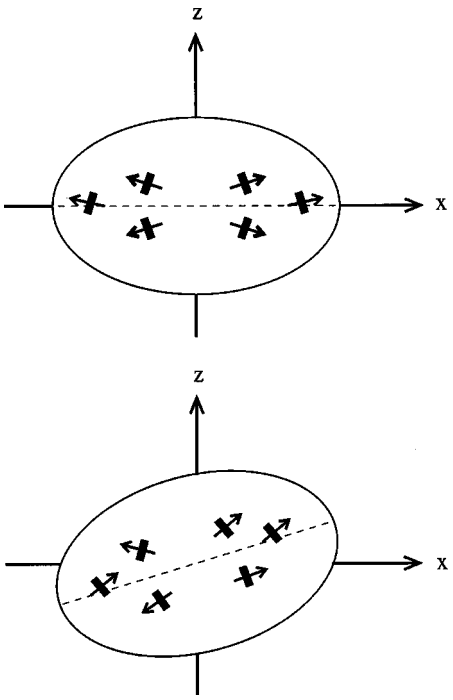

FIG. 11. A classical model of gyroscopes, which demonstrates the possibility of tilted rotation. The principal axis 3 is the dashed symmetry axis. The principal axis 1 lies perpendicular to it. In the upper panel, the gyroscopes are symmetrically arranged. The rotational axis z coincides with 1. In the lower panel, the asymmetric arrangement of the gyroscopes generates an angular momentum component along the 3 axis, which tilts the rotational axis z with respect to the body-fixed frame of the principal axes.

telson, 1975). However a classical body that is not rigid may also uniformly rotate about an axis different from the principal axes of its density distribution. This possibility was already pointed out by Riemann (1860) for an ellipsoidal self-gravitating fluid. The tilt of the rotational axis is due to an intrinsic vorticity of the system. In the case of the nucleus tilted rotation is due to the quantized angular momentum of the nucleonic orbitals. Figure 11 illustrates this by means of a classical model. It consists of a rigid piece of matter with embedded gyroscopes, which simulate the quantized angular momentum of some nucleonic orbitals. The rigid body is characterized by its three principal moments of inertia $\mathcal{J}_\mu$ and the well-known linear relation between the angular momentum $\vec{R}$ and the angular velocity $\vec{\omega}$,

$$R_\mu = \mathcal{J}_\mu \omega_\mu . \tag{55}$$

If the total angular momentum $\vec{J}$ consisted only of this part, uniform rotation would be possible only about the principal axes 1 and 3. However, the system is more complex because there are the gyroscopes, which contribute also to the total angular momentum $\vec{J}$. Assume that $\mathcal{J}_1$ is the maximal moment of inertia. In the upper panel, the gyroscopes are symmetrically distributed, and 1 and 3 remain the axes about which uniform rotation is possible. In the lower panel the gyroscopes are asymmetrically oriented, such that their angular momenta add to a finite component along the 3 axis. The axis of uniform rotation will be different from the principal axes.

The most familiar nuclear examples are the ''high-K bands.'' Consider a well-deformed prolate nucleus with some quasiparticles on orbitals that are strongly coupled to the deformed axial potential. They are the gyroscopes in Fig. 11. Without rotation, for each quasiparticle $j_{3,i} = K_i$, where K_i is quantized because $\hat{J}_3$ is conserved in the axial potential. Also, for finite rotational frequency, $j_{3,i} \approx K_i$ because, in contrast to a classical rotor, the variation of $j_{3,i}$ is strongly restricted by the quantization. The total projection is $J_3 \approx K = \Sigma K_i$. The contributions $j_{1,i}$ of all particles sum up to the collective angular momentum $\vec{R}$, which has a component R_1 on the principal axis 1 but none on the symmetry axis 3. Since the total angular momentum has components on the two principal axes 1 and 3, the rotational axis is tilted. The band starts with $I = K$ and $\vec{J}$ parallel to the 3 axis. The growth of total angular momentum is mainly due to the increase of R_1, while J_3 stays close to K. Hence the vector $\vec{J}$ turns gradually from the 3 to the 1 axis.

Of course, this is just the semiclassical version of the familiar picture of the high-K bands given by the unified model (Bohr and Mottelson, 1975). However, tilted-axis cranking leads further. If the frequency is high and/or the deformation is weak, the component J_3 changes substantially with ω. Titled-axis cranking describes this reorientation. It permits the study of more complex couplings like a combination of high-K quasiparticles with other high-j quasiparticles, which prefer orientations different from the symmetry axis. It is particularly useful for analyzing multi-quasiparticle $\Delta I = 1$ bands in triaxial nuclei, for which K_i is never a good quantum number.

Kerman and Onishi (1981) first pointed out the possibility of uniform rotation about a nonprincipal axis. Frisk and Bengtsson (1987) constructed such solutions for realistic nuclei. Their pioneering work suffered from two shortcomings: (i) They could not give the physical interpretation of the TAC solutions; (ii) They assumed a fixed shape of the nucleus. It was unclear whether taking into account the self-consistency with respect to the shape degrees of freedom would result in rotation about a principal axis. In fact, the investigations of the rotating harmonic oscillator by Cuypers (1987) and a few-level model by Nazarewicz and Szymański (1992) seemed to support the latter view. Frauendorf (1993a) found the first fully self-consistent TAC solutions. His interpretation of the solutions as $\Delta I = 1$ rotational bands made possible a simple analysis of the experiment. Since then, tilted-axis cranking has been used to describe the energies and transition probabilities of various well deformed nuclei: $^{163}_{66}\mathrm{Er}_{97}$ (Brockstedt *et al.*, 1994), $^{164}_{67}\mathrm{Tm}_{97}$ (Reviol *et al.*, 1999), $^{168}_{70}\mathrm{Yb}_{98}$ (Oliveira *et al.*, 1994), $^{178,179}_{74}\mathrm{W}_{104,105}$ (Frauendorf *et al.*, 1994, 2000), $^{181}_{77}\mathrm{Re}_{104}$ (Pearson *et al.*, 1997) and $^{180,182}_{76}\mathrm{Os}_{104,106}$ (Horibata and Onishi, 1994a, 1994b; Lieder *et al.*, 1999). Frauendorf (2000) used the multi-quasiparticle bands in $^{174,175}_{72}\mathrm{Hf}_{102,103}$, $^{175}_{73}\mathrm{Ta}_{102}$, and $^{174}_{71}\mathrm{Lu}_{103}$ as examples to

present the technical details of the TAC calculations. The work on weakly and moderately deformed nuclei is reviewed in Sec. IV.

Marshalek (1987, 1991, 1993) studied tilted rotation generated by superpositions of collective vibrations. Alhassid and Bush (1991), Goodman (1992a, 1992b), and Dodaro and Goodman (1994, 1996) included the tilt of the rotational axis in their analysis of nuclei at nonzero temperature. Goodman (1992a, 1992b) calculated the response of particles in a j-shell to tilted rotation. A recent reinvestigation of the rotating harmonic oscillator by Heiss and Nazmitdinov (1997) claimed the existence of TAC solutions within this model, in contrast to Cuypers (1987). Sheikh (1995) studied the existence of tilted solutions by diagonalizing a cranked shell model Hamiltonian with δ interaction in a single shell.

The self-consistent cranking model always has solutions of the PAC type, for which the laboratory and the intrinsic frames coincide. This is a special case of a general theorem (Ring and Schuck, 1980; Blaizot and Ripka, 1986): if a self-consistent solution spontaneously breaks a symmetry there exist other self-consistent solutions at higher energy which obey this symmetry. Applied to the our case this means: If a solution of the TAC type is the absolute minimum of the energy surface $E'(\omega,q_\mu)$, there are also PAC solutions representing maxima, saddle points, or excited minima. The fact that PAC solutions always satisfy the self-consistency conditions was the reason that the existence of tilted solutions was overlooked for a long time.

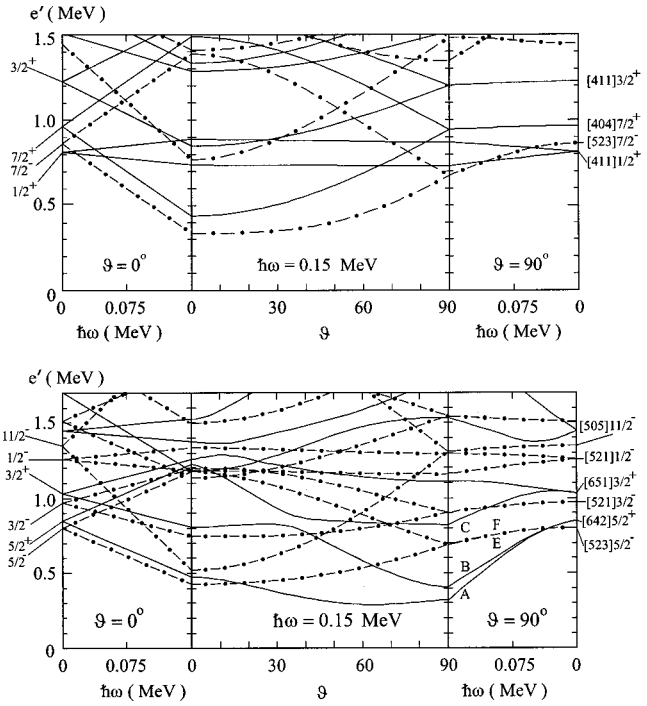

FIG. 12. Quasiproton Routhians for $Z\approx 66$ (upper panel) and quasineutron Routhians for $N\approx 97$ (lower panel) as functions of the tilt angle ϑ at the frequency $\omega=0.15$ (center section of each panel). The variation with ω is shown in the left-hand sections for $\vartheta=0°$ and in the right-hand sections for $\vartheta=90°$. Solid lines, positive parity; dash-dotted lines, negative parity. The parameters are $\varepsilon=0.252$, $\gamma=0°$, $\varepsilon_4=-0.004$, $\Delta_p=0.87$ MeV, $\Delta_n=0.80$ MeV. From Brockstedt *et al.*, 1994.

2. Axial solutions

Planar TAC solutions show up as $\Delta I=1$ bands. The $E2$ transitions between states with I and $I\pm 1$ are strong, because the charge distribution is asymmetric with respect to the tilted axis of rotation. The stretched $M1$ transitions are enhanced, because the transverse magnetic moments of the different quasiparticles add up. The $B(M1)$ values need not be large in all cases, because the transverse magnetic moments of the contributing quasiparticles can have different signs. For PAC solutions, both types of transitions can only be of the order of single-particle transitions, because they connect different quasi-particle configurations.

The most common type of planar TAC solution is found in axially deformed nuclei. The collective angular momentum is directed along the 1 axis and there are quasiparticles aligned with the 3 axis. Some quasiparticles may also align their angular momentum with the 1 axis. At higher frequency, the quasiparticle angular momentum will tend to dealign from the principal axes towards the direction of the rotational axis $\vec{J}$. It may be substantially tilted into the 1-3 plane if the quasiparticles are weakly coupled to the deformed potential.

The appearance of the tilt may be seen as a nuclear Jahn-Teller effect. The Jahn-Teller effect is described in textbooks on molecular physics, for example by Bersuker (1984) and Streitwieser *et al.* (1985). Molecules tend to break away from a certain point-group symmetry when a multiplet of electronic states belonging to a representation of the group is only partially filled. The degenerate multiplet splits as a function of the distortion parameter. A plot of the electronic states as a function of the distortion parameter is called a correlation diagram. Since only the lower levels of the multiplet are occupied, the distortion results in an energy gain. Figure 12 is analogous to a molecular correlation diagram, where the tilt ϑ angle plays the role of the distortion parameter. At $\vartheta=90°$ the pair of quasiparticle states E and F is nearly degenerate. They are the two eigenstates of $\mathcal{R}_z(\pi)$, which generates the point group C_2 (signature quantum number). If in an odd-N nucleus the trajectory E is occupied, a finite distortion $\vartheta<90°$ lowers the energy by breaking the C_2 symmetry (cf. the examples in Sec. III.B.4).

Reinhard and Otten (1984) and Nazarewicz (1994) invoked the Jahn-Teller effect in order to explain the appearance of nuclear deformation, i.e., the breaking of the spherical symmetry. Earlier discussions by Brack *et al.* (1972) and in the textbooks of Bohr and Mottelson (1975) and Ring and Schuck (1980), which did not point out this analogy, described the deformation mechanism along similar lines. As compared to the classical molecular Jahn-Teller effect there are two new aspects. (i) Nuclear deformation appears as the consequence of the simultaneous splitting of several multiplets of given angular momentum j, which form a major shell. By occu-

pying the lowest of these levels, which fan apart, the high density of states near the Fermi level in a partially filled spherical shell is avoided. (ii) The deformation parameter reaches equilibrium where the nucleonic levels rearrange such that their density near the Fermi level is low ("deformed shells," Brack *et al.*, 1972).

This nuclear Jahn-Teller mechanism works for the tilt angle as well. If there are several states with large K_i near the Fermi surface, the nucleus will reduce the level density by tilting the rotational axis. As an example, see Fig. 8. For $N=106$, compare the level densities at $\vartheta=90°$ and 50°. Additional diagrams for the rare earth region were given by Frauendorf (2000). They show low level density for $\vartheta<45°$ around $Z=72$ and $N=106$. The yrast region of these nuclei is dominated by the high-K bands, which cause the well-known K isomerism. There are other regions of low level density in Fig. 8 that are preferred by the orientation of the rotational axis. A systematic survey of the single-particle level density as a function of the orientation and deformation degrees of freedom does not exist.

The PAC energy surfaces are a useful guide to regions that are favorable for tilted solutions, because they permit a comparison of the energy at $\vartheta=90°$ and 0°. As an example, Fig. 10 shows the energy surface $E(\beta,\gamma,J=20)$ for $^{174}_{72}\mathrm{Hf}_{102}$. The shape is well-deformed prolate. The two minima at $\gamma=0°$ and $-120°$ correspond, respectively, to $\vartheta=90°$ (collective rotation) and $\vartheta=0°$ (generation of angular momentum along the symmetry axis by particle-hole excitations). Since they have comparable depth, it takes about the same energy to generate 20 $\hbar$ of angular momentum along either of the two axes. Hence it should not cost much energy to transfer some angular momentum from one to the other axis, i.e., to tilt the rotational axis. The TAC calculation in Fig. 13 confirms this expectation. There are many rotational bands in this nucleus resulting from the redistribution of angular momentum between the 1 and 3 axes. Frauendorf (2000) analyzed this wealth of bands with different orientation in ^{174}Hf and its neighbors.

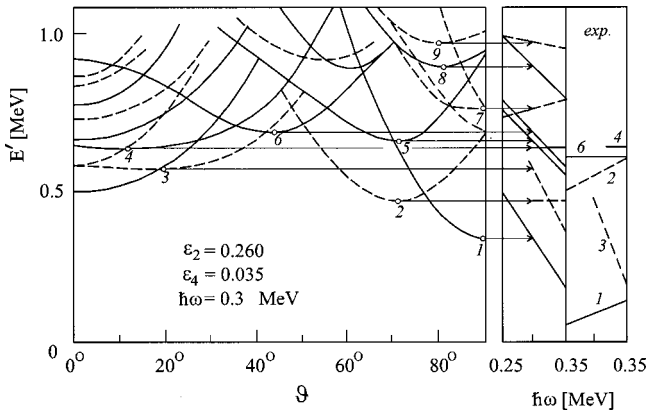

FIG. 13. Total Routhians of $^{174}_{72}\mathrm{Hf}_{102}$ as functions of the tilt angle ϑ (left) and as functions of the frequency ω (right): solid lines, positive parity; dashed lines, negative parity. The energy zero is chosen such that band 4 agrees with the experiment. All slopes in the right part are reduced by 16 $\hbar$. Rounding J_3 to the next integer K, the different bands have $\pi K^{\pi}\nu K^{\pi}$: 1: 0^+0^+, 2: 0^+6^-, 3: 8^-12^+, 4: 8^-10^-, 5: 0^+7^+, 6: 8^-6^+, 7: 0^+0^-, 8: 0^+3^-, and 9: 0^+3^-. All configurations are calculated assuming zero pairing, except 0^+, for which Δ is equal to 80% of the experimental even-odd mass difference. Note the bandheads of 3 and 4. From Frauendorf and May, 1992. Data from Gjørup *et al.*, 1995.

3. Change of symmetry

Along a band, the orientation and shape change with the frequency ω. As a consequence, the symmetries of the mean field may alter. It may become rotational symmetric with respect to $\vec{J}$. Then the band stops. If this happens with decreasing ω the band head is encountered, where the band starts. This possibility is discussed below. If the $\mathcal{R}_z(\psi)$ symmetry is reached with increasing ω, one speaks of *band termination*. This phenomenon will be dealt with in Sec. V. The transition from broken to restored $\mathcal{R}_z(\pi)$ symmetry is a quite common feature of the well deformed axial nuclei. Since the collective part of the angular momentum grows along the bands, the tilt angle ϑ increases and eventually reaches 90°, where $\vec{J}$ has the direction of the 1 axis. The mean-field approximation is good only for a discrete symmetry being well broken or well conserved. It is not able to describe the smooth transition from one to the other symmetry type, which is observed in a finite fermion system like the nucleus. Frauendorf and Meng (1997a) discussed the limitations and the interpretation of the mean field solutions when the $\mathcal{R}_z(\pi)$ symmetry is restored with increasing frequency. They studied the model case of two particles coupled to an axial rotor. Frauendorf (2000) further analyzed these problems.

Let us now discuss the band head. We begin with the familiar case of strong coupling of the quasiparticles to the deformed field. The tilt angle ϑ is given by Eq. (46). The condition $\cos\vartheta\leqslant 1$ is equivalent with the familiar restriction $J\geqslant K$ for the angular momentum. The band head lies at the frequency of $\omega_h=K/\mathcal{J}$. The numerical TAC solutions describe the start of $K>0$ bands in axial nuclei in a similar way. Below a certain finite frequency ω_h, the Routhian $E'(\omega,\vartheta)$ has its minimum at $\vartheta=0°$. At $\omega=\omega_h$ the minimum branches away from the symmetry axis, where a maximum appears. Figure 13 shows bands in different stages of development. There are several minima at $\vartheta=0°$, which represent bands that have not yet started. Bands 3 and 4 have just started, because curvature of $E'(\omega,\vartheta)$ near $\vartheta=0$ is close to zero. Bands 2, 5, and 6 have started earlier ($\omega_h<0.2$ MeV), because they have a maximum at $\vartheta=0$.

The reorientation of $\vec{J}$ from the symmetry axis towards the 1 axis is shown in Fig. 14 for the band K1 in ^{163}Er. It is the consequence of the increasing collective angular momentum along the 1 axis. If quasiparticles are involved which easily align their angular momentum with the 1 axis the tilt angle ϑ does not branch from zero, as in Fig. 14, but rather jumps to a large value at the bandhead. Examples are discussed by Frauendorf (1993a, 2000).

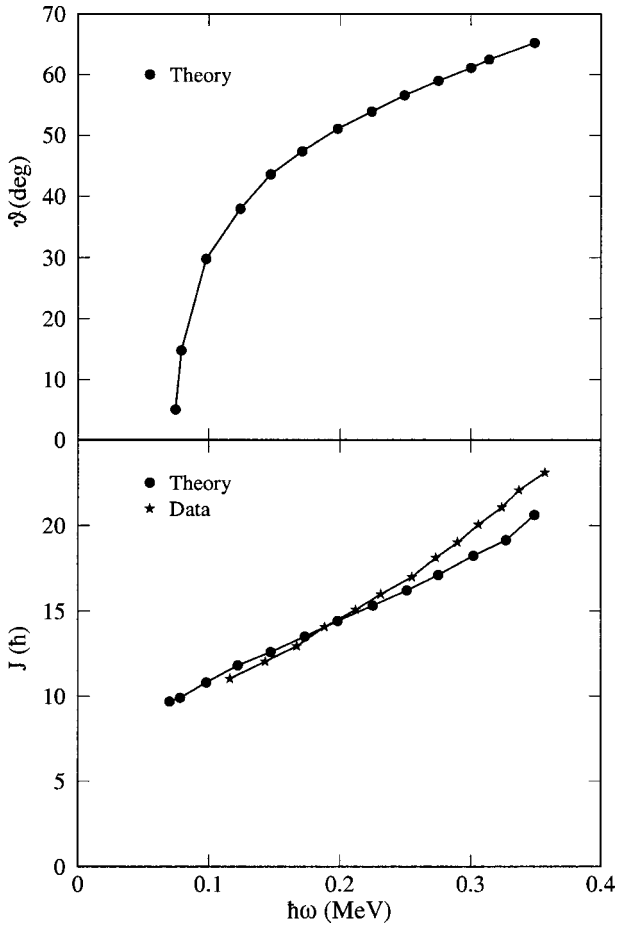

FIG. 14. The tilt angle ϑ (upper panel) and the total angular momentum (lower panel) as functions of the frequency ω for the band K1 in ^{163}Er. The parameters of the TAC calculation are given in Fig. 12. From Brockstedt *et al.*, 1994.

Now let us consider the transition from TAC to PAC solutions at $\vartheta \rightarrow 90°$. The problems accompanying this change of discrete symmetry are explained by means of Fig. 12. Assume that the shallow minimum of A around 60° is substantially deeper, such that there is a solution with $\vartheta < 90°$ for the configuration [A]. This TAC solution is interpreted as a $\Delta I = 1$ band, i.e., there is no splitting between the two signatures. At a higher frequency, ϑ reaches 90°. Now the PAC configuration [A] is interpreted as the positive-signature sequence $I = 1/2 + 2n$ and PAC configuration [B] as the negative-signature sequence $I = -1/2 + 2n$ (cf. Sec. III.A). Hence the energy of the negative-signature branch jumps from E'_A to E'_B when changing from the TAC to the PAC interpretation. This discontinuity is an inevitable consequence of the mean-field approximation, which demands different interpretations of solutions with different discrete symmetries.

The configuration [B] must be discarded as a spurious state when the TAC interpretation is applied for $\vartheta < 90°$. Otherwise the number of states would double when changing from PAC to TAC. For the discussed one-quasiparticle configurations the elimination of the spurious state is quite obvious. It becomes more involved for a larger number of excited quasiparticles. Frauendorf and Meng (1997a) and Frauendorf (2000) have formulated the rules for eliminating the spurious states. The guiding principle is that the number of bands in the TAC interpretation must be the same as in the PAC.

4. Examples

Let us continue to use $^{163}_{66}\mathrm{Er}_{97}$ as an illustrative example. Figure 12 shows the quasiparticle levels as functions of the tilt angle ϑ. Such diagrams permit a rough estimate of the equilibrium angle by adding the quasiparticle Routhians $e'_i(\omega, \vartheta)$ to the vacuum Routhian and looking for the minimum of the sum with respect to ϑ. The vacuum behaves like a collective rotor. If we consider an axial nucleus, it has only the component $R_1 \approx \omega \mathcal{J} \sin \vartheta$ perpendicular to the symmetry axis and its Routhian is $E'_0 \approx -(\omega \sin \vartheta)^2 \mathcal{J}/2$.

The quasineutron levels E and F emanating from the Nilsson state $[523]5/2^-$ are strongly coupled to the deformed potential. They have $j_3 \approx \pm 5/2$ and $j_1 \approx 0$. This is reflected by the ϑ dependence, which is close to $\mp 5/2\omega \cos \vartheta$. An occupied E results in an equilibrium angle $\vartheta < 90°$. As expected for a TAC solution, the band [E] appears as a $\Delta I = 1$ sequence in Fig. 4. Further examples of strong coupling to the deformed potential are the quasineutron level $[505]11/2^-$ and the quasiproton levels $[404]7/2^+$ and $[523]7/2^-$, which are all seen as $\Delta I = 1$ bands.

The Routhian of the quasiproton level $[411]1/2^+$, which is a pseudospin-singlet state (see Sec. VII.D), does not change with ϑ (cf. Sec. II.D). The vacuum Routhian keeps $\vec{J}$ parallel to the 1 axis, and the solution is of the PAC type. Two well separated $\Delta I = 2$ sequences, which correspond to the signatures $\alpha = \pm 1/2$ of the orbital $[411]1/2^+$, are observed in the odd-Z neighbors.

The quasineutron levels A and B emanating from $[642]5/2^+$ are situated in the lower part of the $i_{13/2}$ shell. They show a more complex behavior. The upper level B has its minimum at $\vartheta = 90°$, because high-j particles at the bottom of the shell tend to orient their angular momentum perpendicular to the symmetry axis. The lower level A has a very shallow minimum at $\vartheta \approx 60°$. This quasineutron is only weakly coupled to the deformed potential, because its quadrupole moment is strongly reduced by the pair correlations (it is half particle and half hole). Both [A] and [B] are PAC solutions with $\vartheta = 90°$, which have been discussed in Sec. III.A.

The band K1 is assigned to the three quasiparticle configuration $[\pi 7/2^+, \pi 7/2^-, \nu 5/2^+]$, where each of the quasiprotons occupies the lower of the two branches emanating at $\vartheta = 90°$ in Fig. 12 and the quasineutron occupies the A branch. The angle $\vartheta(\omega)$, shown in Fig. 14, grows as a consequence of the increasing collective angular momentum, but remains below 90°. Accordingly, band K1 is observed as a $\Delta I = 1$ sequence. The composition of the total angular momentum is displayed in Fig. 15.

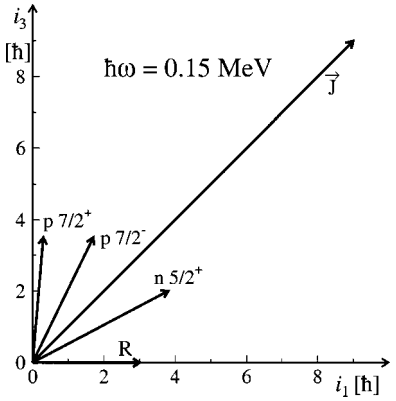

FIG. 15. The angular momentum composition of the three quasiparticle configuration K1 in ^{163}Er at the frequency $\omega = 0.15$ MeV. The collective angular momentum is denoted by R. From Brockstedt *et al.*, 1994.

Figure 14 compares the experimental function $J(\omega)$ of band K1 with the TAC calculation. Figure 4 includes the Routhians calculated by means of TAC for two values of the frequency ω. The agreement between theory and experiment is typical for the other TAC calculations in well deformed nuclei. Tilted-axis cranking is found to be able to account for the experimental ratios $B(M1)/B(E2)$. Discrepancies can be traced back to general problems of the mean-field theories to reproduce the g-factors of the involved quasiparticles with sufficient accuracy.

Now we are going to consider a phenomenon that appears higher up in the neutron shell. Figure 7 shows the quasineutron Routhians near $N=106$. The behavior of the $i_{13/2}$ orbits (solid lines) has changed as compared with the $N=96$ region shown in Fig. 12. The orbit A prefers small values of ϑ, because it already has hole character. It has the angular momentum components $j_1 > 0$ and $j_3 > 0$. For B, the component j_1 is similar to that one of A, but $j_3 < 0$. With decreasing ϑ, B crosses with C, which has $j_3 > 0$. This crossing becomes smeared out at higher values of ω. Hence the configuration with the two lowest $i_{13/2}$ orbits occupied has two minima, which differ by a flip of the j_3 component of the second $i_{13/2}$ quasineutron. Their angular momentum composition is illustrated in Fig. 16, where the reader should disregard the quasineutron E for the moment. The first minimum represents the s band, the second the t band.[8] As illustrated in Fig. 16, the back-bending irregularity of the yrast band in ^{179}W is caused by the encounter of the g band with these *two* configurations, both of which have a large alignment j_1. The experimental points illustrate how the g band (solid circles) is crossed by the t band (open circles), which becomes yrast. At slightly higher frequency the g band turns over because it quasicrosses with the s band.

[8]The name alludes to two characteristics: The t band is similar to the s band (large j_1) but tilted (large j_3).

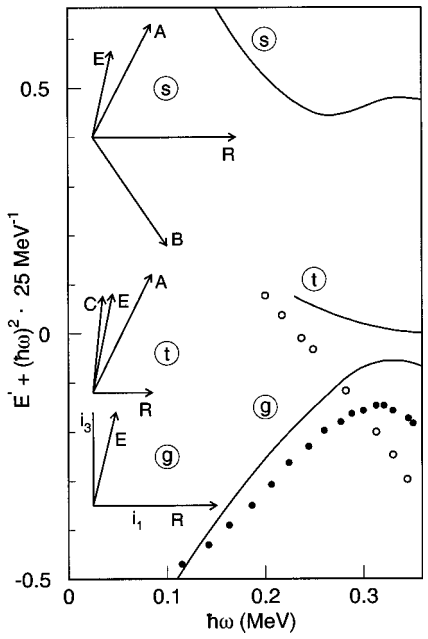

FIG. 16. Total Routhians of the g, s, and t configurations combined with the $[514]7/2^-$ (E) quasineutron in ^{179}W. The insets demonstrate the composition of the angular momentum in the three configurations. The quasiparticles are labeled by the same letters as in Fig. 7, which shows the occupations. The collective angular momentum is denoted by R. The experimental Routhians (Walker *et al.*, 1991) are shown as dots. From Frauendorf, 1993a.

Walker *et al.* (1991, 1994) first observed the coexistence of the s and the t configurations in $^{179}_{74}W_{105}$, where they are combined with an odd quasineutron $[514]7/2^-$. Frauendorf (1993a) gave the interpretation in the framework of TAC, illustrated in Fig. 16, where E is the additional odd quasineutron. Kutsarova *et al.* (1992, 1995) found an analogous structure in $^{181}_{76}Os_{105}$ and Pearson *et al.* (1997) a combination with the odd quasiprotons $[514]9/2^-$ and $[402]5/2^+$ in $^{181}_{77}Re_{104}$. Kutsarova *et al.* (1992, 1995) observed the pure s and t bands in ^{182}Os while Walker *et al.* (1993) observed them in ^{180}W. Horibata and Onishi (1994a, 1994b) demonstrated the coexistence of the s and t configurations in a TAC calculation for $^{182}_{74}Os_{106}$.

In the case of even-even nuclei the TAC interpetation becomes problematic. The s band, which is located at $\vartheta = 90°$, has a good signature of $\alpha = 0$, i.e., even I. The t band, which is located at $\vartheta \ll 90°$, is a $\Delta I = 1$ band. There is no problem at low frequency, where the g, t, and s configurations are well separated. For $\omega > 0.3$ MeV the three configurations meet each other and mix. Since the g and s bands have signature $\alpha = 0$, they can only mix with the even-I levels of the t band. The odd-I levels are not affected. The two signatures, of the t band are no longer degenerate, because the mixing shifts $\alpha = 0$ levels but not these for $\alpha = 1$. A dynamical description of the orientation degrees of freedom by Oi *et al.* (2000), which solves the problem, will be discussed in Sec. VIII.E. The presence of an odd quasiparticle keeps both the t band

and the g and s bands at a finite tilt. That is why tilted-axis cranking works well for these cases.

5. Planar triaxial solutions

The properties of planar solutions in triaxial nuclei have not been studied in any detail so far, although their quantitative description is within the realm of the TAC approach. Only Lieder *et al.* (1999) have discussed TAC solutions with a moderate triaxiality in ^{180}Os.

Since the the $\mathcal{R}_z(\pi)$ symmetry is broken, triaxial planar TAC solutions are observed as $\Delta I=1$ bands. One important difference from axial nuclei is that the moments of inertia of all three principal axes are finite. The vanishing moment of inertia of the symmetry axis has the consequence that the axial high-K bands start at a substantial frequency (see Sec. III.B.3). In triaxial nuclei, the $\Delta I=1$ bands may extend to low frequencies.

In axial nuclei the angle ϑ increases with ω because the collective angular momentum is perpendicular to the symmetry axis. This may lead to a transition from broken to restored $\mathcal{R}_z(\pi)$ symmetry (i.e., signature splitting) when ϑ approaches 90°. In triaxial nuclei there is also the possibility of a transition from conserved to broken $\mathcal{R}_z(\pi)$ symmetry with *increasing* frequency. In order to see this, let us assume that some quasiparticles align their angular momentum with the long (or the short) axis and that the intermediate axis has the largest moment of inertia. If $\vec{R}$ aligns with the quasiparticle angular momentum the $\mathcal{R}_z(\pi)$ symmetry is not broken and the energy gain due to the cranking term $-\vec{\omega}\cdot\vec{J}$ is maximal. If $\vec{R}$ has the direction of the intermediate axis one has a planar TAC solution and the energy of the collective rotation is minimal. The balance of these two energies decides the symmetry. Since the cranking term is linear and the collective rotational energy quadratic, the former should dominate at low and the latter at high ω.

As an example, panel (a) of Fig. 17 shows the case of two high-j holes coupled to a triaxial rotor (Frauendorf and Meng, 1997b). Their angular momentum is aligned with the long (3) axis. At low frequency $\vec{J}$ has the same direction. The configuration represents the lowest $\Delta I=2$ band. There is another $\Delta I=2$ band with the opposite signature, corresponds to a precessional motion of the holes. For larger frequency, the collective angular momentum prefers the intermediate (2) axis with the largest moment of inertia and $\vec{J}$ moves into the 2-3 plane. The breaking of the $\mathcal{R}_z(\pi)$ symmetry manifests itself as the merging of the two signature branches into a $\Delta I=1$ band.

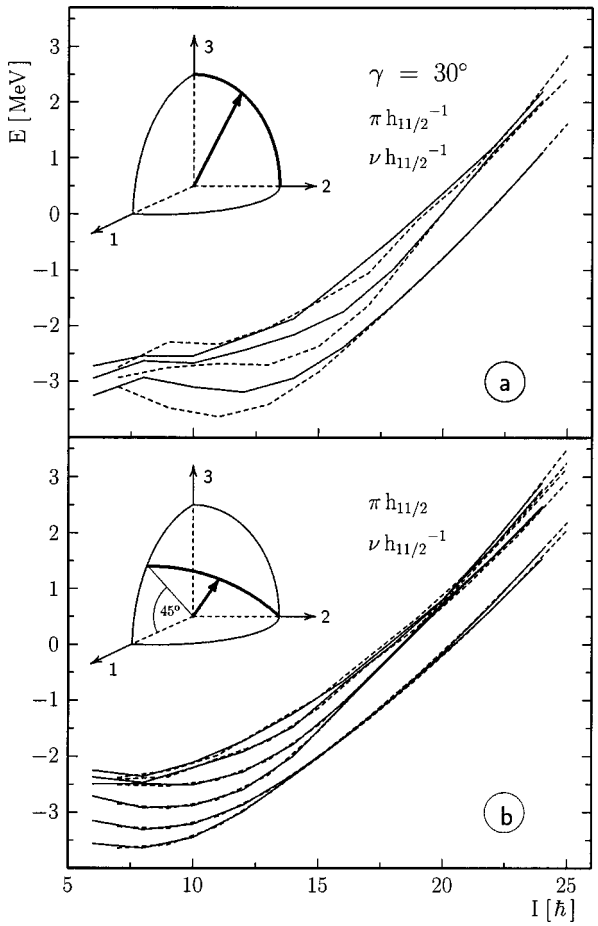

FIG. 17. Rotational levels of $h_{11/2}$ particles and holes coupled to a triaxial rotor with $\gamma=30°$. The upper panel shows the combination of a proton hole and a neutron hole. The combination of a proton particle with a neutron particle, which is obtained by swapping the axes 1 and 3, has the same energies. The lower panel shows the case of a proton particle combined with a neutron hole. Solid lines, $\alpha=0$ (even I); dashed lines, $\alpha=1$ (odd I). The insets show the orientation of the angular momentum with respect to the triaxial potential, where 1, 2, and 3 correspond to the short, intermediate, and long principal axes, respectively. The angular momentum vector moves along the heavy arcs. The position displayed in the lower panel corresponds to the spin interval $13<I<18$, where the two lowest bands are nearly degenerate. The right-handed position is shown. The left-handed is obtained by reflection through the 1-3 plane. From Frauendorf and Meng, 1997b.

C. Chiral rotation

If the angular momentum does not lie in one of the three principal planes of a triaxial nucleus the combination of the three different principal axes with $\vec{J}$ becomes chiral (see Sec. II.F). There are the left-handed $|l\rangle$ and right-handed $|r\rangle$ mean-field solutions, which are related to each other by

$$|l\rangle=\mathcal{TR}_y(\pi)|r\rangle. \tag{56}$$

In the ideal case of strongly broken $\mathcal{TR}_y(\pi)$ symmetry, the matrix elements $\langle l|Q_{22}|r\rangle$, $\langle l|Q_{21}|r\rangle$, and $\langle l|\mu_{11}|r\rangle$ are small because the electromagnetic field does not provide enough angular momentum to turn the long vector $\vec{J}$ from a left- or right-handed position. In order to calculate the transition matrix elements for this ideal case one must take into account that the exact states of the two bands have good $\mathcal{TR}_y(\pi)$ symmetry. One may choose the phases such that

$$\mathcal{TR}_y(\pi)|IM\pm\rangle=|IM\pm\rangle \tag{57}$$

when acting on states $|IM\pm\rangle$ of good angular momentum, which describe the two degenerate bands (see Bohr and Mottelson, 1969). The linear combinations

$$|+\rangle=\frac{1}{\sqrt{2}}(|r\rangle+|l\rangle),\quad |-\rangle=\frac{i}{\sqrt{2}}(|r\rangle-|l\rangle) \tag{58}$$

fulfill the relation (57), i.e., they restore the broken symmetry. Thus for $E2$ transitions one has instead of Eq. (34)

$$B(E2,I\pm\rightarrow I-2\pm)=\frac{5}{8\pi}|\langle r|Q_{22}|r\rangle+\langle l|Q_{22}|l\rangle|^2, \tag{59}$$

$$B(E2,I\pm\rightarrow I-2\mp)=\frac{5}{8\pi}|\langle r|Q_{22}|r\rangle-\langle l|Q_{22}|l\rangle|^2. \tag{60}$$

Equations (35) and (36) are modified in the same way (Dimitirov *et al.*, 2000a).

The $\mathcal{TR}_y(\pi)$ symmetry is broken if the angular momentum has components on all three principal axes. Frisk and Bengtsson (1987) suggested one possibility. High-j particles of one kind of nucleon and high-j holes of the other kind couple with the triaxial deformed potential. The particles tend to align their angular momentum with the short axis and the holes with the long axis, because these orientations maximize the overlap of their density distributions with the potential (cf. Sec. II.D). The collective angular momentum $\vec{R}$ provides the third component along the intermediate axis.

Frauendorf and Meng (1997a, 1997b) studied the above described physical situation for the model case of a high-j particle and a high-j hole coupled to a triaxial rotor with ratios $\mathcal{J}_i=4\mathcal{J}_s=4\mathcal{J}_l$ between the moments of inertia. The results of a numerical diagonalization were compared with an approximation that corresponds to the mean-field description within the model. As shown in panel (b) of Fig. 17, the angular momentum $\vec{J}$ moves out of the 1-3 plane through the chiral region towards the 2 axis. Accordingly the symmetry changes from $\mathcal{R}_z\neq 1$, $\mathcal{TR}_y=1$ to $\mathcal{R}_z\neq 1$, $\mathcal{TR}_y\neq 1$ and then to $\mathcal{R}_z=1$, $\mathcal{TR}_y=1$. The figure also demonstrates how the rotational levels reflect the smooth transitions between the symmetry types. Consider the lowest band. At the bandhead, only the particle and the hole generate the angular momentum, which lies in the 1-3 plane at the angle of $\vartheta=45°$. At low frequency, $\vec{R}$ aligns with the angular momentum of the particle and hole, because this orientation minimizes the cranking term $-\vec{\omega}\cdot\vec{J}$. This is the lowest $\Delta I=1$ band. The first excited $\Delta I=1$ band corresponds to a precessional motion around the axis $\vartheta=45°$. For larger values of ω it is energetically favorable for $\vec{R}$ to take the direction of the intermediate axis, because the moment of inertia is larger. The vector $\vec{J}$ moves out of the 1-3 plane towards the 2 axis. The $\mathcal{TR}_y(\pi)$ symmetry is broken by this aplanar angular momentum geometry. The symmetry breaking manifests itself as the merging of the two lowest bands into the doublet $\Delta I=1$ bands, which are the superpositions (58) of the two opposite chiralities.

Petrache *et al.* (1996) observed in $^{134}_{59}Pr_{75}$ a $\Delta I=1$ band which is merged with another band of the same parity. The configuration was assigned to the combination of a $h_{11/2}$ quasiproton with a $h_{11/2}$ quasineutron which have, respectively, particle and hole character. The levels with $I=14-17$ are very close in energy. Frauendorf and Meng (1997b) suggested that within this limited spin range the pair of bands may have the character of a chiral doublet. They left open the questions whether the suggested configuration in ^{134}Pr has a triaxial equilibrium shape and whether the microscopic moments of inertia are such that a chiral solution appears.

Dimitrov *et al.* (2000a) carried out aplanar TAC calculations based on the shell correction method. They found a stable triaxial deformation of $\varepsilon\approx 0.19$ and $\gamma\approx 30°$. Within the interval $13<I<16$ the angular momentum vector $\vec{J}$ moves out of the 1-3 plane on a trajectory that is similar to the one shown in Fig. 17. Assuming strong chirality, the transition probabilities were calculated by means of Eq. (59) and the analogous expression for the $M1$-transitions. The ratios between the intraband $(\pm\rightarrow\pm)$ and interband $(\pm\rightarrow\mp)$ transition probabilities were found to be consistent with the experimental ones, which are not very stringent though. These results seem to support the suggestion that $^{134}_{59}Pr_{75}$ is an example of a chiral mean field in a restricted spin interval. However, the experimental difference of $|J_+(\omega)-J_-(\omega)|\approx 2\hbar$ points to substantial deviations from the ideal case of strongly broken chiral symmetry with well separated left- and right-handed solutions. The situation is reminiscent of the experimental evidence for breaking of reflection symmetry, which will be discussed in Sec. VI.

The experimental signature of chiral rotation consists of two $\Delta I=1$ bands of the same parity with nearly the same energy. For the examples calculated so far, the interband $E2$ transitions, are strongly suppressed as compared to the intraband $E2$ transitions, whereas the interband and intraband $M1$ transitions are comparable. Of course, there is always the possibility of two planar bands that are accidentally degenerate. Chirality exists only for triaxial nuclei. Thus other experimental evidence for a triaxial shape should be considered as complementary evidence. The possibility of chirality in different mass regions has not yet been investigated in a systematic way. The energy surfaces generated by means of PAC calculations may serve as a guide. Chirality is expected when the energy surface at finite angular momentum has minima of similar depth around $\gamma=30°$, $-30°$, and $-90°$. If this is not fulfilled generation of angular momentum is energetically favored only along one or two principal axes. Frauendorf (1998) used total Routhian surfaces for suggesting the appearance of chirality in nuclei around $^{108}_{43}Tc_{65}$, $^{134}_{59}Pr_{75}$, and $^{188}_{77}Ir_{111}$. By means of self-consistent TAC calculations, Dimitrov *et al.* (2001) confirmed the existence of chiral solutions in the neighborhood of these nucleides.

Chirality appears in molecules and is typical of biomolecules (see, for example, Streitwieser *et al.*, 1985;

March, 1992). The simplest examples are molecules like CH_3CH_2-C≡IHCH$_3$ (2-iodobutene), which contains a stereocenter, that is, a C atom to which four different groups are attached (the bonds are explicitly indicated). The three groups I, H, and CH_3 and the bond to CH_3CH_2 form a left-handed or a right-handed screw. These two ''enantiomers'' are related to each other by mirror reflection. Chirality is also a spontaneously broken symmetry in the molecular case. The exact eigenstates are linear combinations of the two enantiomers. However, the probability of tunneling between enantiomers is usually so small that once a left-handed molecule is formed in a reaction it stays there practically forever. The tunneling times of complex biomolecules (for example, the DNA helix), for which Nature chose the left-handed form, exceed the age of the universe.

In chemistry chirality is of static nature because it characterizes the geometrical arrangement of the atoms. Particle physics is another field in which chirality is encountered. There it has a dynamical character, since it distinguishes between parallel and antiparallel orientations of the spin with respect to the momentum of massless fermions. The chirality of nuclear rotation results from a combination of dynamics (the angular momentum) and geometry (the triaxial shape). Another important difference is that the left- and right-handed states are related by $\mathcal{T}\mathcal{R}_y(\pi)$, which is not a reflection as in molecular and particle physics.

D. C_4 symmetry

As discussed in Sec. II.F.3, the finite rotation $\mathcal{R}_z(\pi)$ generates an important subgroup of the group consisting of all rotations $\mathcal{R}_z(\psi)$. In molecular physics one speaks of a C_n symmetry if the molecule has an n-fold symmetry axis. Using this terminology, the invariance of the mean-field Routhian with respect to $\mathcal{R}_z(\pi)$ is a C_2 symmetry. Another subgroup is $\mathcal{R}_z(\pi/2)$, a rotation about the z axis by an angle of $\pi/2$. If the nuclear mean field had such a symmetry, the quantal levels with $I=I_o+4n$ would form a rotational band. There are many molecules with a C_4 symmetry, for example C_4H_8 (cyclobutene), which is a square of C's with two H's attached to each. They show the expected level sequence. This so-called C_4 bifurcation was discussed by Pavlichenkov (1993).

The observation of a slight $\Delta I=2$ staggering of the levels with $I=I_o+2+4n$ relative to those with $I=I_o+4n$ in one of the superdeformed bands in ^{149}Gd (Flibotte *et al.*, 1993) initiated a discussion about the possibility of a C_4 symmetry in nuclei. Pavlichenkov and Flibotte (1995) suggested that the C_4 axis is perpendicular to the long 3 axis of the axial superdeformed nucleus and almost coincides with the rotational axis. However, it is hard to see why the large difference between the moments of inertia $\mathcal{J}_1\sim 100\,\mathrm{MeV}^{-1}$ and $\mathcal{J}_3\approx 0$, which was ignored in this work, should not completely wipe out any trace of the C_4 symmetry. Hamamoto and Mottelson (1994, 1995) suggested that the C_4 axis is 3. Calculating the quantal levels of a rotor Hamiltonian with such a symmetry they could generate the experimentally observed staggering pattern. Within the same frame, Haslip *et al.* (1998) could explain $\Delta I=2$ staggering, which they also observed in the superdeformed bands of ^{148}Gd and ^{148}Eu.

So far it has not been possible to justify the C_4 rotor Hamiltonian by properties of the rotating mean field. Calculations of the equilibrium shape of the relevant nuclei did not show any tendency towards a C_4 symmetry with respect to the 3 axis (Luo *et al.*, 1995; Magierski, Heenen, and Nazarewicz, 1995; Ragnarsson, 1995). In contrast to these results, Dönau *et al.* (1996) *assumed* a pronounced C_4 symmetry of the deformed potential. Using TAC, they calculated the energy surface $E(\vec{J})$ and the quantal levels by quantizing $\vec{J}$. Since the $\Delta I=2$ staggering turned out to be two orders of magnitude smaller than observed, they also concluded that it is unlikely that a C_4 deformation of the nuclear density causes the staggering. Alternative mechanisms have been suggested (Burzynski *et al.*, 1995; Magierski *et al.*, 1995; Mikhailov and Quentin, 1995; Sun *et al.*, 1995; Reviol *et al.*, 1996; Pavlichenkov, 1997). However, the phenomenon of $\Delta I=2$ staggering remains rather nebulous. It is well established only in the three mentioned cases and $^{131-133}$Ce (Sample *et al.*, 1996). In Sec. IX, the reader can find a beautiful example of C_n symmetry, which spontaneously emerges in the electron system of circular quantum dots.

IV. MAGNETIC ROTATION

As a condition for the appearance of rotational bands in nuclei, Bohr and Mottelson (1975) state: ''A common feature of systems that have rotational spectra is the existence of a 'deformation,' by which is implied a feature of anisotropy that makes it possible to specify an orientation of the system as a whole. In a molecule, as in a solid body, the deformation reflects the highly anisotropic mass distribution, as viewed from the intrinsic coordinate frame defined by the positions of the nuclei. In the nucleus, the rotational degrees of freedom are associated with the deformations in the nuclear equilibrium shape that result from the shell structure.'' The first statement is very general, providing for all kinds of symmetry-breaking mechanisms. However, the low-spin data seemed to indicate that the only way to satisfy this condition is a substantial deformation of the nuclear density distribution, which is measured by the electric quadrupole moment. One suggestive bit of evidence is the correlation between the moment of inertia and the nuclear deformation, often demonstrated by the ratio $\mathcal{J}/B(E2)$ (Grodzin, 1968), which is nearly constant because both the numerator and the denominator are proportional to the square of the deformation parameter.

First Hübel (1991), and then Baldsiefen *et al.* (1991), Fant *et al.* (1991), Clark *et al.* (1992a), and Kuhnert *et al.* (1992) reported the observation of a very regular pattern of γ rays in $^{197-200}$Pb, which can be arranged into rotational bands according to the accepted criteria. At low spin irregular level spacings are observed that are

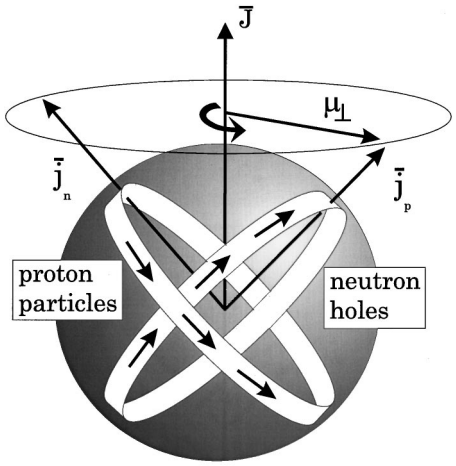

FIG. 18. Magnetic rotation. The high-j proton particles and neutron holes form current loops embedded in the near spherical mass distribution of the nucleus. These current loops as well as the associated transverse magnetic moment $\mu_\perp$ allow us to specify the angle ψ of rotation around the axis $\vec{J}$. The total angular momentum J increases by the gradual alignment of the particle and hole angular momenta $\vec{j}_p$ and $\vec{j}_n$. This is called the shears mechanism. The interaction due to shape polarization tries to keep $\vec{j}_p$ and $\vec{j}_n$ at a right angle, like the spring of a pair of shears. From Clark and Wadsworth, 1998.

typical for these semimagic nuclei with a near spherical shape. The regular band structures appear for $I>10$. The moments of inertia are $\mathcal{J}^{(2)}\sim 20\,\mathrm{MeV}^{-1}$, about one-half of the moments of inertia of the 2^+ states of the well deformed nuclei of the rare-earth region. Figure 3 shows the striking regularity of the bands, which shows up as a picket fence spectrum (ω is equal to the energy of the γ rays). It looks very similar to the spectrum of the superdeformed band shown in Fig. 2, which is an example of the best known collective rotors in nuclei. However, the transitions were shown to be of stretched-dipole type and arguments in favor of a magnetic character were presented. The weak or missing stretched $E2$ transitions pointed to a very small deformation. The lifetime measurements by Wang *et al.* (1992), Hughes *et al.* (1993), Clark *et al.* (1994, 1997, 1998, 1999), Moore *et al.* (1995), Neffgen *et al.* (1995), Krücken *et al.* (1998), and Jenkins *et al.* (1999) showed that the dipole bands have very large values of $B(M1)\sim 3-6\mu_N^2$ and very small values of $B(E2)\sim 0.1(e\ \mathrm{b})^2$. Duprat *et al.* (1994), Porquet *et al.* (1994), and Pohler *et al.* (1999) demonstrated the magnetic character of the transitions conclusively. Clark and Macchiavelli (2000) recently reviewed the peculiar features of the magnetic dipole bands and their interpretation, to be summarized below.

A. Magnetic and antimagnetic rotation

The experimental results are in contradiction with the established view, according to which nuclear rotation is a collective phenomenon that occurs only in well deformed nuclei. The ratio $\mathcal{J}/B(E2)$, which is $\sim 10(e\ \mathrm{b})^{-2}\,\mathrm{MeV}^{-1}$ for well deformed heavy nuclei and $\sim 5(e\ \mathrm{b})^{-2}\,\mathrm{MeV}^{-1}$ for superdeformed nuclei, exceeds $100(e\ \mathrm{b})^{-2}\,\mathrm{MeV}^{-1}$ for the dipole bands. There must be something rotating that carries a long transverse magnetic dipole moment but almost no charge quadrupole moment.

The structure of this novel rotor is illustrated in Fig. 18. In order to be concrete, let us consider a typical case. A pair of protons is excited across the $Z=82$ shell gap into the configuration $[\pi(h_{9/2}i_{13/2}s_{1/2}^{-2})_{11^-}]$. It is combined with two neutron holes in the configuration $[\nu(i_{13/2}^{-2})_{12^+}]$. The angular momenta of the protons and of the neutron holes, which are separately lined up, are represented by the two arrows $\vec{j}_p$ and $\vec{j}_n$, respectively. Since this arrangement breaks the $\mathcal{R}_z(\psi)$ symmetry, a rotational band is the consequence, as observed. There is no $\mathcal{R}_z(\pi)$ symmetry, in accordance with the observed $\Delta I=1$ sequences. The separate configurations $[\pi(h_{9/2}i_{13/2}s_{1/2}^{-2})_{11^-}]$ and $[\nu(i_{13/2}^{-2})_{12^+}]$ have $\mathcal{R}_z(\psi)$ symmetry. They are well known isomeric states in these nuclei. No rotational levels are found on top of these states. The dipole bands appear only when the two structures are combined.

The high-j orbitals have toroidal density distributions, which are illustrated by the two loops. The interaction between the particles and the holes is repulsive and favors an angle of 90°, at which the two loops are as far from each other as possible. Along the band, the total angular momentum is increased by gradually aligning $\vec{j}_p$ and $\vec{j}_n$. This process has been dubbed the shears mechanism (Baldsiefen *et al.*, 1994) because the motion resembles the closing of a pair of sheep-shears, which have a spring to keep them open. The dipole bands are thus referred to as shears bands. Closing the blades of the shears increases the energy because the loops are aligning. If the two blades are long it takes many steps (increments of J by $1\hbar$) until the shears are closed. The energy increases gradually, resulting in the observed smooth increase of the frequency $\omega\ (=dE/dJ)$ with J. The function $\omega(J)$ and its derivative, the inverse of the moment of inertia $\mathcal{J}^{(2)}$, are determined by the interaction between the high-j orbitals. Their form will be discussed in Sec. IV.C.

The shears arrangement of the high-j orbitals gives rise to a large transverse magnetic dipole moment $\mu_\perp$. The protons contribute an orbital part and a spin part $(g_p>0)$ to the magnetic moment $\vec{\mu}$, which are both parallel to $\vec{j}_p$. The spin part of the neutrons is antiparallel to $\vec{j}_n$ $(g_n<0)$. Thus all transverse components add up. It is this long transverse dipole that rotates and generates the strong magnetic radiation. For this type of rotation, the magnetic dipole moment is the order parameter, which specifies the orientation angle.

Frauendorf *et al.* (1994, 1996) suggested calling the new rotational mode "magnetic rotation."[9] The name alludes to the magnetic moment which is the order pa-

[9]The term "magnetic rotation" is also used in optics, solar physics, and nuclear magnetic resonance physics in very different contexts.

rameter that specifies the orientation. There is an analogy with solid-state physics. The magnetic moment (per unit of volume), which is the sum of the atomic dipole moments, is the order parameter of a ferromagnet (see, for example, Kittel, 1988). In contrast to the collective rotation of well deformed nuclei, magnetic rotation is carried by a few high-j orbitals.

When the two blades of the shears close, the transverse component of the magnetic moment becomes shorter. The decrease of the $B(M1)$ values with increasing angular momentum is an inevitable consequence of the shears mechanism. Neffgen *et al.* (1995) found the first evidence for this trend, though the large errors meant that the results were not very convincing. Improvements in gamma-ray detector arrays have made possible the unambiguous demonstration of the decrease in the $B(M1)$ values (Clark *et al.*, 1997, 1998, 1999; Krücken *et al.*, 1998; Jenkins *et al.*, 1999).

In an antiferromagnet one-half of the atomic dipole moments are aligned on one sublattice and the other half are aligned in the opposite direction on the second sub-lattice, such that there is no net magnetic moment. Nevertheless, the state is ordered, i.e., it breaks isotropy like a ferromagnet (see, for example, Kittel, 1998). In this case, one takes the magnetization of one of the sublattices as the order parameter. The rotation of weakly deformed nuclei may also be analogous to an antiferromagnet. Figure 19 shows an example. The proton configuration is $[(g_{9/2})^{-2}]$ and the neutron configuration $[(h_{11/2})^2]$. Each of the proton holes combines with one of the neutron particles, forming a pair of shears. But unlike the case of magnetic rotation they are arranged such that the transverse magnetic moment is zero. The magnetic moment of one of the two shears specifies the orientation, as does the magnetization of one of the sublattices in an antiferromagnet. The angular momentum is generated by simultaneously closing the two shears. Since the mean field has $\mathcal{R}_z(\pi)$ symmetry, the rotational band is a $\Delta I=2$ sequence. Alluding to the analogy with an antiferromagnet, Frauendorf (1997) suggested the name "antimagnetic rotation" for $\Delta I=2$ bands of definite signature, which are regular but have very small $B(E2)$ values. To distinguish this phenomenon from collective rotation it seems reasonable to speak about antimagnetic rotation if the ratio $\mathcal{J}^{(2)}/B(E2)$ is as large as for magnetic rotation, i.e., it should exceed $100\,\mathrm{MeV}^{-1}(e\ \mathrm{b})^{-2}$.

One may also attribute the breaking of the $\mathcal{R}_z(\psi)$ symmetry to the currents that generate the magnetic moments. As illustrated by Fig. 18, the high-j orbitals have a toroidal density distribution along which flows a mass current. This flow is accompanied by an electrical current in the case of the protons. The orbitals resemble current loops. The current in the loop is a distinctive element of anisotropy, which specifies the orientation. Thus one may say that in the cases of magnetic and antimagnetic rotation the orientation is mainly due to the anisotropy in the current distribution, the density distribution being nearly spherical. As is well known, the orientation of well-deformed nuclei manifests itself in the anisotropy of the density and charge distributions. However, a closer examination of the symmetry breaking and its relation to rotational bands in Appendix A shows that nuclei are much better oriented than their distributions of charge and density, which can be traced back to currents.

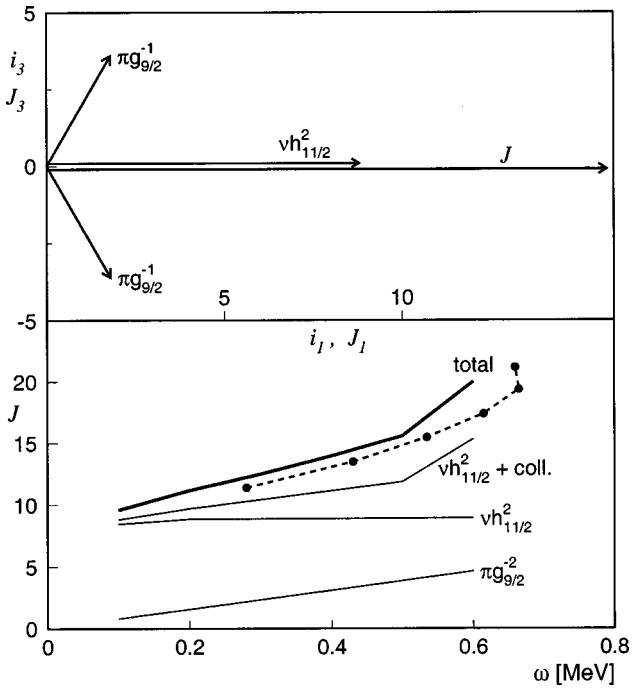

FIG. 19. Antimagnetic rotation of the yrast band in $^{110}_{48}\mathrm{Cd}_{62}$. The results of a principal-axis cranking calculation are compared with the data (dashed lines) from Juutinen *et al.*, 1994. The deformation parameters of the mean field, $\varepsilon=0.1$ and $\gamma=50°$, are the equilibrium values for $\omega=0.3$ MeV. Upper panel: composition of the angular momentum at $\omega=0.3$ MeV. Lower panel: Total angular momentum J and its composition as functions of the frequency ω. The neutron part denoted by "$\nu h_{11/2}^2$ coll." contains in addition to the $\nu h_{11/2}^2$ part the contributions of all particles not shown in the upper panel.

B. Examples

By means of TAC calculations, Frauendorf (1993a) was able to reproduce quantitatively the salient features of the dipole bands: the nearly linear relation between frequency and angular momentum, the large values of $B(M1)$, and the small values of $B(E2)$. As an example, Fig. 20 shows the TAC results for the above discussed high-j configuration[10] $[\pi(h_{9/2}i_{13/2}s_{1/2}^{-2})_{11^-},\nu(i_{13/2}^{-2})_{12^+}]$ in $^{199}_{82}\mathrm{Pb}_{117}$. There is an additional negative parity quasineutron (E) excited, which acts as a spectator by adding $1/2\hbar$ to the total angular momentum (cf. Fig. 32). Within the framework of the TAC approach, the interaction between the the high-j orbitals is due to the slightly oblate average po-

[10]The subscript on the parenthesis gives the angular momentum for stretched coupling of the particles within the subshell.

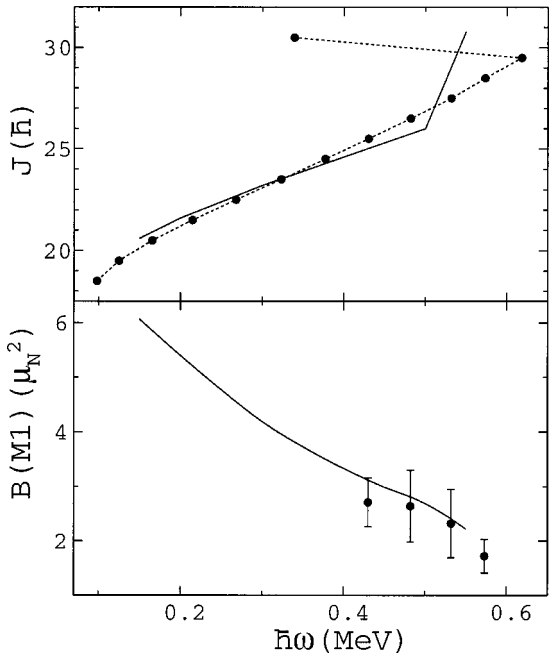

FIG. 20. Angular momentum and $B(M1)$ values as functions of the rotational frequency for the high-j configuration $[\pi(h_{9/2}i_{13/2}s_{1/2}^{-2})_{11^-}][\nu(i_{13/2}^{-2})_{12^+}\nu(pl)]$ in ^{199}Pb. Full lines are the TAC calculation (same parameters as in Fig. 19). Points are the experimental data. From (Frauendorf, 1997).

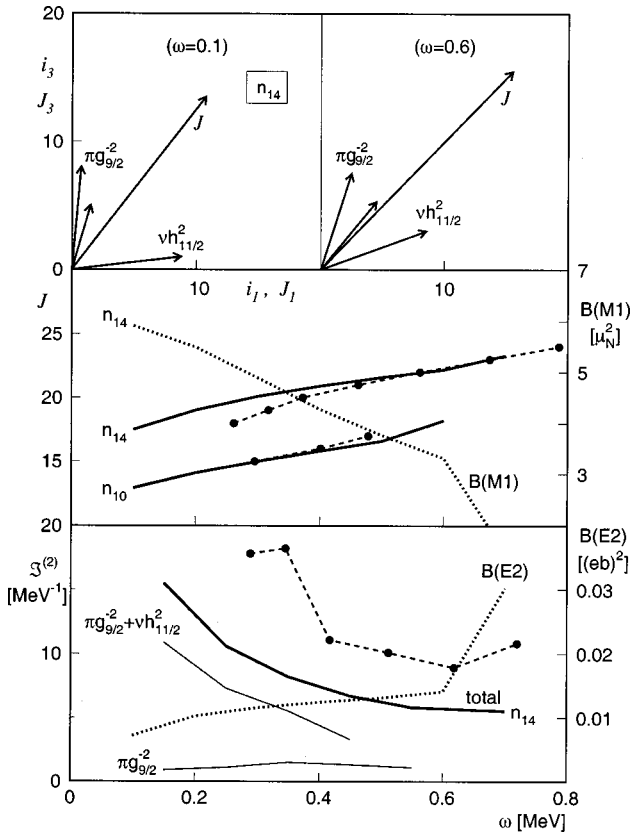

FIG. 21. Magnetic rotation in $^{110}_{48}Cd_{62}$. The data (dashed lines with heavy dots) are from Juutinen *et al.*, 1994. The TAC calculations (solid and dotted lines) assume $\Delta_\pi=0$, $\Delta_\nu=1.1$ MeV and $\varepsilon=0.13$, $\gamma=10°$, which are the equilibrium deformations at $\omega=0.3$ MeV. The two neutron configurations n_{10} and n_{14} differ by the excitation of a $g_{7/2}$ quasineutron pair in the latter. [The recent life time measurements agree with the predicted $B(M1)$ values see Clark *et al.*, 1999. The top panel shows the angular momentum composition of n_{14}, where 3 is the long axis. The bottom panel displays for n_{14} the total moment of inertia and the contributions of the $g_{9/2}$ proton holes and the $h_{11/2}$ quasineutrons].

tential, which is induced by them. It also ensures the alignment of the protons to one blade and of the neutron holes to the other. As discussed in Sec. II.D, the high-j particles tend to align their angular momentum with the symmetry axis, whereas the high-j holes prefer a perpendicular orientation. The angle between the two blades $\vec{j}_p$ and $\vec{j}_n$ results from the balance between the Coriolis force generated by $-\vec{\omega}\cdot\vec{J}$, which tries to align the two vectors with the axis of rotation $\vec{J}$, and the restoring force of the slightly deformed potential, which tries to keep the two loops at 90°. The opening angle decreases with increasing ω, because the Coriolis force gets stronger. The angular momentum vector $\vec{J}$ keeps an angle of about 45° with the principal axes of the density distribution. We shall discuss this balance more quantitatively in Sec. IV.C. It should be stressed at this point that the substantial moments of inertia of the shears bands cannot be attributed to the slight deformation. According to the TAC calculations the shears mechanism is responsible for two-thirds of the moment of inertia $\mathcal{J}^{(2)}$, whereas only one-third is due to the low-j particles, which generate the slightly deformed mean field.

Magnetic rotation may be realized by more complex structures than those just discussed. Figure 21 shows $^{110}_{48}Cd_{62}$ as an example. In the configuration called n_{10}, two proton holes are aligned to $[\pi(g_{9/2}^{-2})_{8^+}]$ and two neutrons to $[\nu(h_{11/2}^2)_{10^+}]$, which form two crossed current loops as in the Pb isotopes. The other dipole band, called n_{14}, has the structure $[\pi(g_{9/2}^{-2})_{8^+}, \nu(h_{11/2}^2)_{10^+}, \nu(d_{5/2}g_{7/2})^2]$. It is the combination of three current loops, which are perpendicular to the $\vec{j}$ vectors shown in the upper panel. The calculated deformation $\varepsilon=0.13$ (at $\omega=0.3$ MeV) is consistent with the experimental limit $B(E2)<0.05(e\ \mathrm{b})^2$, derived from the fact that no stretched $E2$ transitions are found.

Figure 19 shows the $\Delta I=2$ band with antimagnetic character, which is observed in the same nucleus. The rotational degree of freedom may be taken from the two current loops of the $g_{9/2}$ proton holes. The PAC calculations (Frauendorf *et al.*, 1994) account well for the measured function $J(\omega)$. More than one-half of the moment of inertia $\mathcal{J}^{(2)}$ is generated by the gradual alignment of the two $g_{9/2}$ proton holes. The calculated equilibrium deformation of $\varepsilon=0.13$ gives $B(E2)$ values that are nearly constant $0.10(e\ \mathrm{b})^2$. They compare favorably with the experimental values of $0.12(e\ \mathrm{b})^2$ and $0.09(e\ \mathrm{b})^2$ obtained by means of recoil distance method for the transitions from the 12^+ and 14^+ states, respectively (Piiparinen *et al.*, 1993), as well as with $0.11(e\ \mathrm{b})^2$, $0.12(e\ \mathrm{b})^2$, $0.09(e\ \mathrm{b})^2$, and $0.10(e\ \mathrm{b})^2$ obtained by

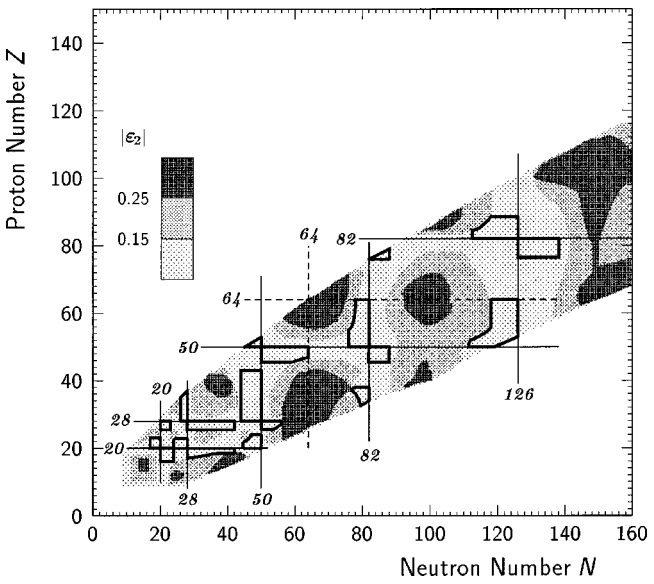

FIG. 22. Appearance of magnetic rotation in different mass regions. The predicted regions are enclosed by heavy lines. From Frauendorf, 1996.

means of Doppler shift attenuation method for the transitions from the 14^+, 16^+, 18^+, and 20^+ states, respectively (Clark, 1999). The experimental ratio $\mathcal{J}^{(2)}/B(E2)\approx 100-200\,\mathrm{MeV}^{-1}(e\ \mathrm{b})^{-2}$ is similar to the one for the magnetic bands. It is much larger than the value $[<10\,\mathrm{MeV}^{-1}(e\ \mathrm{b})^2]$ for the collective rotation of well deformed nuclei.

Below $I=10$, the yrast line of ^{110}Cd is quasivibrational. The transition energies scatter around 0.8 MeV. The experimental values of $B(E2)=0.09,0.18,>0.05$, $>0.08(e\ \mathrm{b})^2$ for the respective transitions from the 2^+, 4^+, 6^+, and 8^+ levels (Piiparinen *et al.*, 1993) indicate that the quasivibrational states have deformations that are comparable with the deformation of the rotational levels above $I=10$. The difference between the quasivibrational and the rotational part of the yrast sequence consists in the presence of the pair of $h_{11/2}$ quasineutrons. As can be seen in Fig. 19, the orientation with respect the $\vec{J}$ is only well specified by one of the two "subshears" $[\pi(g_{9/2})^{-1}\nu h_{11/2}]$ if the long vector $[\nu h_{11/2}^2]$ is present. Accordingly, the rotational band appears only after the configuration has attained antimagnetic character (cf. Sec. IV.A).

We consider small deformation as the salient feature of magnetic rotation. The orientation is specified by a few high-j particles and holes whose current loops are anisotropically arranged. The most straightforward way to achieve this is to combine proton particles with neutron holes or vice versa, because it is easy to find combinations of Z and N for which high-j shells are nearly empty or almost completely filled. Based on these considerations, Frauendorf *et al.* (1994) delineated the mass regions where magnetic rotation can be expected. They are presented in Fig. 22. A complementary chart is given in Frauendorf *et al.*, 1994 and Frauendorf, 1997 showing the active high-j orbitals. Magnetic rotation has been studied in four of the predicted regions: ($Z\geqslant 28$,$N\leqslant 50$), ($Z\leqslant 50$,$N\geqslant 50$), ($Z\geqslant 50$,$N\leqslant 64$), and ($Z\geqslant 80$,$N\leqslant 126$). The reader can find a summary of this work in Appendix B.

C. The shears mechanism

The possibility of generating angular momentum in a rotational band by gradually aligning two long vectors composed of nucleonic angular momenta was first discussed by Danos and Gillet (1967). Their "stretch" scheme looks like Fig. 19, but without the $h_{11/2}$ neutrons. One of the two blades is thought to be constructed by stretched coupling of half of all valence nucleons and the other blade by stretched coupling of the rest of the valence nucleons. The ability of the stretch scheme to account for the energetics of realistic rotational bands was never demonstrated. Frauendorf (1993a) introduced the shears mechanism for explaining the physics underlying his TAC calculations. Macchiavelli *et al.* (1998a, 1998b, 1998) used simple geometry (cf. Fig. 18) for discussing the energies and transition probabilities of the magnetic bands from a more phenomenological point of view. Let us start with their approach and then discuss some general features of the shears mechanism and its relation to the tilted-axis cranking.

In order to keep things simple, we assume that the two blades have the same length $|\vec{j}_p|=|\vec{j}_n|=j$ and all angular momentum is generated by the shears effect. Further it is suggested that the energy depends on the opening angle θ between the two blades as

$$E(\theta)=A\cos^2\theta+E_o,\quad A>0. \tag{61}$$

Macchiavelli *et al.* (1998b) called this a P_2 form because it can be rewritten as a second-order Legendre polynomial $P_2(\cos\theta)$ plus a constant. The opening angle is fixed by the total angular momentum,

$$\cos\theta=(2\overline{J}^2-1),\quad \overline{J}=\frac{J}{2j}. \tag{62}$$

The maximum $2j$ is the natural unit for the angular momentum. The frequency becomes

$$\omega=\frac{dE}{dJ}=\frac{2A}{j}\overline{J}(2\overline{J}^2-1) \tag{63}$$

and the moment of inertia

$$\mathcal{J}^{(2)}=\frac{dJ}{d\omega}=\frac{j^2}{A(6\overline{J}^2-1)}. \tag{64}$$

The shears band starts at $J=\sqrt{2}j$, where $\omega=0$ and $\mathcal{J}^{(2)}=j^2/2A$, and terminates at $J=2j$, where $\omega=2A/j$ and $\mathcal{J}^{(2)}=j^2/5A$. The moment of inertia decreases as in experiment (cf. Figs. 20 and 21). The total angular momentum J also fixes the opening angle when the two blades have different length. Macchiavelli *et al.* (1998b) assumed that $|j_p|$ and $|j_n|$ are equal to their quantized values for a spherical potential. Using the experimental g-factors of the high-j orbitals, which are well known

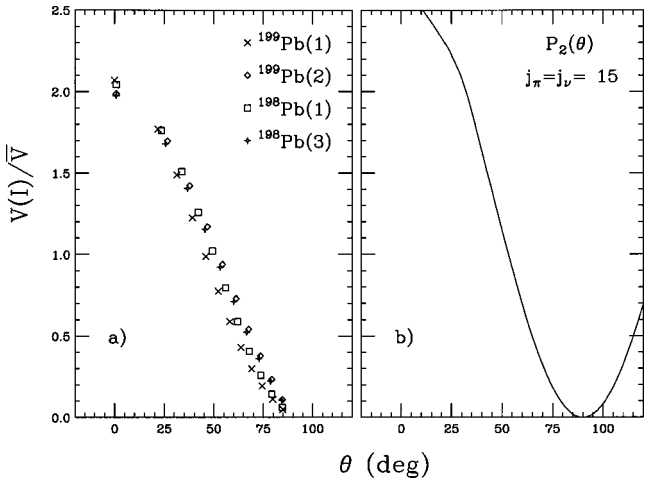

FIG. 23. The experimental energies of magnetic dipole bands in ^{198,199}Pb (a) as functions of the angle between the blades of the shears, compared with the expected dependence of a P_2 term for the case $j=15$ (b). The experimental energies are normalized to the last transition before termination. From Macchiavelli *et al.*, 1998b.

from the spherical shell-model configurations, they determined the transverse component $\mu_\perp$ from geometry. The measured $B(M1)$ values were well reproduced. The contribution of the core particles to the total angular momentum was estimated to be less than 2–3 $\hbar$.

Equation (61) represents the interaction between the blades of the shears. Macchiavelli *et al.* (1998b) used Eq. (62) for determining an empirical function $E(\theta)$ from the experimental energies. Figure 23 demonstrates that for the Pb isotopes this ''interaction between the bladons,'' as called by the authors, is indeed very similar to the suggested P_2 form (61). They attributed the interaction to particle-vibration coupling, which is generated by the exchange of a quantum of the quadrupole vibration of the nuclear shape. Further they found that the coefficient A of the bladon interaction is consistent with the empirical coupling strength of quasiparticles with vibrational excitations (Bohr and Mottelson, 1975). A comprehensive discussion of this model was given in the review by Clark and Macchiavelli (2000).

How does this particle-vibration coupling scheme relate to the TAC mean-field approach? In tilted-axis cranking model, the energy $E(\theta)$ is caused by the interaction of the high-j particles and holes via the average potential V, which has a small quadrupole deformation. The total quadrupole moment is the sum

$$Q_\mu = Q^S_\mu + Q^C_\mu \tag{65}$$

of the moments Q^S_μ of the high-j particles and holes in the shears and the core moment Q^C_μ of all other particles. The value of Q^S_μ is fixed by J via the opening angle of the shears. Let us consider the important case in which TAC calculations give no deformation for the core and assume that the core energy is quadratic in the quadrupole moments,

$$E_C(Q^C_\mu) = \frac{C}{2}\sum\ (-)^\mu Q^C_\mu Q^C_{-\mu}. \tag{66}$$

If the contribution of the shears is included, the total TAC energy (20) becomes

$$E = E_C - \frac{\kappa}{2}\sum\ (-)^\mu (2Q^C_\mu + Q^S_\mu) Q^S_{-\mu}. \tag{67}$$

Minimizing it with respect to Q^C_μ one finds

$$Q_\mu = \left(1+\frac{\kappa}{C}\right) Q^S_\mu. \tag{68}$$

The total TAC energy takes the form (61) with

$$A = \frac{16\pi\kappa}{15}\left(1+\frac{\kappa}{C}\right). \tag{69}$$

That is, with the proper choice of coupling constant κ, TAC is equivalent to the particle-vibration coupling scheme for nuclei commonly classified as spherical. For these nuclei the deformation induced by the valence particles can be treated in linear order. It can be taken into account by means of an effective interaction between the high-j particles and holes (see Bohr and Mottelson, 1975). We have discussed ^{199}Pb as an example in Sec. IV.B.

The other example, ^{110}Cd, presented there, demonstrates that magnetic rotation may be more complex. Intermediate-j orbitals become important in generating the angular momentum. If there are more particles and holes added to the closed shell, the polarization becomes stronger and nonlinear. These transitional nuclei may already have some small deformation without the high-j particles and holes present. Accordingly, the low-spin spectrum has a transitional character between spherical and deformed nuclei. Nevertheless, the deformation of the dipole bands is still small enough to classify the rotation as magnetic. The tilted-axis cranking model permits the treatment of these cases as well.

D. Origin and limits of regularity

Our present understanding of the regular magnetic dipole bands is based on the TAC calculations and the shears model discussed in the preceding section. It may be summarized as follows. These bands appear in near spherical nuclei when high-j particles of one kind are combined with high-j holes of the other kind of nucleons. Each of these high-j particles or holes induces a slight deformation of the average potential which is felt by the other high-j particles and holes. Equivalently one may say that the high-j particles and holes interact by the exchange of quadrupole phonons. This type of interaction causes the particles to couple to the maximal angular momentum, i.e., to form a blade, and the holes to do the same. These long angular momentum vectors break the rotational symmetry with respect to the axis of the total angular momentum, i.e., they specify the orientation degree of freedom. The angular momentum is generated by the gradual alignment of the blades, which

implies the smooth relation (63) between angular momentum and transition energy. The latter looks similar to the linear relation for the perfect rotor, where small deviations from linearity are observed in experiment. In Appendix A, we analyze more quantitatively the relation between symmetry breaking by the mean field and the appearance of regular rotational bands.

The simplest shears structure can be constructed by adding a high-j particle and a high-j hole to closed proton and neutron shells. The sequence of states obtained by coupling their angular momenta $\vec{j}$ to different values of J is commonly called a multiplet. Multiplets are well studied, both experimentally and theoretically. Schiffer (1971) analyzed the particle-hole interaction by a method similar to the determination of the bladon interaction described above. He found a function $E(\theta)$ which exhibits staggering, that is, which is different for the even and odd values of J. One branch has a minimum at $\theta=90°$ and increases towards $\theta=0°$, whereas the other branch is close to zero. A quantal calculation with a short-range force reproduces $E(\theta)$. One expects an increasing function $E(\theta)$ for a short-range repulsive interaction, which prefers a minimal overlap of the doughnutlike wave functions of the high-j particles and holes (see Fig. 18). Staggering arises when the angular momentum is treated quantum mechanically. It can be traced back to the symmetry of the wave function $\Psi(\Omega_1,\Omega_2)_{LL}$ of two particles with the orbital angular momenta l_1 and l_2, which are coupled to the total orbital angular momentum $L,M=L$. When the angle coordinates Ω are exchanged, one has $\Psi(\Omega_1,\Omega_2)_{LL}=(-)^{l_1+l_2-L}\Psi(\Omega_2,\Omega_1)_{LL}$. Hence $\Psi(\Omega_1,\Omega_1)_{LL}=0$ for l_1+l_2-L odd. For these L the matrix element of a short-range force is small as compared to the one for the other L. The staggering of $E(J)$ reflects by this L dependence. An extended discussion can be found in the textbook of deShalit and Feshbach (1974). The staggering is much weaker for a long-range residual interaction like the quadrupole interaction (8).

What is the difference between the regular shears bands and the staggering multiplets? How does one structure develop into the other when the particle number changes? A complete understanding has not yet been reached. For the regular bands to appear it seems important that the blades be composed of more than one high-j particle or hole. Combining several high-j particles and holes tends to suppress staggering, because the different interacting particle-hole pairs, which contribute to the total $E(\theta)$, are not expected to be in phase. Furthermore, the long-range polarization interaction should be dominant. It is smooth and favors the stretched coupling of high-j particles into one blade and high-j holes into the other. Long blades make it possible to change J in many steps. The short-range interaction between two identical high-j particles or holes does not favor their stretched coupling (Schiffer, 1971), that is, it does not stabilize the shears blades if they are composed of particles or holes from the same j shell.

The quadrupole polarizability has a minimum for the closed shells (see, for example, Bohr and Mottelson, 1975). Hence, in the immediate vicinity of double magic nuclei the short-range residual interaction between the valence particles dominates. There, one observes the multiplets. When enough valence particles (or holes) are added the nucleus becomes soft with respect to quadrupole polarization, which then dominates the interaction between high-j particles and holes. In this regime regular $M1$ bands appear. In between there are sequences of states with enhanced $M1$ transitions that are caused by the perpendicular orientation of the proton and neutron angular momenta. But these states will only arrange into bandlike sequences. The level spacings are irregular, because the energy needed to close the two blades is comparable to the energy gained by rearranging the angular momenta of the particles (or holes) forming one blade.

These qualitative considerations are supported by investigations of the $M1$ bands in the frame of the spherical shell model, which will be discussed in Sec. VIII.A. The experimental spectra of the Cd, In, and Sn isotopes, which are reviewed in Appendix B, change from regular magnetic bands via irregular $M1$ sequences to multiplets when N approaches 50 from above.

V. BAND TERMINATION

Band termination appears as a consequence of the quantization of the angular momentum. Consider a nucleus that is not too strongly deformed, such that the the single-particle levels are still grouped into spherical shells. The angular momentum of the high-j orbitals remains close to j, its value in the spherical potential. The total angular momentum J is generated by gradually aligning the angular momentum vectors $\vec{j}$ of the particles and holes in the incompletely filled shells. Eventually all vectors $\vec{j}$ are aligned in accordance with the Pauli principle. The mean-field state $|\rangle$ is $\mathcal{R}_z(\psi)$ symmetric for this stretched coupling. In order to increase the angular momentum further, particles from the core must be excited, i.e., a new configuration must be generated. That is, termination is reached. The shape may change appreciably before attaining $\mathcal{R}_z(\psi)$ symmetry at termination.

Experimentally, band termination is seen as a break in the smooth relation $J(\omega)$ between angular momentum and rotational frequency. In contrast to the situation after a band crossing, where another smooth sequence $J(\omega)$ starts, after a termination the level distances become irregular and there are competing parallel decay paths.

Termination may also occur for nuclei with a substantial deformation. Nucleons in a deformed harmonic-oscillator potential, which rotates about a principal axis, is an illustrative example. Band termination within this model was comprehensively discussed by Afanasjev *et al.* (1999), who also give references to the numerous earlier studies. The rotating harmonic oscillator separates into independent oscillations along the three principal axes, as the nonrotating oscillator does. A band is defined by a fixed number of oscillator quanta along

each of the principal axes. Consider rotation about the 1 axis. The maximal angular momentum of a given configuration is

$$J_{1,max}=|\Sigma_2-\Sigma_3|, \quad \Sigma_\nu=\sum_{i,occ}\left(n_{\nu,i}+\frac{1}{2}\right), \tag{70}$$

where $n_{\nu,i}$ is the number of quanta on the ν axis in the state i. When this value is reached the density becomes symmetric with respect to the 1 axis and the band terminates. Again, termination is due to restriction of the accessible angular momentum by quantization.

Termination does not have to take place. For near spherical nuclei, the deformation may change in such a way that the spherical shell structure dissolves. Then core angular momentum becomes accessible in addition to the angular momentum of the valence particles. For a harmonic oscillator Afanasjev *et al.* (1999) delineated shapes that terminate and shapes that do not.

The two mechanisms idealize different features of real nuclei. The high-j intruder orbitals behave like spherical ones, whereas the low-spin orbitals are better accounted for by a deformed harmonic oscillator. Only realistic self-consistent cranking calculations describe band termination quantitatively.

Band termination was discussed by Bohr and Mottelson (1975) for light nuclei in the sd shell. Nilsson and Ragnarsson (1995) and Afanasjev *et al.* (1999) reviewed subsequent work. Röpke and Endt (1998) and Röpke (2000) used mean-field configurations for classifying many bands, which all terminate when the amount of angular momentum available for the particles in the sd shell is exhausted. The oscillator model accounts fairly well for the termination of bands in these light nuclei.

Terminating bands in heavy nuclei were predicted by Bengtsson and Ragnarsson (1983) for the region $Z\approx 66$ and $N\approx 90$ and experimentally verified by Simpson *et al.* (1984) and Tjøm *et al.* (1985). The termination appears when the angular momentum of the protons above $Z=64$ and the neutrons above $N=82$ is exhausted. Nilsson and Ragnarsson (1995) and Simpson *et al.* (1994) reviewed the theoretical and experimental work on these nuclei. Ragnarsson *et al.* (1995) invoked the concept of terminating bands in order to explain the experiment by Janzen *et al.* (1994) on $^{109}_{51}Sb_{58}$. Since then a large number of terminating bands has been observed in nuclei with several valence particles outside the $Z=N=50$ core. Extensive theoretical analyses have been carried out in the framework of the configuration-dependent cranked Nilsson-Strutinsky model (see Sec. III.A.2). Afanasjev *et al.* (1999) recently reviewed these investigations and also discussed other regions with terminating bands.

Band termination may occur for all of the discrete symmetries discussed in Sec. II.F. The case with $\mathcal{R}_z(\pi)$ symmetry is well studied. Since it is presented in the above-mentioned reviews, we restrict ourselves to one illustrative example and discuss the termination of magnetic bands.

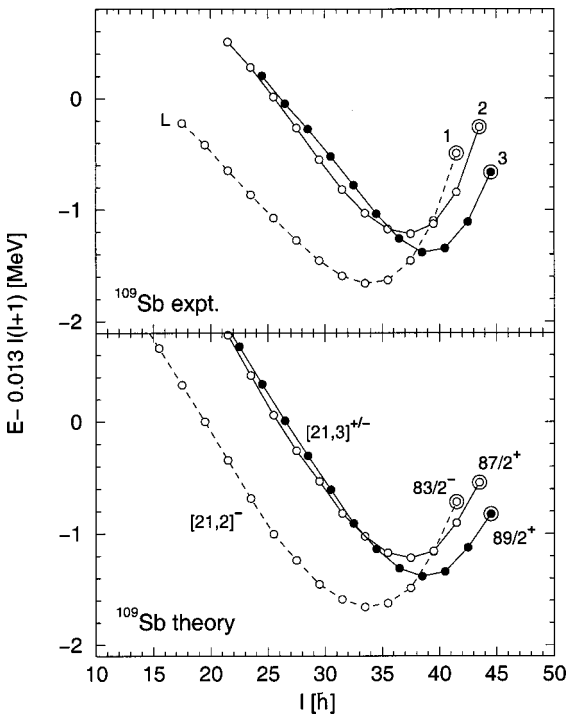

FIG. 24. The energies of the bands 1–3 in $^{109}_{51}Sb_{58}$ relative to the energy of a rigid rotor with a moment of inertia of $\mathcal{J}=38\,\mathrm{MeV}^{-1}$. The terminating states are shown as large circles labeled by the spin and parity I^π. Band 2 and 3 are not linked to the known part of the spectrum. The unknown energy of the lowest level is chosen to give agreement with the cranked Nilsson-Strutinsky calculations in the lower panel. The configuration assignment $[lm,n]^\pm$ in the lower panel is as follows. l, number of $g_{9/2}$ proton holes; m, number of $h_{11/2}$ proton particles; n, number of $h_{11/2}$ neutron particles and $\pm$ gives the signature $\alpha=\pm 1/2$. From Afanasjev *et al.*, 1999.

A. Terminating bands with good signature

Figure 24 shows three terminating bands in $^{109}_{51}Sb_{58}$. Band 1 with $(\pi,\alpha)=(-,-1/2)$ has the proton configuration $[(g_{9/2})^{-2}_8(d_{5/2}g_{7/2})^2_6(h_{11/2})^1_{11/2}]$ and the neutron configuration $[(h_{11/2})^2_{10}(d_{5/2}g_{7/2})^6_{12}]$. Stretched coupling of all the angular momenta gives $I^\pi=83/2^-$, as observed. Bands 2 and 3 with $(\pi,\alpha)=(+,-1/2)$ and $(+,1/2)$ have the same proton configuration combined with neutron configurations $[(h_{11/2})^3_{27/2}(d_{5/2}g_{7/2})^5_{21/2}]$ and $[(h_{11/2})^3_{27/2}(d_{5/2}g_{7/2})^5_{23/2}]$, respectively. As expected, they terminate at $I^\pi=87/2^+$ and $89/2^+$. Figure 25 shows that band 1 starts with the substantial prolate deformation of $\varepsilon\approx 0.25$. Generating angular momentum by gradual alignment of the valence particle angular momenta, the shape becomes triaxial and then oblate and symmetric with respect to $\vec{J}$ at termination. The corresponding decrease in the $B(E2)$ values has been confirmed experimentally and agrees well with the cranked Nilsson-Strutinsky calculations (Wadsworth *et al.*, 1998; Afanasjev *et al.*, 1999). The dispersion ΔJ, which measures the symmetry breaking (see Appendix A), and the moment of inertia $\mathcal{J}^{(2)}$ decrease along this path. The path in the ε-γ plane is similar for bands 2 and 3.

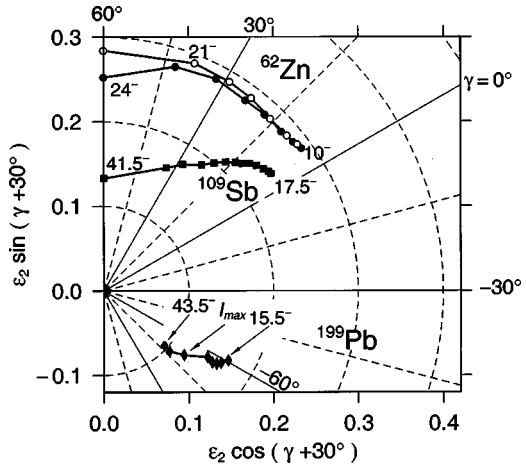

FIG. 25. The calculated deformation parameters of bands in $^{199}_{82}Pb_{117}$, $^{109}_{51}Sb_{58}$, and $^{62}_{30}Zn_{32}$ as functions of the angular momentum. Each spin value is represented by a symbol, where $\Delta I=2$. From Ragnarsson, 2000.

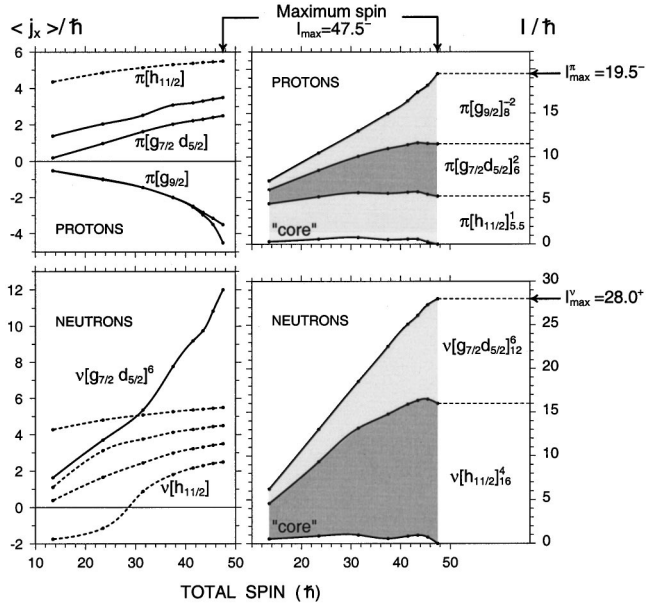

FIG. 26. Contributions of the valence particles and holes to the total angular momentum of a terminating band in $^{111}_{51}Sb_{60}$. The calculations follow the deformation path relevant for the specific configuration shown in Fig. 25. From Afanasjev *et al.*, 1999.

Afanasjev *et al.* (1999) compare the energies to those of a rotor with a rigid-body moment of inertia. They call the characteristic U shape of the function $E(I)-E(I)_{rotor}$ in Fig. 24 a *smooth unfavored termination*. ''Smoothness'' is just one of the criteria for a sequence of levels to qualify for a rotational band. The possibility of observing the bands up to termination is due to the low level density, which is caused by gaps in the single-particle spectrum at $Z=50$ and $N=58$. If such gaps appear, the smoothness condition is well satisfied [see Eq. (A9) in Appendix A]. ''Unfavored'' means that the rotational energy is larger than that of the reference rotor. This feature, which is seen in Fig. 24 as a sharp increase in the relative energy at the highest spins, reflects the decrease of $\mathcal{J}^{(2)}$.

Afanasjev *et al.* (1999) characterize the terminating bands in the mass 110 region as starting with ''collective rotation'' and then ''gradually losing the collectivity.'' This terminology is used to describe the gradual restoration of $\mathcal{R}_z(\psi)$ symmetry, which is substantially broken at a bottom of the band. A detailed discussion of why the substantial symmetry breaking does not necessarily imply high collectivity is offered in Appendix A. Figure 26 shows that the rotation is not very collective. The angular momentum is generated by a relatively small number of particles. The bands have antimagnetic character in the upper part. In the lower part, the deformation is larger than 0.15, which is our upper limit for qualifying as an anti-magnetic rotor. Hence these bands are in between good collective and antimagnetic rotors. This characterization is supported by the experimental ratio $\mathcal{J}^{(2)}/B(E2)\approx 100\,\mathrm{MeV}^{-1}(e\ \mathrm{b})^2$ (Janzen *et al.*, 1994; Wadsworth *et al.*, 1998).

Classifying the different types of bands, Afanasjev *et al.* (1999) referred to ''rigid-rotor-like'' and ''favored'' terminations if $E(I)$ is about the same or lower than the energy of the reference rotor, respectively. Their comparison with the reference rotor seems appropriate because the nucleus would have the rigid-body moment of inertia if there were no shell structure (this case is discussed by Bohr and Mottelson, 1975). As examples they discuss sequences of fast $E2$ transitions that are not quite regular when termination is approached. They call these ''unsmooth'' bands. These sequences appear for nuclei with a higher level density near the Fermi surface, where the smoothness criterion (A9) is no longer well satisfied. There is a noticeable change in the structure between the adjacent states. In our scheme such sequences do not qualify as real bands. We prefer to call them quasirotational bands, because they are intermediate between regular bands and the irregular sequences that are characteristic of $\mathcal{R}_z(\psi)$ symmetry.

B. Termination of magnetic bands

The $\Delta I=1$ bands should terminate in a similar way to the $\Delta I=2$ bands, which have antimagnetic character. In Sec. IV.C we discussed the shears model of two blades of length j interacting via phonon exchange. Termination is reached at $J=2j$ and $\omega=2A/j$, i.e., when the blades of the shears are closed. The moment of inertia decreases from $\mathcal{J}^{(2)}=j^2/2A$ at the bottom to $\mathcal{J}^{(2)}=j^2/5A$ at termination. However, following the band all the way to termination may be energetically more expensive than a particle-hole excitation, which would be seen as a crossing band.

The systematic appearance of terminating $\Delta I=2$ bands in the region above $Z=N=50$ strongly suggests that magnetic bands in this region also terminate. Some of these were studied by Afanasjev *et al.* (1999) and found to terminate. For the question of termination their restriction to principal-axis cranking should not be

problematic because as $\mathcal{R}_z(\psi)$ symmetry is approached the difference between conserved and broken $\mathcal{R}_z(\pi)$ symmetry becomes unimportant. The TAC calculations of Jenkins *et al.* (1998) and Jenkins, Wadsworth, Cameron, Clark, *et al.* (1999) gave very small opening angles at the highest frequencies considered. Whether the shape attains the expected $\mathcal{R}_z(\psi)$ symmetry could be answered, because the deformations were calculated only for $\omega=0.3$ MeV and kept fixed for the other ω values. Some of the observed terminating bands started as $\Delta I=1$ sequences. Near termination, the $\Delta I=1$ bands began to split into two signature branches, because when $\mathcal{R}_z(\psi)$ symmetry is approached, $\mathcal{R}_z(\pi)$ symmetry is approached too. The band in ^{62}Zn, shown in Fig. 25, is an example of such behavior in another mass region.

Whether shears bands of the Pb isotopes terminate is a question that has not yet been answered. The above discussed phenomenological analysis of the shears mechanism by Macchiavelli *et al.* (1998a, 1998b, 1998) assumes that shears bands have been observed up to the terminating angular momentum. This is seen in Fig. 23, which assigns $\theta=0$ to the last transition. A contribution of about four units from the pf shell neutrons is estimated. The emerging consistent picture for the energies and transition probabilities can be taken as evidence that termination must be close. Hübel *et al.* (1997) suggested that in ^{199}Pb the band ABE11 (see Fig. 20) terminates at $I=57/2$ and ABC11 at 63/2. They could not identify transitions, that would continue the bands to higher spins. The stretched coupling of the high-j particles and holes forming two blades gives an angular momentum, that is 4–5 $\hbar$ less than the upper spin of the the last regular transition. The difference can be generated by the neutrons in the partially filled pf shell, Hence the experimental evidence seems to favor termination.

Ragnarsson (2000) investigated the termination of the two $M1$ bands in ^{199}Pb by means of the cranked Nilsson-Strutinsky approach. As can be seen in Fig. 25, the deformation shrinks within the considered interval of angular momentum, but $\mathcal{R}_z(\psi)$ symmetry is not reached. At yet higher spin he found an admixture of core excitations accompanied by an increase of deformation. Using TAC, Chmel *et al.* (2000) calculated the deformation as a function of the frequency. For the bands ABE11 and ABC11 in ^{199}Pb they obtained $\gamma\approx 50°$ and ε decreasing from 0.08 at $\omega=0.1$ MeV to 0.06 at 0.6 MeV, where termination was reached. The function $J(\omega)$ did not differ much from the one calculated with fixed deformation (see Fig. 20).

The theoretical results are controversial. The cranked Nilsson-Strutinsky calculations give a deformation of $\varepsilon\approx 0.16$ for the lower part of the band, which agrees with calculations by means of the shell correction version of TAC without pairing (Frauendorf and Meng, 1994). The TAC calculations based on the quadrupole interaction (see Sec. IV.B) give a smaller deformation of $\varepsilon\sim 0.08-0.11$ for the lower part of the bands. Since the TAC accounts well for the spectra and lifetime measurements, the deformations obtained by means of the Nilsson-Strutinsky calculations seem to be too large. Hence it is possible that the latter approach overestimates the quadrupole polarizability. This may lead to an increase in the deformation for large spin. Altogether, it seems likely that the shears bands in the Pb isotopes terminate. However, more systematic calculations are needed for putting this conjecture on firm ground.

VI. REFLECTION-ASYMMETRIC NUCLEI

Various aspects of breaking the reflection symmetry have recently been reviewed by Ahmad and Butler (1993) and Butler and Nazarewicz (1996). Therefore we shall focus on the symmetries that result from unrestricted combination of the angular momentum vector with the reflection-asymmetric density distribution and their consequences for the rotational bands.

Bohr and Mottelson (1975) discussed the consequences of a reflection-asymmetric shape for rotational bands and the underlying symmetries in the frame of their unified model.

A. Discrete symmetries

The expectation values of the electric octupole moments $\langle Q_{3\mu}\rangle$ must be zero for a reflection-symmetric mean field. They are finite for a reflection-asymmetric mean field and lead to fast $E3$ transitions. Thus the electric octupole moment can be taken as the order parameter, which measures the deviation from reflection symmetry. Similarly, the expectation values of the electric dipole moments are finite only for a reflection-asymmetric mean field. Thus fast $E1$ transitions between the members of a band are a clear indication of reflection asymmetry. However, the enhancement strongly varies with particle number, because there is substantial cancellation between dipole moments of the contributing particles. In this respect the $E1$ transitions are similar to enhanced $M1$ transitions, which appear in reflection-symmetric nuclei when the the rotational axis is tilted (cf. Sec. III.B).

Let us start the discussion by assuming that the mean field has no discrete symmetry at all. There is no restriction of I by $\mathcal{R}_z(\pi)$. The operations $\mathcal{P}$ and $\mathcal{T}R_y(\pi)$, which leave the two-body Routhian invariant, define four nonequivalent degenerate mean-field solutions $|\rangle$, $\mathcal{P}|\rangle$, $\mathcal{T}R_y(\pi)|\rangle$, and $\mathcal{P}\mathcal{T}R_y(\pi)|\rangle$. This means that the bands appear as fourfold-degenerate $\Delta I=1$ sequences. For each value of I, there are two levels of positive and two levels of negative parity. The cases when symmetries reduce this degeneracy are summarized in Table II. Figures 27 and 28 illustrate the symmetries, which arise from combining the angular momentum vector $\vec{J}$ with the density distribution. The other cases involve time-odd components of the mean field.

Figure 27 shows the symmetry types when the density distribution has two symmetry planes. In the middle panel the rotational axis stands perpendicular to one of the symmetry planes. Frauendorf and Pashkevich (1984) and Nazarewicz *et al.* (1984) studied the important special case of axial symmetry with the axis of rotation per-

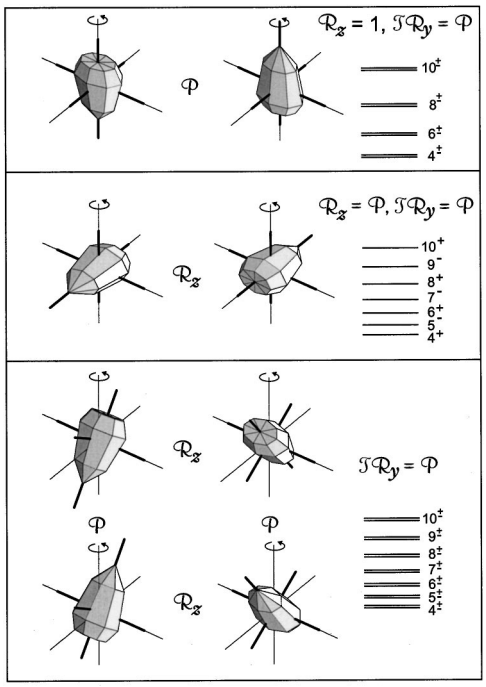

FIG. 27. The discrete symmetries of the mean field of a rotating nucleus with two symmetry planes. See caption of Fig. 9.

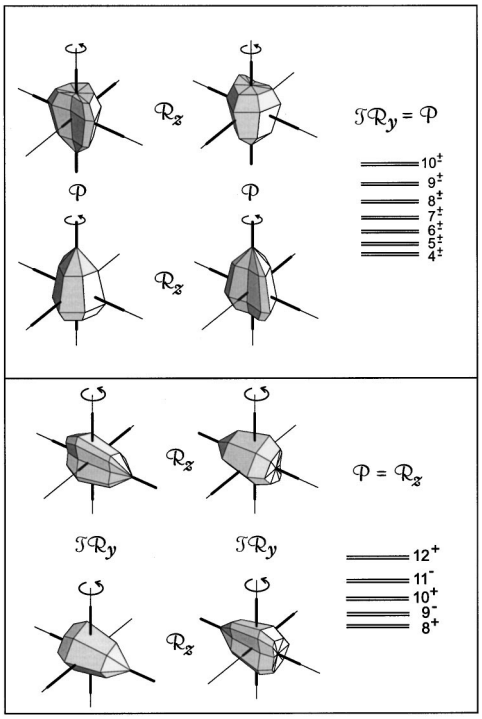

FIG. 28. Discrete symmetries of the mean field of a rotating nucleus with one symmetry plane. See caption of Fig. 9.

pendicular to the symmetry axis. There are two symmetries. $\mathcal{T}R_y(\pi)=1$ ensures that there is only one state for a given parity. The symmetry $\mathcal{S}=\mathcal{P}R_z(\pi)=1$ defines the simplex quantum number σ by[11]

$$\mathcal{S}|\rangle = e^{-i\sigma\pi}|\rangle. \tag{71}$$

The simplex fixes the parity for a given spin I,

$$\pi = (-)^{I-\sigma}. \tag{72}$$

The relation can be derived like Eq. (53) by decomposing $|\rangle$ into states of good I and π. This symmetry type can be viewed as the generalization of the PAC solutions to reflection asymmetric shapes. It is well studied in the framework of the self-consistent cranking model and thoroughly presented in the review by Butler and Nazarewicz (1996).

In the lower panel of Fig. 27 the rotational axis lies in one of the two symmetry planes but is not perpendicular to the other plane. Since the simplex is no longer a good quantum number, the parity is no longer fixed by the spin. There is a parity doublet for each spin I. This symmetry type can be viewed as a generalization of the planar TAC solutions to reflection-asymmetric shapes. So far, it has been discussed only in the context of the Unified Model and the particle rotor model. The references are given in the review by Butler and Nazarewicz (1996).

For the important case of axial nuclei, only the two above-discussed symmetries appear. For a nonaxial shape, the symmetry type $\mathcal{T}R_y(\pi)=\mathcal{P}$, $\mathcal{R}_z(\pi)=1$ in the upper panel of Fig. 27 also leads to a rotational band. Since the signature is a good quantum number, the band is a $\Delta I=2$ sequence. As in the reflection-symmetric case, $I=\alpha+2n$. However, each level is a parity doublet. Tilting the axis of rotation out of the symmetry plane breaks all symmetries, i.e., it results in full fourfold degeneracy of the rotational levels.

The upper panel of Fig. 28 shows one of the two symmetries that are possible when the rotating mean field has only one symmetry plane. Due to the relation $\mathcal{T}R_y(\pi)=\mathcal{P}$ there is one $\Delta I=1$ sequence of each parity. Each level is a parity doublet. Tilting the axis of rotation within the symmetry plane does not change the symmetry. Tilting it out of the plane breaks all symmetries.

The lower panel shows the other symmetry, which appears when the rotational axis is perpendicular to the symmetry plane. As in the case with two symmetry planes, $\mathcal{S}$ defines the simplex quantum number σ. Since $\mathcal{T}R_y(\pi)\neq 1$ or $\mathcal{P}$, there is a doubling of states with the same simplex σ. This corresponds to two degenerate $\Delta I=1$ sequences with alternating parity. They are the even and odd linear combinations of the two mean-field solutions with $\vec{J}$ pointing to the left or to the right side of the symmetry plane. This case represents another type of chirality. The asymmetry of the shape with respect to the two axes in the symmetry plane makes it possible to specify a positive half axis for each. The angular momentum selects one of the half axes perpendicular to the symmetry plane. This results in a left-handed or a right-handed coordinate system.

[11]We use the notation introduced by Frauendorf and Pashkevich (1984). Nazarewicz *et al.* (1984) introduced another, frequently used convention, which follows Bohr and Mottelson (1975). They call simplex $s=e^{-i\sigma\pi}$.

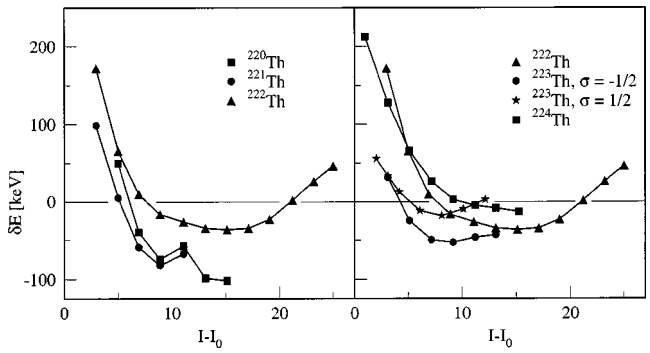

FIG. 29. Splitting between states with opposite parity of rotational bands with a definite simplex in the Th isotopes. The spins are given relative to the ground-state spin I_o. The quantity shown is $\delta E = E(I^-) - E_{int}(I^+)$, where $E_{int}(I^+)$ is obtained by interpolating by means of the $I(I+1)$ function between the two adjacent levels of positive parity. From Dahlinger *et al.*, 1988.

B. Examples

According to Ahmad and Butler (1993) and Butler and Nazarewicz (1996), the best examples of rotational bands in reflection-asymmetric nuclei were found for $Z = 88, 89, 90$ and $N = 130-136$. In the even-even nuclei of this region, the high-spin part of the yrast band is composed of a $\Delta I = 1$ sequence with alternating parities. The levels are connected by fast $E1$ transitions. These bands have the symmetry shown in the middle panel of Fig. 27. The simplex is $\sigma = 0$, i.e., the parity is even for even I and odd for odd I. The reflection symmetry is not strongly broken. There is a noticeable tunneling between the mean-field solutions $|\rangle$ and $\mathcal{P}|\rangle$, which causes an energy difference between the two branches $1/\sqrt{2}(|\rangle \pm \mathcal{P}|\rangle)$ of opposite parity within the same simplex. Figure 29 shows that the parity splitting is largest at small angular momentum. Butler and Nazarewicz (1996) mentioned several reasons why rotation may enhance the breaking of reflection symmetry.

Figure 29 also shows the two lowest bands in ^{223}Th, which have the simplex $\sigma = \pm 1/2$. The parity splitting is less than for the even-even nuclei. Butler and Nazarewicz (1996) reviewed the physics of this reduction, which is also observed in other odd-A nuclei.

The two bands of opposite simplex in ^{223,225}Th are very close in energy. This suggests that the $\mathcal{S}$ symmetry is broken. Since one expects that the odd-mass nuclei have a shape with two symmetry planes as their even-even neighbors, the symmetry is most likely of the type shown in the lower panel of Fig. 27. That is, the breaking of the $\mathcal{S}$ symmetry is a consequence of tilting the rotational axis. This is quite analogous with breaking the $\mathcal{R}_z(\pi)$ symmetry in reflection-symmetric nuclei by tilting the rotational axis (cf. Sec. III.B). The distance between levels of the same I and opposite parity, which measures the splitting between the two branches of opposite simplex, is some 10 keV, i.e., of the same order of magnitude as the parity splittings in Fig. 29.

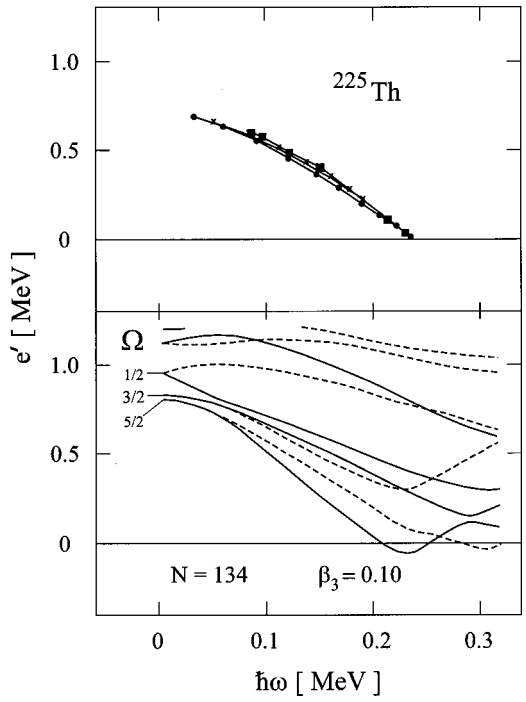

FIG. 30. Comparison of the experimental and calculated Routhians in ^{225}Th. Upper panel: experimental Routhians calculated by means of Eq. (4) from the four observed $\Delta I = 2$ sequences with $(\pi = \pm, \alpha = \pm 1/2)$. The Routhian of the zero-quasiparticle configuration is subtracted. For a more detailed explanation of this way to present the data the reader is referred to Bengtsson and Frauendoef, 1979b. Lower panel: quasineutron Routhians for an axial rotating Woods-Saxon potential with a finite octupole deformation. The line type indicates the simplex: solid lines, $\sigma = -1/2$, dashed lines, $\sigma = 1/2$. The parameters of the calculation are $\beta_2 = 0.14$, $\beta_3 = 0.10$, $\beta_4 = 0.08$, which are the equilibrium deformations of ^{224}Th, and $\Delta = 0.8$ MeV. From Hughes *et al.*, 1990.

Figure 30 shows the experimental Routhians of the four lowest $\Delta I = 2$ sequences in $^{225}_{90}\mathrm{Th}_{135}$, which have the parity and signature $(\pi = \pm, \alpha = \pm 1/2)$. They can also be grouped into two $\Delta I = 1$ sequences of alternating parity with the simplex $\sigma = \pm 1/2$. The experimental Routhians of these one-quasineutron configurations can be compared with the calculated Routhians in the lower panel. The calculation, which assumes $\mathcal{S}$ symmetry, shows a substantial splitting between the lowest quasineutron Routhians with simplex $\sigma = -1/2$ and $1/2$. In contrast, the experimental simplex splitting is small. This discrepancy can be resolved by assuming a tilt of the rotational axis into one of the symmetry planes. Due to the breaking of $\mathcal{S}$ symmetry, the simplex splitting disappears like the signature splitting in the case of reflection-symmetric nuclei when the $\mathcal{R}_z(\pi)$ symmetry is broken by a tilt of the rotational axis. (cf. Sec. III.B).

The data in the light actinide region seem to be consistent with the existence of two symmetry planes. The self-consistent cranking calculations for this region assume an axial shape, which is a special case. They find stable octupole deformation for those nuclides whose rotational bands show the signatures of a parity-

breaking mean field. For details see the reviews by Ahmad and Butler (1993) and Butler and Nazarewicz (1996), who also discuss other mass regions. Yamagami and Matsuyanagi (2000) did a SCC calculation for ^{32}S. They found a nonaxial solution with two symmetry planes as shown in the upper panel of Fig. 27. The existing data do not permit us to look for the expected $\Delta I=2$ sequence of parity doublets.

Since the relation between breaking of $\mathcal{R}_z(\psi)$ symmetry and the appearance of rotational bands is quite general, one may expect for reflection-asymmetric nuclei similar phenomena to those discussed in Secs. IV and V for weakly deformed reflection-symmetric nuclei. One may think of a rotating magnetic dipole combined with an electric dipole but not much of an electric quadrupole, which would be the reflection-asymmetric version of magnetic rotation. This analogy is not far fetched, because the known reflection-asymmetric nuclei are only slightly deformed.

VII. NONSPATIAL SYMMETRIES

A. Rotation in gauge space

This symmetry is broken by the field P generated by a pair of protons or a pair of neutrons [Eq. (11)],

$$e^{-i\chi\hat{N}}P^+e^{i\chi\hat{N}}=e^{-2i\chi}P^+. \tag{73}$$

Its expectation value $\langle P^+\rangle$ is the order parameter commonly used in condensed-matter physics (Ashcroft and Mermin, 1976). The pair field is still invariant with respect to the gauge rotation by π. The consequences are *pair rotational bands* (Broglia *et al.*, 1973; Bohr and Mottelson, 1975). This concept is based on the analogy with rotational bands, which appear when the $\mathcal{R}_z(\psi)$ symmetry is broken but $\mathcal{R}_z(\pi)$ conserved. Pair rotational bands show up as similar quasiparticle configurations in nuclei with N, $N\pm2$, $N\pm4,\ldots$ nucleons, which are connected by strong two-nucleon transfer matrix elements $\langle N|P^+|N\pm2\rangle$. At large angular momentum, gauge rotational symmetry is restored because the spatial rotation destroys the pair field in the same way as a magnetic field destroys superconductivity. There are no longer pair rotational bands, i.e., the similarity between the spectra of nuclei with N and $N\pm2$ nucleons disappears. Zhang *et al.* (1986) demonstrated this by comparing the experimental spectra of isotope chains at low and high spins.

B. Isospin

For nuclei with $N\approx Z$ it becomes important that the two-body Routhian is (approximately) invariant with respect to the rotations generated by the isospin operators. This symmetry is broken by the isovector pair field. This field is defined by generalizing the pair operators (11) to P^+_{nn}, P^+_{np}, P^+_{pn}, and P^+_{pp}, which generate pairs of two neutrons, a neutron and a proton, a proton and a neutron, and two protons in time-reversed orbits. The pair fields $\langle P^+_{pp}\rangle$, $(1/\sqrt{2})\ \langle P^+_{np}+P^+_{pn}\rangle$, $\langle P^+_{nn}\rangle$ are the spherical components 1, 0, -1 of a vector in isospace. As for spatial anisotropy, this symmetry breaking leads to the appearance of *isorotational bands*, sequences of states with increasing isospin T, which have similar structure. They are connected by strong matrix elements of the isovector pair field, which plays the role of an order parameter. For the lowest values of T their relative energy is approximately given by

$$E(T)-E(T=0)=\frac{T(T+1)}{2\mathcal{J}_T}. \tag{74}$$

Broglia *et al.* (1973) reviewed the work on this symmetry breaking, emphasizing the analogies with ordinary rotational bands (see also Bohr and Mottelson, 1975; Bes *et al.*, 1977).

More recently, Vogel (2000) and Macchiavelli *et al.* (2000) presented experimental evidence for a substantial isovector pair field at low spin in nuclei with $N\approx Z$ and $40<A<80$. Frauendorf and Sheikh (1999) discussed its consequences for the excitation spectra. They pointed out that among the different orientations of the isovector pair field, which all represent one and the same intrinsic state, the y direction has the special property $\langle P^+_{pp}\rangle=\langle P^+_{nn}\rangle$ and $(1/\sqrt{2})\ \langle P^+_{np}+P^+_{pn}\rangle=0$. Since the pair field has no proton-neutron component, the intrinsic excitation spectrum can be constructed by combining pure quasiproton and quasineutron excitations. The scheme was discussed in Sec. III.A when N is very different from Z. The difference from this familiar case consists in the invariance of the mean-field Routhian with respect to $e^{i\pi T_y}$. This additional symmetry restricts the possible quasiparticle configurations to those with $T_y|\rangle=0$. For a more detailed discussion the reader is referred to Frauendorf and Sheikh (1999). There it is shown that the available experimental spectra of $N=Z$ and $N=Z\pm1$ nuclei can be interpreted by combining the intrinsic quasiparticle configurations with the lowest isorotational excitations. It must be underlined that the success of the mean-field description without an explicit proton-neutron pair field by no means implies that there is no proton-neutron pair field. It is just the consequence of the particular choice of broken-symmetry intrinsic state. States with good isospin, which are linear combinations of all orientations of the isovector pair field, contain a proton-neutron part, which is as strong as the like-particle part.

C. Isoscalar pair field

Detailed studies of $N=Z$ nuclei in the mass 80 region have come within reach of experiment. This progress has rekindled interest in the possible existence of an isoscalar pair field $\langle P^+_0\rangle$, where

$$P^+_0=\frac{1}{\sqrt{2}}(P^+_{np}-P^+_{pn}). \tag{75}$$

The mean-field equations that determine the structure of the quasiparticles in the presence of a proton-neutron

pair field were reviewed by Goodman (1979). More recent mean-field calculations are discussed or cited by Terasaki *et al.* (1998), Kaneko *et al.* (1999), and Goodman (2000). The isoscalar pair field conserves the total isospin. The quasiparticle operators have isospin $T=1/2$ and $T_z=\pm 1/2$, i.e., they are mixtures of protons and neutron holes or vice versa. Frauendorf and Sheikh (2000) discussed this type of mean-field solution and its interpretation in the case of strong symmetry breaking.

The field conserves the parity of the total number of particles,

$$[e^{-i(\hat{Z}+\hat{N})\pi},P_0^+]=0, \quad e^{-i(\hat{Z}+\hat{N})\pi}|\rangle=\pm|\rangle. \tag{76}$$

This means that even-A and odd-A nuclei correspond to configurations with an even or odd number of quasiparticles. However, since

$$e^{-i\hat{N}\pi}P_0^+e^{-i\hat{N}\pi}=-P_0^+, \tag{77}$$

the individual parities of the neutron and proton numbers are not conserved. This has the consequence that even-even and odd-odd nuclei will join into a pair rotational band, i.e., they will have similar spectra.

Since the isoscalar pair field is antisymmetric in its isospin part it must be symmetric in its space-spin part, i.e., isoscalar pairs must carry finite angular momentum. The deuteron-like pairs with spin $S=1$ and orbital momentum $L=0$ are one example. The spatial and gauge symmetries become connected. Let us consider the case in which the deformed potential rotates about a principal axis. The protons and neutrons which occupy states with good signature (cf. III.A) combine to form pairs of definite signature. When the pair field has odd signature,

$$\mathcal{R}_z(\pi)P_0^+\mathcal{R}_z(\pi)^{-1}=-P_0^+, \tag{78}$$

the quasiparticle Routhian is invariant with respect to the combined operation $\mathcal{S}_N=e^{-i(\hat{J}_z+\hat{N})\pi}$ and

$$\mathcal{S}_N|\rangle=e^{-i\gamma\pi}|\rangle. \tag{79}$$

The additional symmetry implies the quantum number γ, which restricts the states of the pair rotational bands to $I+N=\gamma+2n$. That is, the rotational states with odd (even) I in odd-odd $N=Z$ nuclei become similar to those with even (odd) I in their even-even neighbors.

It is not clear whether an isoscalar pair field exists that is sufficiently strong to generate the described pair rotational bands. There is no experimental evidence for it from the low-spin states in $N=Z$ nuclei, which differ markedly between adjacent even-even and odd-odd nuclei. This is consistent with the mean-field calculations (see Goodman, 2000a), which give only a strong isovector pair field. Some SCC calculations predict a transition from an isovector pair field at low spin to an isoscalar one at high spin in ^{48}Cr (Terasaki *et al.*, 1998) and ^{80}Zr (Goodman, 2001). No experimental data are available in the interesting spin range.

D. Pseudospin

Hecht and Adler (1969) and Arima *et al.* (1969) observed that the normal parity levels, which are well separated from the high-j intruder levels in heavy spherical nuclei, arrange into pairs with the quantum numbers $(l_1, j_1=l_1+1/2)$ and $(l_2=l_1+2, j_2=j_1+1)$. They suggested that these pairs are obtained by coupling the pseudo-orbital momentum $\tilde{l}=l_1+1$ with the *pseudospin* $\tilde{s}$ to $j_{1,2}=\tilde{l}\pm 1/2$. The interpretation of the single-particle states becomes simpler, because the pseudospin-orbit coupling is found to be small and can be treated in perturbation theory (Ratna Raju *et al.*, 1973). Bohr *et al.* (1982) generalized the concept to rotating deformed potentials. They pointed out that the pseudospin-orbit splitting may be smaller than or comparable to the rotational frequency. As a consequence, the pseudospin tends to decouple from the deformed potential and to align with the rotational axis.

The pseudospin-singlet states have a zero pseudospin-orbit splitting because the projection of the pseudo-orbital momentum on the symmetry axis is zero. In this case the pseudospin decouples completely from the deformed potential. The decoupling is plainly visible in the spaghetti diagrams $e_i'(\vartheta)$ as two parallel horizontal trajectories, which correspond to the pseudospins being aligned or antialigned with $\vec{\omega}$. As examples, we have discussed $[411]1/2^+$ in Sec. III.B.4 and $[521]1/2^-$ in Sec. V.B. There are more manifestations of the pseudospin in rotating nuclei. One example and further references can be found in Baktash *et al.*, 1995.

The relativistic mean-field approach has permitted us to relate pseudospin symmetry to the strength of the meson fields. Ginoccio (1997) showed that the symmetry becomes exact when the potentials generated by scalar and vector mesons are equal and that the pseudo orbital angular momentum is the orbital angular momentum of the lower component of the Dirac spinor. Since the difference between the two potentials, which is the nuclear potential, is much smaller than each, the pseudospin symmetry is somewhat broken. Meng *et al.* (1998) showed that the relativistic mean-field approach gives the right pseudospin-orbit splitting and central potential with one and the same parameter set, which fixes the meson masses and their coupling constants.

VIII. BEYOND THE MEAN FIELD

The focus of this review has been the symmetries of the rotating mean field and their manifestation by different types of rotational bands. In order to relate nuclear states to the mean-field solutions one has to restore the broken symmetries. We have restricted ourselves to the simplest possibility, which stays within the mean-field approximation. We connected the classical rotation of the mean field to quantal levels of the rotational bands by means of semiclassical quantization (see Appendix A). In the case of twofold discrete symmetries we assumed no tunneling between the two equivalent mean-field solutions (see Sec. III.C). Of course, simplicity has its price. It limits the accuracy of the results, and there are phenomena, like the gradual transition from one to another type of discrete symmetry, which cannot be ac-

counted for. In this section we shall review selected work that starts with but goes beyond the mean-field approximation. We have chosen some representative articles that are devoted to high spin states and that contain good lists of references. Our aim is to put the new aspects of rotation discussed in this review into the broader perspective of nuclear many-body theory.

A. The spherical shell model

The shell model is described in textbooks, for example, those of Ring and Schuck (1980) and Blaizot and Ripka (1986). The nucleons occupy the lowest single-particle states in a spherical potential. A configuration space is generated by subsequent particle-hole excitations, within which the exact eigenstates are found by numerical diagonalization of the two-body Hamiltonian. Thanks to the progress in computer technology as well as to the development of efficient algorithms it is now possible to study nuclei with many valence nucleons in the *fp* shell. The advantage of large-scale shell-model calculations is their accurate description of the experiment, which is the main goal in many applications, as for example in astrophysics. Their disadvantage is the complexity of the state vectors, which consist of a huge number of components. In contrast, the rotating mean field permits us to understand the basic structure of rotational bands, but it is an approximation with limited accuracy. Hence it is instructive to study one and the same nucleus by means of both approaches. On the one hand, an interpretation of the shell-model results can be found and, on the other hand, the mean-field approximation can be compared with the exact solution. Here are some examples.

Röpke and Endt (1998) and Röpke (2000) used shell-model calculations for interpreting the spectra of *sd*-shell nuclei in terms of configurations of the rotating mean field. They took unobserved level energies as well as structure information from the shell-model states in order to classify the spectra in terms of rotational bands.

Caurier *et al.* (1995) reproduced very well the experimental yrast states of ^{48}Ca by means of a shell-model calculation in the full *fp* configuration space. They could explain the first major structural change (a back bend) in terms of two crossing configurations of the rotating mean field, which was calculated by means of the self-consistent cranking model. Applying the cranked Nilsson-Strutinsky approach (see Sec. V.A), Juodogalvis *et al.* (2000) interpreted the second structural change at $I=16$ as the termination of the yrast band.

Frauendorf *et al.* (1996) studied magnetic rotation of the Pb isotopes. The physics of their shell-model calculation was essentially to freeze the proton blade (in order to keep the configuration space manageable) and let the neutrons do what they like. The $\Delta I=1$ level sequence depended on the number of neutrons in the normal-parity *pf* subshell. The level spacings were irregular when it was empty or full. The irregularity was due to changes in the orientation of the two $i_{13/2}$ neutron holes relative to each other. Regular bands appeared when the *pf* subshell was half filled. In this case the two $i_{13/2}$ neutron holes were predominantly coupled to $J=12$. The *pf* neutrons acted as a kind of glue which kept the two neutron holes in a stretched coupling and generated the P_2 type of interaction between the blades.

Frauendorf and Reif (1997) studied the In isotopes by means of the spherical shell model. They found irregular sequences for $N<58$. The angular momentum turned out to be generated by various recouplings of the valence neutrons. For larger N the neutrons organized into aligned structures and regular bands appeared. This transition from irregular to regular $M1$ bands was discussed in Sec. IV.D, where it was related to the growth of the quadrupole polarizability with the number of valence neutrons above $N=50$. It can be seen in the experimental spectra of the In isotopes and its neighbors (cf. Appendix B). Brown (1999) investigated $M1$ bands in the Ni isotopes. He was also able to describe the transition from irregular to regular bands with changing N.

B. Projection methods

In nuclear physics the symmetries are often only weakly broken. Then the mean-field approximation is not very good. It can be improved by projecting the mean-field state onto the correct symmetry. The techniques are well presented in the textbooks of Ring and Schuck (1980) and Blaizot and Ripka (1986). Part or all of the parameters that determine the mean field are found by minimizing the energy of the projected state. This quickly becomes a very demanding task, because the calculation of the energy is complicated. Schmid (1992) and co-workers have progressed farthest with this approach. They start from a mean field with a number of broken symmetries, which are restored by projection. The accuracy is further improved by admixing excited quasiparticle configurations, as described in the following paragraph. A recent example can be found in the article of Hjelt *et al.* (2000), who calculated the spectra of several *pf* shell nuclei assuming that the mean field possesses only reflection symmetry. The results come very close to those of a full shell-model diagonalization. It would be interesting to analyze the optimized mean fields along the lines discussed in this review.

The projected shell model (Hara and Sun, 1995) starts from an axial symmetric nonrotating mean field, which defines the multi-quasiparticle configurations. Projecting all these states onto good angular momentum generates a nonorthogonal basis (the ''unperturbed bands''), which is used for diagonalizing a pairing-plus-quadrupole Hamiltonian. The approach is a good compromise between a large-scale shell-model diagonalization and a microscopic version of the strong-coupling picture (cf. Sec. I.B) for rotational bands. Their unperturbed bands differ from our definition of bands as configurations of the *rotating* mean field. Our bands are a mixture of their unperturbed bands. If the rotating mean field differs strongly from the nonrotating one, the heavy mixture obscures a simple interpretation and may become intractable due to the limitations of the configura-

tion space. Veláquez *et al.* (1999) accounted very well for the back bend (cf. Sec. III.A) in the yrast line of heavy nuclei. Sheikh *et al.* (1998) studied the t bands (see Sec. III.B).

The pair field, which breaks gauge rotational symmetry, is destroyed at high spin. Although projection onto a good particle number has become a standard tool for describing this transition in the principal-axis cranking scheme, we are not aware of a comprehensive review. Shimizu (1993) who reported recent developments, cited some of the relvant references. Almehed *et al.* (1999) included particle number projection in the TAC approach.

C. The random-phase approximation

The random-phase approximation (RPA) studies small oscillations of the mean field around its equilibrium value, which is determined by the self-consistency conditions. It is described in the textbooks by Ring and Schuck (1980) and Blaizot and Ripka (1986). Its application to the rotating mean field has a long history, which cannot be reviewed here. The reader can find the the important references in Kvasil and Nazmitdinov (1986) and Shimizu and Matsuzaki (1995).

Among the various vibrational modes the ''wobbling motion'' is most relevant to this review. Bohr and Mottelson (1975) discussed it in the frame of the rotor model. The triaxial nucleus rotates uniformly about the principal axis with the maximal moment of inertia. In addition the angular momentum vector $\vec{J}$ executes precessional oscillations, which are quantized. The RPA is the tool for treating this mode microscopically. Whereas earlier work had mainly studied the structure of the RPA equations, Shimizu and Matsuzaki (1995) calculated the properties of the wobbling quanta for selected nuclei. Recently first evidence for the wobbling mode in ^{163}Lu has been reported by Ødegård *et al.* (2001). The RPA should also be capable of describing the oscillations of $\vec{J}$ with respect to a nonprincipal axis of uniform rotation. A low-lying ''chiral vibration'' may appear as the precursor of the chiral rotation discussed in Sec. III.C.

The RPA permits one to calculate the correlation energy due to the fluctuations of an order parameter, provided one is not too close to the transition between broken and conserved symmetry. Shimizu *et al.* (1989) used this capability for obtaining the pair-correlation energy of nuclei rotating about a principal axis. Almehed *et al.* (1999) did the same for tilted rotation.

The RPA restores broken continuous symmetries within the small-amplitude approximation. Among the normal modes appear ''spurious'' or Nambu-Goldstone modes, which have zero energy. The case of broken $\mathcal{R}_z(\psi)$ symmetry was analyzed by Reinhardt (1982) and Marshalek (1982). One Nambu-Goldstone mode carries the angular momentum J_{NG}, which is not quantized. The total energy and angular momentum are, respectively, given by

$$E=E_{SCC}+\frac{J_{NG}^2}{2\mathcal{J}^{(2)}},\quad J=J_{SCC}+J_{NG}, \tag{80}$$

where the subscripts SCC indicate the quantities calculated from the mean-field solution and $\mathcal{J}^{(2)}$ is the dynamic moment of inertia [Eq. (27)] of the self-consistent cranking model. There is a second, quantized Nambu-Goldstone model. It is the ''excitation'' from the vacuum state with angular momentum projection $M=I$ to the state with $M=I-1$, which lies at ω in the rotating frame. Its zero point motion contributes $-1/2$ to J, which is restricted to the values I by semiclassical quantization. This is the quantum correction that we referred to in Sec. I.D when we associated the quantum number I with the classical angular momentum $J-1/2$ calculated by the self-consistent cranking model.

The other finite-energy modes represent excited bands. The RPA ensures that they are orthogonal to the spurious modes. The RPA correlations are expected to modify the interband transition probabilities obtained from the quasiparticle configurations of the self-consistent cranking model. Hamamoto and Sagawa (1979) calculated transition probabilities between principal-axis cranking quasiparticle configurations. They corrected the $M1$ transitions by substituting for the single-particle g factors $g-g_R$, where g_R is the gyromagnetic factor for collective rotation. Such a correction accounts for the conservation of angular momentum.

D. The time-dependent Hartree-Fock method

The time-dependent Hartree-Fock (TDHF) scheme (see Ring and Schuck, 1980; Blaizot and Ripka, 1986) describes how a Slater determinant evolves in time, if it is required to remain a Slater determinant. The uniformly rotating Slater determinant, which we discussed at the beginning of Sec. II, is a solution of the TDHF equations, which become the self-consistent cranking equations in this case. Starting from the exact many-body problem formulated in terms of path integrals, Reinhardt (1982) obtained the TDHF equations as a result of the stationary phase approximation. He showed how to quantize classical rotational motion and calculated the lowest-order quantum corrections, which agree with the results of the RPA discussed in the previous section.

The TDHF approach is not restricted to uniform rotation. It permits us to calculate how the orientation angles ϑ and φ change with time, when $\vec{J}$ and $\vec{\omega}$ are not parallel. Thouless and Valatin (1962) first studied this nuclear offshoot of the classical Euler equations. Vassanji and Harvey (1980) requantized the classical Hamiltonian in the attempt to describe the wobbling motion of ω. For the orientation degrees of freedom, Zelevinsky (1980) discussed the equivalence of the small-amplitude limit with the RPA. The TDHF approach has not attained much significance for concrete calculations in high-spin physics.

One remark concerning terminology seems appropriate. In the literature one speaks of one-, two-, and three-

dimensional cranking in order to indicate the dimension of the rotational degrees of freedom, where one does not specify whether the mean-field solution is self-consistent, i.e., $\vec{\omega} \| \vec{J}$, or not. We suggest reserving the terms two-dimensional and three-dimensional cranking for the general case when $\vec{\omega}$ is not parallel to $\vec{J}$ and using the acronyms PAC, (planar) TAC, and aplanar or chiral TAC for indicating the three symmetry types of uniformly rotating self-consistent cranking solutions.

E. The generator coordinate method

Horibata *et al.* (1995, 1999) and Oi *et al.* (1998, 2000), applied the generator coordinate method (see Ring and Schuck 1980; Blaizot and Ripka 1986) combined with angular momentum projection to the orientation degrees of freedom. They studied in detail the coupling between the t and s bands in $^{182}_{76}\mathrm{Os}_{106}$. They were able to qualitatively reproduce experimental findings that the even-I branches of the s and t bands strongly perturb each other, whereas the odd-I branch of the t band remains unaffected (cf. Sec. III.B.4). In the context of the generator coordinate method, band mixing appears as a collective motion in the ϑ degrees of freedom between the tilted minimum (t) and the minimum at 90° (g+s). Since the $\alpha=1$ wave function (odd) must be equal to zero at 90°, this branch of the t band can only weakly mix with the s band. This is not the case for the $\alpha=0$ wave function (even), which has a maximum at 90°.

Dönau *et al.* (1999) studied the $[633]7/2^+$ quasineutron band in $^{175}_{72}\mathrm{Hf}_{103}$ by using the orientation angle ϑ as the generator coordinate (see also Dönau, 1992). This band starts as a $\Delta I=1$ sequence and develops signature splitting. The mean-field approximation leads to an unphysical jump of the signature splitting from zero to a finite value, when changing from the TAC to the PAC interpretation (cf. Sec. III.B.3). Dönau *et al.* (1999) were able to reproduce the gradual onset of the signature splitting in the energy and $B(M1)$ values.

The generator coordinate and other many-body methods have been used to describe the transition from conserved to broken reflection symmetry. This work was reviewed by Butler and Nazarewicz (1996).

F. Decay of K isomers

The decay of high-K bands into low-K is usually strongly hindered and proceeds via many steps, each of which changes K by a small amount. This is a manifestation of the conservation J_z in an axial nucleus (see Bohr and Mottelson, 1975). Recently direct decays from states with $K>10$ to $K\approx 0$ have been observed (see Walker and Dracoulis, 1999). In a direct decay, the deformed mean field changes from $\vec{J}$ being parallel to the long symmetry axis to $\vec{J}$ being perpendicular to it. There are two competing paths: (i) through a sequence of triaxial shapes while $\vec{J}$ remains parallel to a principal axis or (ii) by the reorientation of the fixed shape relative to $\vec{J}$.

Bengtsson *et al.* (1989), Crowell *et al.* (1996), and Narimatsu *et al.* (1996) studied (i) by means of a Hamiltonian that described the dynamics of the quadrupole deformations β and γ. They used the cranking energy surface $E(\beta,\gamma,J)$ discussed in Sec. III.A.2 as the potential energy. The mass parameter was obtained from the hopping model (Barranco *et al.*, 1990), which quantifies the dominant mechanism of shape changes at low spin: The nucleus hops from one to another shape by scattering pairs of like nucleons in time-reversed states from one to another configuration. After a systematic comparison with experiment, Narimatsu *et al.* (1996) concluded that not only path (i) but also path (ii) must contribute to the decay of the high-K isomers.

Frauendorf (1993b) discussed some aspects of (ii). He suggested that the motion has a diffusive character, which consists of hopping between many low-lying configurations with a different orientation of $\vec{J}$. Each hop involves the transfer of a pair carrying finite angular momentum. It is controlled by a stochastic matrix element. The model reproduces the experimental fact that ^{174}Hf has many relatively fast decays via large changes of K, whereas ^{178}Hf decays slowly via small steps in K. The higher density of hopping configurations in ^{174}Hf as compared to ^{178}Hf is responsible for the difference.

Frauendorf (1993b) argued that the strength of the hopping matrix element increases with rotational frequency and deviation from axial shape. This points to the importance of the mechanism (i). Probably the actual decay path combines the orientation angles ϑ and φ with the deformation parameters β and γ.

Walker *et al.* (1991) and Frauendorf (1993b) suggested that high-K isomers may decay directly into low-K bands via coupling to the t bands (see Sec. III.B). The t band has both a large angular momentum projection on the 1 axis, like the s band, and a large projection on the 3 axis, like the high-K bands. But unlike the latter it has a wide distribution in the K quantum number, which indicates large fluctuations in the direction of the quasiparticle angular momentum. The wide distribution of K components around a substantial mean value of J_3 can make the t band the preferred decay path of a high-K isomer into low-K bands.

A satisfying theoretical description of the decay of the high-K isomers has not been reached. The problem is interesting because it concerns collective motion when the pair correlations are weak. It remains to be seen whether a conventional description in terms of a potential energy and a mass parameter or a model with diffusive character is more appropriate. Perhaps both aspects must be taken into account. For the further development of the theory it is important to study experimentally the decay of $\Delta I=1$ bands both in triaxial nuclei and in axial nuclei at high angular momentum.

IX. NON-NUCLEAR SYSTEMS

The nucleus is one of the best studied small many-fermion systems. Certain results may be of interest in

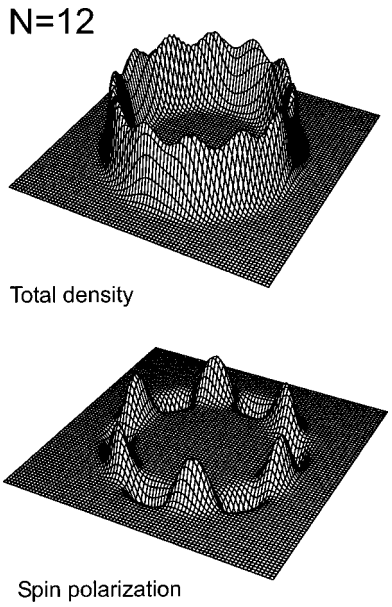

FIG. 31. Density and spin polarization of 12 electrons in a quantum ring. From Reimann *et al.*, 1999.

the study of non-nuclear finite many-fermion systems. Obviously, some of the phenomena considered in this review should find their counterpart in small rotating He_3 clusters, about which very little is known. There is a less direct but rather far-reaching analogy with confined electrons in a strong magnetic field. Metallic clusters and quantum dots are realizations in three and two dimensions, respectively. The analogy is seen best if the magnetic field B is expressed by the Larmor frequency $\omega_L = -eB/2m$. The electronic Hamiltonian h is modified to $h-\vec{\omega}_L\cdot(\vec{L}+2\vec{S})+m(\vec{\omega}_L\times\vec{r})^2/2$. The linear term is almost identical with the cranking term $\vec{\omega}\cdot\vec{J}$. The quadratic term may be viewed as an additional axial potential felt by the electrons.

Ralph *et al.* (1997) measured the quasiparticle levels in superconducting Al clusters of size ~ 5 nm. Plotted as functions of ω_L, the experimental levels show a remarkable similarity to quasiparticle diagrams like Fig. 5. Since the spin-orbit coupling is very small and the irregular shape of the cluster quenches the orbital angular momentum, the slope of all quasiparticle trajectories is close to ± 1, which is the spin contribution.

Nowadays it is possible to fabricate two-dimensional structures that are as small as ~ 10 nm. One type of these ''quantum dots,'' also called ''artificial atoms,'' is realized by layered semiconductors. Near the boundary between two layers a two-dimensional electron gas is formed, which is laterally confined by an external electric potential. Reimann *et al.* (1999) studied a ''quantum ring.'' They assumed that the electrons move in the external potential $V(\vec{r})=C(r-R)^2$. The interaction between the electrons was treated in mean-field approximation (density-functional theory). For large electron density the kinetic energy dominates. The electron density along the ring is constant, i.e., it conserves circular symmetry. At low density this symmetry is broken, as illustrated by Fig. 31. Now the Coulomb repulsion dominates, which tries to locate the electrons equidistantly. The 12-electron system has a C_{12} symmetry. Thus bands with $I=I_o+12n$, where n is an integer, are expected (cf. Sec. III.D). If there are 6 electrons in the ring the symmetry is C_6. Koskinen *et al.* (2000) calculated the exact states of this system by means of a shell-model diagonalization. They found the expected $\Delta I=6$ rotational bands. Moreover, they demonstrated that the electron states are similar to the rotational and vibrational states of a heaxagonal molecule composed of the six electrons.

The Nambu-Jona-Lasinio model and soliton models describe the structure of baryons in terms of quarks and their effective interactions. The review articles of Alkover *et al.* (1996) and Birse (1990) give an introduction to these models, which are invariant with respect to rotations in ordinary space and isospace. Mean-field solutions are found, which are called *hedgehogs*. These have neither good angular momentum nor good isospin. Only the ''grand spin'' $\vec{J}+\vec{T}$ is conserved, which is zero for a hedgehog. This implies $J=T$. The rotation of an anisotropic hedgehog generates a rotational band that includes the nucleon $J=T=1/2$ and the Δ resonance $J=T=3/2$. Their mass difference is determined by the moment of inertia, which, for nuclei at low spin, is calculated by angular momentum projection or by adding a cranking term to the field equation and treating it in perturbation theory. Blaizot and Ripka (1988) solved the latter system of equations in a nonperturbative way. They found that the band terminates at $J=T=5/2$ due to a complete alignment of the quark angular momenta, which is analogous to the mechanism described in Sec. V.

X. CONCLUSIONS AND PERSPECTIVES

The symmetries of a rotating mean field are reflected by the ordering of quantal levels with respect to the quantum numbers of angular momentum I and parity π. Thus the mean-field is more than just a concept appearing in an approximation scheme. It attains a physical meaning of its own by allowing us to classify different types of rotational bands according to its symmetries.

The point-group symmetries of a molecule provide a classification scheme for its rotational spectra. In the same way the symmetries of the nuclear shape have been used to classify rotational bands at low angular momentum. At high angular momentum the rotating mean field behaves in a more complex way than a molecular rotor with its simple classical relation between angular velocity and momentum. It becomes important that it be composed of nucleons carrying a quantized amount of angular momentum. This coarse microstructure leads to a highly nonlinear relation between angular velocity and momentum, with new phenomena and symmetries as a consequence. Not surprisingly, such phenomena became apparent only when the development

of large arrays of γ-ray detectors opened the door to detailed spectroscopic studies of nuclei at high angular momentum.

Unlike molecules, nuclei may uniformly rotate about an axis that is tilted with respect to the principal axes of the density distribution. This new freedom gives rise to a variety of discrete symmetries, which are obtained by combining the deformed density distribution with the vector of the angular momentum $\vec{J}$. In the most common case of a reflection-symmetric axial shape, $\vec{J}$ may either be perpendicular to the symmetry axis or not. The corresponding bands are $\Delta I=2$ or $\Delta I=1$ sequences, respectively. The high-K bands, which have tilted-axis symmetry, are a new testing ground for our ideas about cold, rapidly rotating nuclei: The angular momenta of the different nucleonic orbits align more or less with the rotational axis, which itself changes direction. As an example of this intricate interplay we have discussed the t bands. At experimentally accessible angular momenta, even the orbits most strongly coupled to the deformd potential begin to react to the inertial forces. How far does the resulting erosion of the K quantum number go and what is the interplay with the shape degrees of freedom? The tilted-axis cranking mean-field approach may serve as a tool in such studies.

In the case of triaxial nuclei one has to distinguish two cases: planar solutions, when $\vec{J}$ lies in one of the principal planes, and aplanar solutions when it is out of the planes. The planar solutions show up as $\Delta I=1$ bands. There are *two* aplanar solutions with opposite chirality, which differ from each other in having long, intermediate, and short axes, arranged in clockwise or counterclockwise order with respect to $\vec{J}$. These two solutions combine into two degenerate $\Delta I=1$ bands of the same parity.

Not much is known about triaxial nuclei. Even the existence of stable triaxial shapes is still debated. The observation of chiral sister bands would be clearcut evidence. Moreover, it would be the nuclear counterpart to the chirality of complex molecules and chirality in the realm of particle physics. The calculations and some experiments point to weak chirality in nuclei with $A\approx 134$ and 188. However, there may be better examples. Triaxial shapes are expected to be more common at high than at low spin. Planar solutions may have properties that can serve as evidence for triaxiality. For example, only in triaxial nuclei do two $\Delta I=2$ sequences merge into a $\Delta I=1$ band with *increasing* I.

The combination of $\vec{J}$ with a reflection-asymmetric density distribution results in several discrete symmetries. Only the case of $\vec{J}$ perpendicular to the axis of an axial symmetric shape is well studied; it appears as $\Delta I=1$ bands of alternating parity. Such bands are found in the region around $A=224$. If $\vec{J}$ is tilted with respect to the symmetry axis the corresponding band is a $\Delta I=1$ sequence of parity doublets. There is some experimental evidence for such parity doubling at high spin in the same region. For a theoretical description, the tilted-axis cranking approach must be generalized to reflection asymmetric shapes. There are additional symmetry types if the shape is nonaxial. They manifest themselves in yet other structures of the rotational bands, which, if observed, would provide a clue as to the shape.

The number of discrete symmetries and corresponding types of rotational bands increases further if the possibility is taken into account that the mean field contains a substantial time-odd part. Observation of the corresponding bands would be direct evidence for such components. The strong currents at high spin induce time-odd terms. It remains to be seen how important these are and whether they can change the symmetry. In order to address these questions, we need to base the tilted-axis cranking approach on more realistic two-body interactions.

A number of problems require going beyond the mean-field approximation. For example: The low-K bands often change from the $\Delta I=1$ to the $\Delta I=2$ type. The calculated breaking of chiral symmetry is weak and transient in ω. Likewise, the asymmetry of the nuclear shape is not very strong. How do bands with substantially different orientation (high-K and low-K) couple and decay into each other? The necessary dynamical treatment of the nuclear shape and its orientation with respect to the vector $\vec{J}$ remains a challenge to the theory.

The observation of very regular rotational bands consisting of magnetic dipole transitions in near spherical nuclei is another peculiar feature of nuclear rotation that has been revealed by high-spin studies. A few particles and holes in high-j orbitals may be arranged such that their currents break rotational symmetry with respect to the angular momentum vector $\vec{J}$, although the nucleon density is almost spherical. The quantized rotation of these current loops is observed as a regular $\Delta I=1$ rotational band. The currents carry a magnetic dipole moment along, which generates electromagnetic radiation. This phenomenon of ''magnetic rotation'' is found in many nuclides and well studied. The high-j particles and holes may also be arranged such that they break rotational symmetry but their magnetic dipole moments cancel. This ''antimagnetic rotation'' will show up as regular $\Delta I=2$ bands with a low probability for electric quadrupole transitions, which reflects the small deformation of the charge distribution. The bands investigated so far seem to be in between good antimagnetic and well deformed rotors. It remains to be seen if there exist better antimagnetic rotors.

The high-spin studies permit us a deeper insight into the nature of nuclear rotation. It has been considered as an established fact that a rotational band appears only when the nuclear density distribution has substantial deformation. This is a well known principle in molecular physics. Only molecules that have an anistropic mass distribution show rotational bands, not atoms. The absence of well-localized masses in nuclei is the obvious difference between them and molecules. It has led us to view the nucleus as a microdroplet, which develops a rotational spectrum if it is substantially deformed. This concept accounts for many features of rotational bands. Yet the picture of a liquid with a simple flow pattern is

incomplete. The rotating nucleus is interspersed with current loops, which reflect the quantization of the nucleonic motion. They are mainly responsible for breaking the isotropy of the mean field with respect to the rotational axis. The pair correlations tend to pair off the loops with opposite currents, where they act most effectively at small deformation. That is why droplet behavior appears at low spin. At high spin, not much of this pairing off is left. Already a few loops may combine to a magnetic or antimagnetic rotor. These structures remind one of molecules, but, instead of massive atoms, the building blocks are current loops, which act like gyroscopes. With increasing numbers of particles in the open shells, the deformation grows and the pattern of currents becomes more complicated. For very large deformation the flow pattern of rigid rotation is expected.

In the case of magnetic and antimagnetic rotors, a few valence particles and holes gradually align their individual angular momenta. This ''shears mechanism'' is the major source of angular momentum. It is directly visible as a decrease in the rate of magnetic dipole radiation. The increment of angular momentum per unit of angular frequency is conventionally referred to as the moment of inertia. In contrast to molecular inertia, it is determined by the interaction between quantal orbits of the valence particles and not by the mass distribution. It seems that this interaction is mainly mediated by a small quadrupole polarization of the mass distribution, induced by the high-j orbitals. This simple picture needs to be worked out. Are isovector quadrupole or hexadecapole polarizations of importance? What about polarizations of the time-odd type? What is the role of the short-range residual interaction? For the case of many nucleons and large deformation one expects the moment of inertia to become independent of the interaction and to approach the classical rigid-body value given by the mass distribution. Superdeformed nuclei seem to be close to this limit. How close are normally deformed nuclei at high spin? The study of the transition from magnetic to classical rotation is an open field for theory and experiment.

The angular momentum grows along a rotational band because the nucleons in the incompletely filled shells gradually align their angular momenta. The band terminates when all these angular momenta are fully aligned in accordance with the Pauli principle. During this process the mean field changes substantially, attaining rotational symmetry with respect to $\vec{J}$ at termination. A further increase in angular momentum requires a particle-hole excitation, which means a break in the regular sequence of levels. Hence the quantization of nucleonic motion restricts the nuclear rotational bands to a finite interval of angular momentum. In well deformed nuclei, the upper limit is too high to be seen. Termination is observed in nuclei with a small or moderate deformation, where it appears at lower angular momentum. This phenomenon is well studied for $\Delta I = 2$ bands. Much less is known about the termination of $\Delta I = 1$. It remains to be seen whether bands without reflection symmetry also terminate.

There are cascades of γ rays that neither strictly meet the smoothness criterion for rotational bands nor show the pronounced irregularity that is characteristic of angular momentum generated along a symmetry axis. These quasirotational sequences appear as the precursors of rotational bands when N and Z change towards the open shells but also as relicts when the band structures dissolves with increasing excitation energy for a given spin. The development of an appropriate theoretical description is of general interest, because the quasirotational sequences may represent the first traces of phase transitions in large systems.

The concepts of spontaneous symmetry breaking and of an order parameter, which were developed to characterize the phase transitions of infinite systems, can be applied to the mean field in finite systems. They enable us to understand what is going round in a nuclear rotational band and how the discrete symmetries of this object are reflected by the ordering of the quantum states with respect to the symmetry quantum numbers. These questions are of a general nature. The nucleus is an ideal system in which to study them, because one can excite it to high spin and measure its quantum levels. The insight gained from rotating nuclei is relevant for non-nuclear finite systems: hadrons on a smaller scale and mesoscopic systems on a larger scale.

ACKNOWLEDGMENTS

I should like to thank D. Jenkins and R. Wadsworth for carefully reading the manuscript. Part of the work was carried out under Grant No. DE-FG02-95ER40934.

APPENDIX A: SYMMETRY BREAKING AND ROTATIONAL BANDS

In order to clarify the physics of rotational bands in weakly deformed nuclei it seems useful to extend the discussion in Sec. II.F. The overlap between two mean-field solutions rotated with respect to each other by the angle ψ about $\vec{J}$ can be well approximated by a periodic Gaussian (Frauendorf *et al.*, 1971; Ring and Schuck, 1980),

$$|\langle \mathcal{R}_z(\psi)\rangle|^2 \approx \exp\left[-\frac{1}{\Delta\psi^2}\sin^2(\psi)\right]$$
$$\text{or} \quad \approx \exp\left[-\frac{4}{\Delta\psi^2}\sin^2\left(\frac{\psi}{2}\right)\right], \tag{A1}$$

where the first expression holds if there is $\mathcal{R}_z(\pi)$ symmetry and the second if there is not. The width of the overlap $\Delta\psi^2$ is the inverse of the angular momentum dispersion ΔJ^2 of the state $|\rangle$. The latter can be thought of as being composed of the angular momentum eigenstates $|I, M=I\rangle$ forming the band

$$|\rangle = \sum c_I |I, M=I\rangle. \tag{A2}$$

Viewed in this way, it represents a coherent state.[12] The periodic Gaussian form (A1) implies a near Gaussian distribution of the coefficients,

$$c_I^2 \propto \exp\left[-\frac{(I-J+1/2)^2}{\Delta J^2}\right]. \tag{A3}$$

The width ΔJ measures how much angular momentum can be generated from the mean field state $|\rangle$, i.e., it is an estimate of how much angular momentum is available before the band terminates. As expected, the width $\Delta\psi$ of the overlap (A1) and the width ΔJ of the angular momentum distribution (A4) are connected by the uncertainty principle $\Delta\psi\Delta J\sim 1$. The condition for a well defined orientation can be written as

$$\Delta\psi \approx \Delta J^{-1} \ll 2\pi. \tag{A4}$$

The dispersion

$$\Delta J^2 = \langle \hat{J}_z^2\rangle - \langle \hat{J}_z\rangle^2 = \sum_{ph} \langle ph|\hat{J}_z|0\rangle^2 \tag{A5}$$

is the sum over the particle-hole or quasiparticle excitations, depending on the version of the mean-field theory.

Let us formulate the condition for similar intrinsic structure of adjacent levels in a quantitative way. Since we are interested in small changes of the wave function we may use perturbation theory for comparing adjacent states of the band. When the frequency is incremented by $\Delta\omega$, the state $|\omega\rangle$ changes as

$$|\omega+\Delta\omega\rangle = |\omega\rangle + \Delta\omega \sum_{ph} |ph\rangle \frac{\langle ph|\hat{J}_z|0\rangle}{e_p+e_h}, \tag{A6}$$

and the total angular momentum increases by

$$J(\omega+\Delta\omega) = J(\omega) + \mathcal{J}^{(2)}\Delta\omega. \tag{A7}$$

The dynamical moment of inertia

$$\mathcal{J}^{(2)} = dJ/d\omega = 2\sum_{ph} \frac{\langle ph|\hat{J}_z|0\rangle^2}{e_p+e_h} \tag{A8}$$

measures the local increment of the angular momentum with the frequency ω. The state $|\omega(I+1)\rangle$ has a structure similar to $|\omega(I)\rangle$ if it differs only by particle-hole excitations with small amplitudes,

$$\alpha_{ph} = \frac{|\langle ph|\hat{J}_z|0\rangle|}{\mathcal{J}^{(2)}(e_p+e_h)} \ll 1. \tag{A9}$$

If this relation is fulfilled, $\mathcal{J}^{(2)}(\omega)$ will change little from I to $I+1$, because such changes are of higher order in α_{ph}. The spacing ω between the levels I and $I+1$ will be a smooth function of I.

If the more stringent condition $\Delta I\alpha_{ph} \ll 1$ holds for an interval $\Delta I \gg 1$, the band is not only regular, but will have a nearly linear relation between the spin and the level spacing. This is because the nonlinear terms of a perturbation expansion of $J(\omega)$ are of higher order in α_{ph}. The $I(I+1)$ rule of the rotor model follows from the assumption that the Hamiltonian is quadratic in the angular momentum, which means a linear relationship between angular momentum and frequency.

An overall measure of structural similarity is the overlap $|\langle\omega(I)|\omega(I+1)\rangle|^2 = 1-D$. Its deviation from one is given by

$$D = \sum_{ph} \alpha_{ph}^2. \tag{A10}$$

This overlap defect should be much smaller than unity.

Table III compares the indicators of rotational behavior for the different types of bands found in nuclei with super, normal, and weak deformation. Realistic calculations for the yrast band of ^{152}Dy and ^{174}Hf and one dipole band in ^{199}Pb (classified as ABE11; see Appendix B) are taken as examples.

Let us start with super and normal deformation. The nuclei are very well oriented. In fact, they are much better oriented than one might expect from the anisotropy of the density distribution. The superdeformed nucleus has an axis ratio of 2:1. Two density distributions with this axis ratio still have an appreciable overlap at a relative angle of 90°, whereas the overlap of the mean-field states becomes already very small at an angle of 10°. This needle-like behavior can be attributed to the nodal structure of the incompletely filled spherical states which represents a strong element of anisotropy. The number of nodes of the wave functions determines the momentum of the particles. Hence one may say that in the case of well and superdeformed nuclei symmetry breaking is primarily due to the anisotropy caused by the momentum distribution of the particles at the Fermi surface. In order to understand this better one may invoke the stretch picture (Danos and Gillet, 1967), which separates the particles into two groups, one with $j_x > 0$ and the other with $j_x < 0$. (We assume that the symmetry axis lies in the x-z plane.) Each generates a strong current in the y-z plane, which represents the element of anisotropy. The fact that the net current in the y-z plane is zero is not relevant for the orientation (see the discussion of antimagnetic rotors in Sec. IV.A).

The overlap defect is very small. The small value of $\alpha_{\max}$ ensures a near-linear relation $J(\omega)$ over an extended range. The quadrupole moment of the charge distribution with respect to the axis of rotation Q_t is large. The rotation has electric character because it is the asymmetric charge distribution that rotates and generates the strong $E2$ radiation connecting the members of the band.

Table III also illustrates how the band criteria are fulfilled for a typical case of magnetic rotation. Although the value of $\Delta\psi$ is about twice as large as for a well deformed nucleus, the nucleus is still sufficiently well oriented to develop quantal rotation. We consider a configuration with two protons excited into the orbitals $i_{13/2}$ and $h_{9/2}$ and two quasineutrons, which have hole character, excited into the $i_{13/2}$ orbitals. These four high-j qua-

[12] See Blaizot and Ripka (1986). A coherent state is a wave packet for which the product $\Delta p\Delta x$ of the momentum and coordinate takes a minimum. It behaves much like a classical object as permitted by the laws of quantum mechanics.

siparticles contribute $4\hbar^2$ to ΔJ^2; the remaining $3\hbar^2$ come from the low-j neutrons in the fp orbitals. Thus most of what is going round are the four high-j orbitals, which form the current loops in Fig. 18. The value of Q_t reflects the almost symmetric distribution of charge with respect to the axis $\vec{J}$. The rotation has magnetic character because it is the magnetic dipole that goes round, generating the observed strong $M1$ radiation which connects the members of the band.

The value $\alpha_{\max}=0.15$ ensures the regularity of the band, but it is too large to imply a linear relation $J(\omega)$ over many transitions. The largest amplitudes α_{ph} belong to the four high-j quasiparticles, which contribute 10 MeV^{-1} to the total moment of inertia $\mathcal{J}^{(2)}$. This part of the angular momentum is generated by the shears mechanism, the energetics of which are discussed in Sec. IV.C. The low-j neutrons in the fp orbitals contribute 4 MeV^{-1} to $\mathcal{J}^{(2)}$. This part is nearly ω independent because of the small particle-hole amplitudes $\alpha_{ph}<0.02$. It adds a linear contribution to $J(\omega)$.

Let us compare the degree of collectivity. One way is to count the number of ''active'' particles or holes in the incompletely filled shells. The particles in the filled shells contribute very little to $\mathcal{J}^{(2)}$ and ΔJ^2. In the case of magnetic rotation, the 4 high-j particles and holes give 2/3 of $\mathcal{J}^{(2)}$ and 4/7 of $\mathcal{J}^{(2)}$. The rest comes from the 7 neutron holes in the fp shell. A well deformed nucleus has altogether 32 active particles and holes and a superdeformed nucleus 46. The number of particles and holes contributing to $\mathcal{J}^{(2)}$ and ΔJ^2 grows with increasing deformation, i.e., the rotation becomes more and more collective.

Another way to quantify the degree of collectivity is to count the number of particle-hole excitations in the sums (A5) and (A8). There is the problem that the sums contain many tiny terms. In order to come up with a definite number we set a lower limit for the matrix element $\langle ph|\hat{J}_z|0\rangle^2$. Table III shows two cases. If the limit is set to 0.1, the truncated sums exhaust almost the full value. Again, magnetic rotation is much less collective than the rotation of the normal and superdeformed nuclei. Nevertheless, it fulfills the criteria for rotational bands and shows up as such. If the limit is increased to 0.5, there are only three terms in the case of magnetic rotation, which come from the high-j particles and holes. They account for half of $\mathcal{J}^{(2)}$ and ΔJ^2. This part is not very collective indeed. The other half comes from nine fp neutron terms and two high-j terms, which are below the limit. These numbers illustrate the qualitative statement made in Sec. IV.A that magnetic rotation consists of the rotation of a few high-j current loops accompanied by some collective rotation of the core.

TABLE III. Top panel: Character of the different types of nuclear rotational bands. The overlap defect D is calculated for a $\Delta I=2$ transition in the case of super and normal deformation and for a $\Delta I=1$ transition in the case of weak deformation. The amplitude (A9) of the strongest p-h transition is given in the line α_{max}. Middle panels: Only the terms with $\langle ph|\hat{J}_z|0\rangle^2$ larger than indicated are included in the sums (A5) and (A8). The number of terms is given by n_{ph}. Lowest panel: The parameters of the calculations for which $\omega=0.3$ MeV. The moments of inertia are in MeV^{-1}, the quadrupole moments in e b, the magnetic moment in μ_N, and the pair gaps in MeV.

Deformation	Super	Normal	Weak
$\mathcal{J}^{(2)}$	97	56	14
ΔJ	14	7.1	2.9
$\Delta\psi$	4°	8°	20°
$\alpha_{\max}$	0.003	0.01	0.15
D	0.005	0.03	0.05
Q_t	5.2	2.6	0.7
μ_t	0	0	3.5
$\langle ph\|\hat{J}_z\|0\rangle^2>0.1$			
$\mathcal{J}^{(2)}$	96	52	11
ΔJ	14	6.6	2.0
n_{ph}	96	76	14
$\langle ph\|\hat{J}_z\|0\rangle^2>0.5$			
$\mathcal{J}^{(2)}$	92	44	7
ΔJ	14	5.6	1.5
n_{ph}	58	22	3
Z	64	72	82
N	88	104	117
ε	0.6	0.3	0.1
Δ_p	0	0.75	0
Δ_n	0	0.70	0.75

APPENDIX B: MAGNETIC ROTATION IN DIFFERENT MASS REGIONS

The experimental indicators for magnetic rotation can be summarized as follows.

(1) A $\Delta I=1$ sequence of strong magnetic dipole transitions, corresponding to a reduced transition probability $B(M1)\sim$ a few μ_N^2.

(2) Weak or absent quadrupole transitions, corresponding to a deformation parameter of $\beta<0.15$.

(3) A smooth increase in the γ transition energy with angular momentum.

(4) A substantial moment of inertia, corresponding to $\mathcal{J}^{(2)}/B(E2)>100\,\mathrm{MeV}^{-1}(e\ \mathrm{b})^{-2}$.

Naturally there is a gradual transition between magnetic and collective rotation and the limits are to some extent arbitrary. Therefore the global scaling of $\mathcal{J}^{(2)}$ and $B(E2)$ with the Z and A is not taken into account in their ratio. As long as $A>50$ the variation remains below a factor of 3. For antimagnetic rotation, point (1) does not apply. The band consists of a $\Delta I=2$ sequence.

Amita *et al.* (2000) collected magnetic dipole bands according to these criteria. The bands are localized in the following four regions:

I: $(80\leqslant Z\leqslant 86, 109\leqslant N\leqslant 120)$,

II: $(56\leqslant Z\leqslant 64, 74\leqslant N\leqslant 80)$,

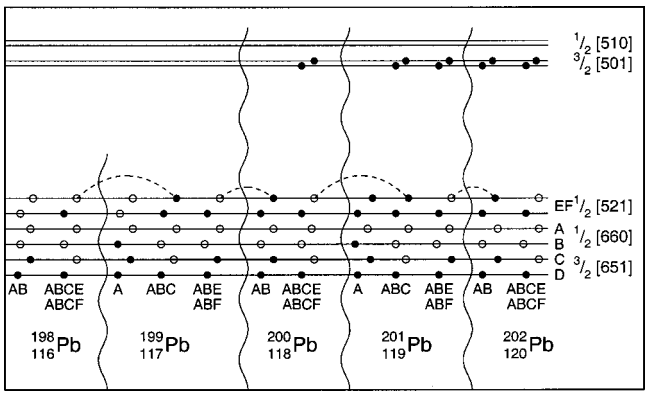

FIG. 32. The configurations of the neutron holes for various shears bands in $^{198-202}$Pb at low frequency ω. The levels are labeled both with the Nilsson quantum number relevant for $\omega=0$ and with the letter code for the corresponding quasiparticle configurations at finite pairing used by Baldsiefen *et al.* 1994, 1995. The dashed lines connect configurations that differ by a hole in E or F, which have nearly identical transition energies. From Baldsiefen *et al.*, 1995.

III: $(48\leqslant Z\leqslant 51, 55\leqslant N\leqslant 64)$, and

IV: $(35\leqslant Z\leqslant 37, 42\leqslant N\leqslant 48)$,

as expected from Fig. 22. Not all of the collected $M1$ sequences qualify as magnetic bands. Some show signature splitting, i.e., they have a character in between magnetic and antimagnetic (analogous to ferrimagnetism; see Kittel, 1988). Some have irregular level spacings, i.e., they are only quasirotational. Some seem to have larger deformations than accepted, i.e., they are in between magnetic and collective rotational bands. Now let us review the results of TAC calculations in these mass regions. The collection by Amita *et al.* (2000) contains many $M1$ bands for which no calculations have been carried out.

In region I, the Pb isotopes are most thoroughly investigated, since the concept of magnetic rotation was developed on the basis of the experiments on these nuclei. Clark *et al.* (1992a, 1992b), and Kuhnert *et al.* (1992) carried out principal-axis cranking calculations, which clarified the quasiparticle configurations of the bands. They found a small oblate deformation and demonstrated that their configuration assignment was consistent with the experimental pattern of decay of the dipole bands into the known low-spin states. After the first calculations by Frauendorf (1993a), Baldsiefen *et al.* (1996, 1994, 1995) interpreted the $M1$ bands of $^{193,198-202}_{82}\mathrm{Pb}_{111,116-120}$ in the framework of tilted-axis cranking. To most of the bands they assigned combinations of the proton configuration $[h_{9/2}i_{13/2}s_{1/2}^{-2}]$ with neutron holes $[i_{13/2}]^{-n}, n=1,2,3$ and different configurations of the neutrons in the pf orbitals. Figure 32 summarizes the configurations of the $M1$ bands in the heavier Pb isotopes. The deformation parameters of the mean field $\varepsilon\approx 0.1$ and $\gamma=50^\circ$ were calculated at $\omega=0.3$ MeV. The lifetime measurements by Clark *et al.* (1997, 1998) and Krücken *et al.* (1998) confirmed the predicted decrease of the $B(M1)$ values and thus the existence of the shears mechanism in the whole isotope chain. The measured $B(M1)$ values agree quite well with the TAC calculations. The experimental $B(E2)$ values are within larger errors consistent with the TAC calculations.

Chmel *et al.* (1997) provided additional evidence for the shears geometry by measuring the g-factor of a dipole band in ^{193}Pb. They demonstrated that at the bandhead the longitudinal component of the magnetic moment $\mu_\parallel$ has the value expected for an opening angle of 90° of the two blades, composed of the suggested particles and holes. The $M1$ bands in the Pb isotopes become less regular when N approaches 110 and are rather irregular in the Hg chain. The reason is not understood. The Bi isotopes seem similar to their Pb isotones. This is expected because the difference consists in just one of the $s_{1/2}$ proton holes' being filled. For larger Z, there is only one band in $^{205}_{86}\mathrm{Rn}_{119}$, which was interpreted as magnetic rotation. The suggested configuration is $[\pi(h_{9/2}i_{13/2})\nu(i_{13/2}^{-1})]$ (Novak *et al.*, 1999).

In region II the $h_{11/2}$ proton particles combine with $h_{11/2}$ neutron holes to form magnetic bands. Brandolini *et al.* (1996) studied a magnetic dipole band in $^{139}_{62}\mathrm{Sm}_{77}$. Both the energies and the measured lifetimes can be reproduced by TAC calculations, which are based on the configuration $[\pi(h_{11/})^2,\ \nu(h_{11/2})^{-1}]$. The calculated shapes are prolate, with a deformation of $\varepsilon=0.12$. Figure 22 shows that the deformation substantially increases for $N<76$. This is reflected by the experimental ratios $B(M1)/B(E2)<6(\mu_n/e\ \mathrm{b})^2$ and $\mathcal{J}^{(2)}/B(E2)\approx 15\ \mathrm{MeV}^{-1}(e\ \mathrm{b})^{-2}$. These dipole bands are intermediate between magnetic rotation and the high-K bands of well deformed nuclei. The TAC analysis of $^{128}_{56}\mathrm{Ba}_{72}$ by Dimitrov *et al.* (2000b) accounts well for the experimental properties of the two observed $M1$ bands. It ascribes a deformation of $\varepsilon\approx 0.2$ to the dipole bands, which is consistent with numerous studies of the mass 130 region within the traditional PAC frame (e.g., Wyss *et al.*, 1989).

In region III, the combination of $g_{9/2}$ proton holes with $h_{11/2}$ neutron particles causes magnetic rotation. The magnetic bands are more complex than the simple shears bands in the Pb isotopes because the mixed $d_{5/2}g_{7/2}$ orbitals above the $Z=N=50$ shell gap, which also have a relatively high j value, participate as current loops. We discussed the TAC calculations for ^{110}Cd in Sec. IV.B as an example. The deformation of $\varepsilon=0.13$ is not far from the upper limit we set for magnetic rotation. The $M1$ bands in the lighter Cd isotopes have a smaller deformation and, thus, more pronounced magnetic character, as expected for N approaching the magic number 50. Chiara *et al.* (2000) studied $^{109}_{48}\mathrm{Cd}_{61}$. Both the measured energies and lifetimes were well reproduced by their TAC calculations. The deformation parameters of the various bands with magnetic and antimagnetic character are between $\varepsilon=0.10$ and 0.12. Thorslund *et al.* (1993) found a ratio of $B(M1)/B(E2)>100(\mu_N/e\ \mathrm{b})^2$ for the most intense dipole band in $^{108}_{48}\mathrm{Cd}_{60}$, which is larger than for $^{109,110}_{48}\mathrm{Cd}_{61,62}$. The re-

cent lifetime measurements by Kelsall *et al.* (1999) give a deformation of $\beta \approx 0.11$ at the bottom and 0.06 at the top of this band. Their TAC calculations assign configuration $[(g_{9/2})^{-3} d_{5/2} g_{7/2}]$ to this band, the proton part of which is different from $[(g_{9/2})^{-2}]$ in ^{109,110}Cd.

Macchiavelli *et al.* (1998b) analyzed the Cd data in terms of their phenomenological shears model. Assuming $j_\pi = 8$ and $j_\nu = 15$, they incorporated the $d_{5/2} g_{7/2}$ quasineutron pair into the neutron blade. They extracted an interaction $E(\theta)$ that deviates from the P_2 form for induced deformation. However, it is not clear to what extent the phenomenological two-blade analysis is applicable.

Gadea *et al.* (1997) and Jenkins *et al.* (1998) studied the isotopes $^{105,106,108}_{50}\mathrm{Sn}_{55,56,58}$. Their TAC calculations assign configurations of the type $(\pi(g_{9/2}^{-1}, d_{5/2} g_{7/2}) \nu[h_{11/2}, (d_{5/2} g_{7/2})^n])$ to the $M1$ bands. In the neutron system pairing is taken into account and $(d_{5/2} g_{7/2})^n$ stands for the number of quasiparticle excitations. The bands are perturbed by a back bending due to the excitation of an extra pair of $(g_{7/2} d_{5/2})$ quasineutrons. The calculated deformations at $\omega = 0.3$ MeV are $\varepsilon = 0.14$, 0.11, and 0.12 for $N = 58$, 56, and 55, respectively. The TAC results agree reasonably well with the experimental energies.

The lifetime measurement of Jenkins *et al.* (1999) gave a ratio of $\mathcal{J}^{(2)}/B(E2) > 1000\,\mathrm{MeV}^{-1}(e\ \mathrm{b})^{(-2)}$ for $^{106}_{50}\mathrm{Sn}_{56}$. Since this is the largest observed, one may consider this band as the purest realization of magnetic rotation. In order to reproduce the observed $B(E2)$ values and the rapid decrease of the $B(M1)$ values, Jenkins *et al.* (1999) had to adjust the the quadrupole coupling constant. The resulting deformations $\varepsilon = 0.08$ (before the back bend) and 0.11 (after the back bend) for $N = 58$ and 0.03 for $N = 56$ are smaller than the values obtained by means of the cranked shell correction method. In the case of very small deformations it is not guaranteed that the latter will provide a reliable estimate of the quadrupole polarizability. One could try to determine the quadrupole coupling constant from the properties of vibrational excitations (see, for example, Bohr and Mottelson, 1975). So far, TAC has only considered isoscalar quadrupole deformations. This is a natural restriction for well-deformed nuclei because the symmetry energy keeps the ratio of the proton to the neutron density close to Z/N. However for small deformations this argument no longer holds. In fact, the polarization charges for quadrupole transitions in spherical nuclei point to a substantial isovector part of the polarization (Górska *et al.*, 1997; Lipoglavšek *et al.*, 1998). Including isovector deformations appears to be straightforward in the framework of the pairing-plus-quadrupole version of TAC.

The ratios $B(M1)/B(E2)$ of the $M1$ bands in $^{104}_{48}\mathrm{Cd}_{56}$ observed by Jenkins *et al.* (2001) are similar to those in $^{108}_{50}\mathrm{Sn}_{58}$. The same holds for the lower limits of these ratios in $^{102}_{48}\mathrm{Cd}_{54}$ (Persson *et al.*, 1997) and $^{106}_{50}\mathrm{Sn}_{56}$. The sequences of $M1$ transitions in the light Cd, In, and Sn isotopes become less regular with N approaching 50. They are examples of the transition from regular magnetic bands to irregular sequences which we discussed in Sec. IV.D.

In region IV, Schnare *et al.* (1999) found magnetic dipole bands in $^{82,84}_{37}\mathrm{Rb}_{45,47}$. The $B(M1)/B(E2)$ ratios reach values up to about 20 $(\mu_N/e\ \mathrm{b})^2$, which are comparable with the ratios in other regions of magnetic rotation. The ratios decrease smoothly with increasing rotational frequency ω, manifesting the shears mechanism. The bands were interpreted as the configuration $[\pi(fp)\pi g_{9/2}^2 \nu g_{9/2}^{-1}]$.

REFERENCES

Åberg, S., H. Flocard, and W. Nazarewicz, 1990, Annu. Rev. Nucl. Sci. **40**, 439.

Afanasjev, A.V., D.B. Fossan, G.J. Lane, and I. Ragnarsson, 1999, Phys. Rep. **322**, 1.

Ahmad, I., and P.A. Butler, 1993, Annu. Rev. Nucl. Part. Sci. **43**, 71.

Alhassid, Y., and B. Bush, 1991, Nucl. Phys. A **531**, 39.

Alkover, R., H. Reinhardt, and H. Weigel, 1996, Phys. Rep. **265**, 139.

Almehed, D., S. Frauendorf, and F. Dönau, 2001, Phys. Rev. C **63**, 044311.

Amita, A., K. Jain, and B. Singh, 2000, At. Data Nucl. Data Tables **74**, 283.

Andersson, C.G., S.E. Larsson, G. Leander, P. Möller, S.G. Nilsson, I. Ragnarsson, S. Åberg, R. Bengtsson, J. Dudek, B. Nerlo-Pomorska, K. Pomorski, and Z. Szymanski, 1976, Nucl. Phys. A **268**, 205.

Arima, A., M. Harvey, and K. Shimizu, 1969, Phys. Lett. **30B**, 517.

Ashcroft, N.W., and N. D. Mermin, 1975, *Solid State Physics* (Saunders, Philadelphia).

Baktash, C., B. Haas, and W. Nazarerewicz, 1995, Annu. Rev. Nucl. Part. Sci. **45**, 485.

Baldsiefen, G., H. Hübel, D. Mehta, B.V. Thirumala Rao, U. Birkental, G. Fröhlingsdorf, M. Neffgen, N. Nenoff, S.C. Pancholi, N. Singh, W. Schmitz, K. Theine, P. Willsau, H. Grawe, J. Heese, H. Kluge, K.H. Maier, M. Schramm, R. Schubart, and H.J. Maier, year, in *Proceedings X. International School on Nuclear Physics and Nuclear Energy*, Varna, 1991, edited by W. Andreitscheff and D. Elenkov.

Baldsiefen, G., *et al.*, 1992, Phys. Lett. B **275**, 252.

Baldsiefen, G., H. Hübel, W. Korten, D. Mehta, N. Nenoff, B.V. Thirumala Rao, P. Willsau, H. Grawe, J. Heese, H. Kluge, K.H. Maier, R. Schubart, S. Frauendorf, and H.J. Maier, 1994, Nucl. Phys. A **574**, 521.

Baldsiefen, G., P. Maagh, H. Hübel, W. Korten, S. Chmel, M. Neffgen, W. Pohler, H. Grawe, K.H. Maier, K. Spohr, R. Schubart, S. Frauendorf, and H.J. Maier, 1995, Nucl. Phys. A **592**, 365.

Baldsiefen, G., M.A. Stoyer, J.A. Cizewski, D.P. McNabb, W. Younes, J.A. Becker, L.A. Bernstein, M.J. Brinkman, L.P. Farris, E.A. Henry, J.R. Hughes, A. Kuhnert, T.F. Wang, B. Cederwall, R.M. Clark, M.A. Deleplanque, R.M. Diamond, P. Fallon, I.Y. Lee, A.O. Macchiavelli, J. Oliveira, F.S. Stephens, J. Burde, D.T. Vo, and S. Frauendorf, 1996, Phys. Rev. C **54**, 1106.

Banerjee, B., H.J. Mang, and P. Ring, 1973, Nucl. Phys. A **215**, 366.

Barranco, F., G. F. Bertsch, R. A. Broglia, and E. Vigezzi, 1990, Nucl. Phys. A **512**, 253.
Bengtsson, R., and S. Bengtsson, 1999, unpublished. Web sites: http://www.matfys.lth.se/ragnar/ultimate.html and http://www.matfys.lth.se/ragnar/nusma-manual.html.
Bengtsson, R., and S. Frauendorf, 1979, Nucl. Phys. A **314**, 27.
Bengtsson, R., and S. Frauendorf, 1979, Nucl. Phys. A **327**, 139.
Bengtsson, R., S. Frauendorf, and F.R. May, 1986, At. Data Nucl. Data Tables **35**, 15.
Bengtsson, R., H. Frisk, and C.-S. Wu, in *Proceedings of the XXII Zakopane School on Physics*, Zakopane, Poland, 1987; Lund Institue of Technology Report Lund-Mph-87/10, p. 1.
Bengtsson, R., and J.D. Garrett, 1984, in *Collective Phenomena in Atomic Nuclei*, International Review of Nuclear Physics Vol. 2, p. 193.
Bengtsson, T., 1989, Nucl. Phys. A **496**, 56.
Bengtsson, T., and I. Ragnarsson, 1983, Phys. Scr. **T5**, 165.
Bengtsson, T., and I. Ragnarsson, 1985, Nucl. Phys. A **436**, 14.
Bengtsson, T., R. A. Broglia, E. Vigezzi, F. Barranco, F. Dönau, and Jing-ye Zhang, 1989, Phys. Rev. Lett. **62**, 2448.
Bersuker, I. B., 1984, *The Jahn-Teller Effect and Vibronic Interactions in Modern Chemistry* (Plenum, New York).
Bes, D., R. A. Broglia, O. Hansen, and O. Nathan, 1977, Phys. Rep. **34**, 53.
Birse, M. C., 1990, Prog. Part. Nucl. Phys. **26**, 1.
Blaizot, J.P., and G. Ripka, 1986, *Quantum Theory of Finite Systems* (MIT, Cambridge, Massaschusetts/London).
Blaizot, J.P., and G. Ripka, 1988, Phys. Rev. D **38**, 1556.
Bohr, A., and B. Mottelson, 1969, *Nuclear Structure I* (Benjamin, New York/Amsterdam).
Bohr, A., and B. Mottelson, 1975, *Nuclear Structure II* (Benjamin, London/Amsterdam; Don Mills, Ontario/Sydney/Tokyo).
Bohr, A., and B. Mottelson, 1980, Phys. Scr. **22**, 461.
Bohr, A., I. Hamamoto, and Ben R. Mottelson, 1982, Phys. Scr. **26**, 267.
Bonche, P., H. Flocard, and P.H. Heenen, 1987, Nucl. Phys. A **467**, 11.
Brack, M., J. Damgaard, A.S. Jensen, H.C. Pauli, V.M. Strutinsky, and C.Y. Wong, 1972, Rev. Mod. Phys. **44**, 320.
Brandolini, F., M. Ionescu-Bujor, N.H. Medina, R.V. Ribas, D. Bazzacco, M. De Poli, P. Pavan, C. Rossi Alvarez, G. de Angelis, S. Lunardi, D. De Acuña, D.R. Napoli, and S. Frauendorf, 1996, Phys. Lett. B **388**, 468.
Brockstedt, A., J. Lyttkens-Lindén, M. Bergström, L.P. Ekström, H. Ryde, J.C. Bacelar, J.D. Garrett, G.B. Hagemann, B. Herskind, F.R. May, P.O. Tjøm, and S. Frauendorf, 1994, Nucl. Phys. A **571**, 337.
Broglia, R. A., O. Hansen, and C. Riedel, 1973, Adv. Nucl. Phys. **6**, 287.
Brown, A., 1999, Bull. Am. Phys. Soc. **44**, 32.
Burzynski, K., P. Magierski, J. Dobaczewski, and W. Nazarewicz, 1995, Phys. Scr. **T56**, 228.
Butler, P.A., and W. Nazarewicz, 1996, Rev. Mod. Phys. **68**, 349.
Caurier, E., J. L. Egido, G. Martinez-Pinedo, A. Poves, J. Retamosa, L. M. Robledo, and A. P. Zuker, 1995, Phys. Rev. Lett. **75**, 2466.
Chiara, C.J., S.J. Asztalos, B. Busse, R.M. Clark, M. Cromaz, M.A. Deleplanque, R.M. Diamond, P. Fallon, D.B. Fossan, D.G. Jenkins, S. Juutinen, N. Kelsall, R. Krücken, G.J. Lane, I.Y. Lee, A.O. Macchiavelli, R.W. MacLeod, G. Schmid, J.M. Sears, F. Smith, F.S. Stephens, K. Vetter, R. Wadsworth, and S. Frauendorf, 2000, Phys. Rev. C **61**, 034318.
Chmel, S., F. Brandolini, R.V. Ribas, G. Baldsiefen, A. Görgen, M. De Poli, P. Pavan, and H. Hübel, 1997, Phys. Rev. Lett. **79**, 2002.
Chmel, S., S. Frauendorf, and H. Hübel, 2000, unpublished.
Clark, R., 1999, private communication.
Clark, R.M., S.J. Asztalos, G. Baldsiefen, J.A. Becker, L. Bernstein, M.A. Deleplanque, R.M. Diamond, P. Fallon, I.M. Hibbert, H. Hübel, R. Krücken, I.Y. Lee, A.O. Macchiavelli, R.W. MacLeod, G. Schmid, F.S. Stephens, K. Vetter, R. Wadsworth, and S. Frauendorf, 1997, Phys. Rev. Lett. **78**, 1868.
Clark, R.M., S.J. Asztalos, B. Busse, C.J. Chiara, M. Cromaz, M.A. Deleplanque, R.M. Diamond, P. Fallon, D.B. Fossan, D.G. Jenkins, S. Juutinen, N. Kelsall, R. Krücken, G.J. Lane, I.Y. Lee, A.O. Macchiavelli, R.W. MacLeod, G. Schmid, J.M. Sears, J.F. Smith, F.S. Stephens, K. Vetter, R. Wadsworth, and S. Frauendorf, 1999, Phys. Rev. Lett. **82**, 3220.
Clark, R.M., and A.O. Macchiavelli, 2000, Annu. Rev. Nucl. Part. Sci. **50**, 1.
Clark, R.M., R. Krücken, S.J. Asztalos, J.A. Becker, B. Busse, S. Chmel, M.A. Deleplanque, R.M. Diamond, P. Fallon, D. Jenkin, K. Hauschild, I.M. Hibbert, H. Hübel, I.Y. Lee, A.O. Macchiavelli, R.W. MacLeod, G. Schmid, F.S. Stephens, U.J. van Severen, K. Vetter, R. Wadsworth, and S. Wan, 1998, Phys. Lett. B **440**, 251.
Clark, R., and B. Wadsworth, 1998, Phys. World **11**(7), 25.
Clark, R.M., R. Wadsworth, H.R. Andrews, C.W. Beausang, M. Bergstrom, S. Clarke, E. Dragulescu, T. Drake, P.J. Dagnall, A. Galindo-Uribarri, G. Hackman, K. Hauschild, I.M. Hibbert, V.P. Janzen, P.M. Jones, R.W. MacLeod, S.M. Mullins, E.S. Paul, D.C. Radford, A. Semple, J.F. Sharpey-Schafer, J. Simpson, D. Ward, and G. Zwartz, 1994, Phys. Rev. C **50**, 84.
Clark, R.M., R. Wadsworth, E.S. Paul, C.W. Beausang, I. Ali, A. Astier, D.M. Cullen, P.J. Dagnall, P. Fallon, M.J. Joyce, M. Meyer, N. Redon, P.H. Regan, J.F. Sharpey-Schafer, W. Nazarewicz, and R. Wyss, 1992a, Z. Phys. A **342**, 371.
Clark, R.M., R. Wadsworth, E.S. Paul, C.W. Beausang, I. Ali, A. Astier, D.M. Cullen, P.J. Dagnall, P. Fallon, M.J. Joyce, M. Meyer, N. Redon, P.H. Regan, W. Nazarewicz, and R. Wyss, 1992b, Phys. Lett. B **275**, 247.
Crowell, B., P. Chowdhury, D.J. Blumenthal, S.J. Freeman, C.J. Lister, M.P. Carpenter, R.G. Henry, R.V.F. Janssens, T.L. Khoo, T. Lauritsen, Y. Liang, F. Soramel, and I.G. Bearden, 1996, Phys. Rev. C **53**, 1173.
Cuypers, F., 1987, Nucl. Phys. A **468**, 237.
Dahlinger, M., E. Kankeleit, D. Habs, D. Schwalm, B. Schwartz, R.S. Simon, J.D. Burrows, and P.A. Butler, 1988, Nucl. Phys. A **484**, 337.
Danos, M., and V. Gillet, 1967, Phys. Rev. **161**, 1034.
Dean, D., S. Koonin, K. Langanke, and P. Radha, 1997, Phys. Lett. B **399**, 1.
deShalit, A., and H. Feshbach, 1974, *Theoretical Nuclear Physics I* (Wiley, New York/Chichester/Brisbane/Toronto/Singapore).
de Voigt, M.J.A., J. Dudek, and Z. Szymanski, 1983, Rev. Mod. Phys. **55**, 949.
Dimitrov, V., S. Frauendorf, and F. Dönau, 2000a, Phys. Rev. Lett. **84**, 5732.
Dimitrov, V., F. Dönau, and S. Frauendorf, 2000b, Phys. Rev. C **62**, 024315.

Dimitrov, V., S. Frauendorf, and F. Dönau, 2001, unpublished.
Dobaczewski, J., J. Dudek, S.G. Rohozinski, T.R. Werner, 2000, Phys. Rev. C **62**, 014310 (Part I); **62**, 014311 (Part II).
Dodaro, F.A., and A.L. Goodman, 1994, Phys. Rev. C **49**, 1482.
Dodaro, F.A., and A.L. Goodman, 1996, Nucl. Phys. A **596**, 91.
Dönau, F., 1992, Nucl. Phys. A **517**, 125.
Dönau, F., 1987, Nucl. Phys. A **471**, 469.
Dönau F., and S. Frauendorf, 1983, in *High Angular Momentum Properties of Nuclei*, Nuclear Science Research Conference Series Vol. 4, edited by N.R. Johnson (Harwood, New York), p. 143.
Dönau, F., S. Frauendorf, O. Vogel, A. Gelberg, and P. von Brentano, 1994, Nucl. Phys. A **584**, 241.
Dönau, F., S. Frauendorf, and J. Meng, 1996, Phys. Lett. B **387**, 667.
Dönau, F., Jing-je Zhang, and L.L. Riedinger, 1999, Phys. Lett. B **450**, 313.
Duprat, J., C. Vieu, F. Azaiez, G. Baldsiefen, C. Bourgeois, R.M. Clark, I. Deloncle, J.S. Dionisio, B. Gall, F. Hannachi, H. Hübel, M. Kaci, A. Korichi, Y. Le Coz, M. Meyer, N. Perrin, M.G. Porquet, N. Redon, C. Schück, H. Sergolle, and R. Wadsworth, 1994, Z. Phys. A **347**, 289.
Edmonds, A.R., 1957, *Angular Momentum in Quantum Mechanics* (Princeton University Press, Princeton, NJ).
Egido, J.L., and L.M. Robledo, 1993, Phys. Rev. Lett. **70**, 2876.
Fant, B., R.J. Tanner, P.A. Butler, A.N. James, G.D. Jones, R.J. Poynter, C.A. White, K.L. Ying, D.J.G. Love, J. Simpson, and K.A. Connell, 1991, J. Phys. G **17**, 319.
Fleckner, J., U. Mosel, P. Ring, and H.J. Mang, 1979, Nucl. Phys. A **331**, 288.
Flibotte, S., H.R. Andrews, G.C. Ball, C.W. Beausang, F.A. Beck, G. Belier, T. Byrski, D. Curien, P.J. Dagnall, G. de France, D. Didier, G. Duchene, Ch. Finck, B. Haas, G. Hackman, D.S. Haslip, V.P. Janzen, B. Kharraja, J.C. Lisle, J.C. Merdinger, S.M. Mullins, W. Nazarewicz, D.C. Radford, V. Rauch, H. Savajols, J. Styczen, Ch. Theisen, P.J. Twin, J.P. Vivien, J.C. Waddington, D. Ward, K. Zuber, and S. Åberg, 1993, Phys. Rev. Lett. **71**, 4299.
Frauendorf, S., 1982, in *Contemporary Research Topics in Nuclear Physics*, edited by D.H. Feng, M. Vallières, M.W. Guidry, and L.L. Riedinger (Plenum, New York/London), p. 1.
Frauendorf, S., 1993a, Nucl. Phys. A **557**, 259c.
Frauendorf, S., 1993, in *Proceedings of the International Conference on the Future of Nuclear Spectroscopy*, Crete, edited by W. Gelletly, C.A. Kalfas, R. Vlastou, S. Harissopulos, and D. Loukas (I. N. P., National Center for Scientific Research Demokritos, Athens, Greece), p. 12.
Frauendorf, S., 1996, in *Proceedings of the Workshop on Gamma Sphere Physics*, Berkeley, edited by M.A. Deleplanque, I.Y. Lee, and A.O. Macchiavelli (World Scientific, Singapore), p. 272.
Frauendorf, S., 1997, Z. Phys. A **358**, 163.
Frauendorf, S., 1998, in *Proceedings of the Workshop on GRETA Physics*, Berkeley (LBNL-41700, CONF-98028), p. 143.
Frauendorf, S., 2000, Nucl. Phys. A **677**, 115.
Frauendorf, S., D. Janssen, and L. Münchow, 1971, Phys. Lett. **34B**, 469.
Frauendorf, S., and F.R. May, 1992, in *Proceedings of the International Conference on Nuclear Structure at High Angular Momentum*, Ottawa (AECL 10613), Vol. 2, p. 177.
Frauendorf, S., and J. Meng, 1994, unpublished.
Frauendorf, S., and J. Meng, 1997a, Z. Phys. A **356**, 263.
Frauendorf, S., and J. Meng, 1997b, Nucl. Phys. A **617**, 131.
Frauendorf, S., J. Meng, and J. Reif, 1994, in *Proceedings of the Conference on Physics from Large γ-Ray Detector Arrays*, Berkeley (LBL-35687, CONF-940888), Vol. 2, p. 52.
Frauendorf, S., K. Neergard, J.A. Sheikh, and P.M. Walker, 2000, Phys. Rev. C **61**, 064324.
Frauendorf, S., and V.V. Pashkevich, 1984, Phys. Lett. **141B**, 23.
Frauendorf, S., and J. Reif, 1997, Nucl. Phys. A **621**, 736.
Frauendorf, S., J. Reif, and G. Winter, 1996, Nucl. Phys. A **601**, 41.
Frauendorf, S., and J.A. Sheikh, 1999, Nucl. Phys. A **645**, 509.
Frauendorf, S., and J.A. Sheikh, 2000, Phys. Scr. **T88**, 162.
Frisk, H., and R. Bengtsson, 1987, Phys. Lett. B **196**, 14.
Gadea, A., G. de Angelis, C. Fahlander, M. De Poli, E. Farnea, Y. Li, D.R. Napoli, Q. Pan, P. Spolaore, D. Bazzacco, S.M. Lenzi, S. Lunardi, C.M. Petrache, F. Brandolini, P. Pavan, C. Rossi Alvarez, M. Sferrazza, P.G. Bizzeti, A.M. Bizzeti Sona, J. Nyberg, M. Lipoglavsek, J. Persson, J. Cederkäll, D. Seweryniak, A. Johnson, H. Grawe, F. Soramel, M. Ogawa, A. Makishima, R. Schubart, and S. Frauendorf, 1997, Phys. Rev. C **55**, R1.
Garrett, J.D., G. Hagemann, and B. Herskind, 1986, Annu. Rev. Nucl. Sci. **36**, 419.
Ginoccio, J., 1997, Phys. Rev. Lett. **78**, 436.
Gjørup, N., P.M. Walker, G. Sletten, M.A. Bentley, M.B. Fabricius, and J.F. Sharpey-Schafer, 1995, Nucl. Phys. A **582**, 369.
Goodman, A.L., 1974, Nucl. Phys. A **230**, 466.
Goodman, A.L., 1976, Nucl. Phys. A **265**, 113.
Goodman, A.L., 1979, Adv. Nucl. Phys. **11**, 263.
Goodman, A.L., 1992a, Phys. Rev. C **45**, 1649.
Goodman, A.L., 1992b, Nucl. Phys. A **542**, 237.
Goodman, A.L., 2000, Phys. Scr. **T88**, 170.
Goodman, A.L., 2001, Phys. Rev. C **63**, 044325.
Goodman, A.L., J.P. Vary, and R.A. Sorensen, 1976, Phys. Rev. C **13**, 1674.
Górska, M., M. Lipoglavšek, H. Grawe, J. Nyberg, A. Ataç, A. Axelsson, R. Bark, J. Blomqvist, J. Cederkäll, B. Cederwall, G. de Angelis, C. Fahlander, A. Johnson, A. Leoni, A. Likar, M. Matiuzzi, S. Mitarai, L.-O. Norlin, M. Palacz, J. Persson, H.A. Roth, R. Schubart, D. Seweryniak, T. Shizuma, Ö. Skeppstedt, G. Sletten, W.B. Walters, and M. Weiszflog, 1997, Phys. Rev. Lett. **79**, 2415.
Grodzin, L., 1968, Annu. Rev. Nucl. Sci. **18**, 291.
Hagemann, G.B., H. Ryde, P. Bosetti, A. Brockstedt, H. Carlsson, L.P. Ekström, A. Nordlund, R.A. Bark, B. Herskind, S. Leoni, A. Bracco, F. Camera, S. Frattini, M. Mattiuzzi, B. Million, C. Rossi-Alvarez, G. de Angelis, D. Bazzacco, S. Lunardi, and M. De Poli, 1997, Nucl. Phys. A **618**, 199.
Hamamoto, I., 1976, Nucl. Phys. A **271**, 15.
Hamamoto, I., and B. Mottelson, 1994, Phys. Rev. B **333**, 294.
Hamamoto, I., and B. Mottelson, 1995, Phys. Scr. **T56**, 27.
Hamamoto, I., and H. Sagawa, 1979, Nucl. Phys. A **327**, 99.
Hara, K., and Y. Sun, 1995, Int. J. Mod. Phys. E **4**, 637.
Haslip, D.S., S. Flibotte, C.E. Svensson, and J.C. Waddington, 1998, Phys. Rev. C **58**, R1893.
Hecht, K.T., and A. Adler, 1997, Nucl. Phys. A **137**, 129.
Heiss, W.D., and R.G. Nazmitdinov, 1997, Phys. Lett. B **397**, 1.
Herzberg, G., 1945, *Molecular Spectra and Molecular Structure II* (Van Nostrand, New York).

Herzberg, G., 1950, *Molecular Spectra and Molecular Structure I* (Van Nostrand, New York).
Herzberg, G., 1966 *Molecular Spectra and Molecular Structure III* (Van Nostrand, New York).
Hjelt, K., K.W. Schmid, E. Hammarén, A. Feassler, 2000, Eur. Phys. J. A **7**, 201.
Horibata, T., and N. Onishi, 1994a, Phys. Lett. B **325**, 283.
Horibata, T., and N. Onishi, 1994b, Nucl. Phys. A **596**, 251.
Horibata, T., M. Oi, and N. Onishi, 1995, Phys. Lett. B **355**, 433.
Horibata, T., M. Oi, N. Onishi, and A. Ansari, 1999, Nucl. Phys. A **646**, 277.
Hübel, H., 1991, lecture at the Wethrill Symposium, Philadelphia, 1991, unpublished.
Hübel, H., G. Baldsiefen, R.M. Clark, S.J. Asztalos, J.A. Becker, L. Bernstein, M.A. Deleplanque, R.M. Diamond, P. Fallon, I.M. Hibbert, R. Krücken, I.Y. Lee, A.O. Macchiavelli, R.W. MacLeod, G. Schmid, F.S. Stephens, K. Vetter, and R. Wadsworth, 1997, Z. Phys. A **358**, 237.
Hughes, J.R., J.A. Becker, M.J. Brinkman, E.A. Henry, R. Hoff, M.A. Stoyer, T.F. Wang, B. Cederwall, M.A. Deleplanque, R.M. Diamond, P. Fallon, I.Y. Lee, J.R.B. Oliveira, F.S. Stephens, J.A. Cizewski, L.A. Bernstein, J.E. Draper, C. Duyar, E. Rubel, W.H. Kelly, and D. Vo, 1993, Phys. Rev. C **48**, R2135.
Hughes, J.R., R. Tölle, J. De Boer, P.A. Butler, C. Günther, V. Grafen, N. Gollwitzer, V.E. Holliday, G.D. Jones, C. Lauterbach, M. Marten-Tölle, S.M. Mullins, R.J. Poynter, R.S. Simon, N. Singh, R.J. Tanner, R. Wadsworth, D.L. Watson, and C.A. White, 1990, Nucl. Phys. A **512**, 275.
Inglis, D.R., 1954a, Phys. Rev. **96**, 1059.
Inglis, D.R., 1954b, Phys. Rev. **97**, 701.
Janssens, R.V.F., and T.L. Khoo, 1991, Annu. Rev. Nucl. Sci. **41**, 321.
Janzen, V.P., D.R. LaFosse, H. Schnare, D.B. Rossan, A. Galindo-Uribarri, J.R. Hughes, S.M. Mullins, E.S. Paul, L. Persson, S. Pilotte, D.C. Radford, I. Ragnarsson, P. Vaska, J.C. Waddington, R. Wadsworth, D. Ward, J. Wilson, and R. Wyss, 1994, Phys. Rev. Lett. **72**, 1160.
Jenkins, D.G., I.M. Hibbert, C.M. Parry, R. Wadsworth, D.B. Fossan, G.J. Lane, J.M. Sears, J.F. Smith, R.M. Clark, R. Krücken, I.Y. Lee, A.O. Macchiavelli, V.P. Janzen, J. Cameron, and S. Frauendorf, 1998, Phys. Lett. B **428**, 23.
Jenkins, D.G., R. Wadsworth, J. Cameron, R.M. Clark, D.B. Fossan, I.M. Hibbert, V.P. Janzen, R. Krücken, G.J. Lane, I.Y. Lee, A.O. Macchiavelli, C.M. Parry, J.M. Sears, J.F. Smith, and S. Frauendorf, 1999, Phys. Rev. Lett. **83**, 500.
Jenkins, D.G., R. Wadsworth, J. Cameron, M.P. Carpenter, C.J. Chiara, R.M. Clark, M. Devlin, P. Fallon, D.B. Fossan, I.M. Hibbert, R.V.F. Janssens, V.P. Janzen, R. Krücken, D.R. La Fosse, G.J. Lane, T. Lauritzen, I.Y. Lee, A.O. Macchiavelli, C.M. Parry, D.G. Sarantities, J.M. Sears, D. Swernyaiak, J.F. Smith, K. Starosta, D. Ward, I. Wiedenhoever, A.N. Wilson, J.N. Wilson, and S. Frauendorf, 2000, ''Incipient magnetic rotation? A magnetic dipole band in ^{194}Cd,'' e-print nucl-ex/0007004.
Juodogalvis, A., I. Ragnarsson, and S. Åberg, 2000, Phys. Lett. B **477**, 66.
Juutinen, S., R. Julin, M. Piiparinen, P. Ahonen, B. Cederwall, C. Fahlander, A. Lampinen, T. Lönnroth, A. Maj, S. Mitarai, D. Müller, J. Nyberg, P. Šimeček, M. Sugawara, I. Thorslund, S. Törmänen, A. Virtanen, and R. Wyss, 1994, Nucl. Phys. A **573**, 306.
Kaneko, K., M. Hasegawa, and Jing-ye Zhang, 1999, Phys. Rev. C **59**, 740.
Kelsall, N.S., R. Wadsworth, S.J. Asztalos, B. Busse, C.J. Chiara, R.M. Clark, M.A. Deleplanque, R.M. Diamond, P. Fallon, D.B. Fossan, D.G. Jenkins, S. Juutinen, R. Krücken, G.J. Lane, I.Y. Lee, A.O. Macchiavelli, C.M. Parry, R.W. Schmid, J.M. Sears, F.S. Stephens, J.F. Smith, and K. Vetter, 1999, Phys. Rev. C **61**, 011301(R).
Kerman, A.K., and N. Onishi, 1981, Nucl. Phys. A **361**, 179.
Kittel, C., 1986 *Introduction to Solid State Physics* (Wiley, New York/Chichester/Brisbane/Toronto/Singapore).
Koepf, W., and P. Ring, 1989, Nucl. Phys. A **493**, 61.
Koskinen, M., M. Manninen, B. Mottelson, and S.M. Reimann, 2000, ''Rotational and Vibrational Spectra of Quantum Rings,'' e-print cond-mat/0004095.
Krane, K.S., 1988, *Introductory Nuclear Physics* (Wiley, New York/Chichester/Brisbane/Toronto/Singapore).
Krücken, R., R.M. Clark, A. Dewald, M.A. Deleplanque, R.M. Diamond, P. Fallon, K. Hauschild, I.Y. Lee, A.O. Macchiavelli, R. Peusquens, G.J. Schmid, F.S. Stephens, K. Vetter, and P. von Brentano, 1998, Phys. Rev. C **58**, R1876.
Kuhnert, A., M.A. Stoyer, J.A. Becker, E.A. Henry, M.J. Brinkman, S.W. Yates, T.F. Wang, J.A. Cizewski, F.S. Stephens, M.A. Deleplanque, R.M. Diamond, A.O. Macchiavelli, J.E. Draper, F. Azaiez, W.H. Kelly, and W. Korten, 1992, Phys. Rev. C **46**, 133.
Kutsarova, T., W. Gast, S. Frauendorf, R.M. Lieder, H. Schnare, G. Sletten, and P. Walker, 1992, in *International Conference on Nuclear Structure at High Angular Momentum*, Ottawa (AECL 10613), Vol. 1, p. 28.
Kutsarova, T., R.M. Lieder, H. Schnare, G. Hebbinghaus, D. Balabanski, W. Gast, A. Krämer-Flecken, M.A. Bentley, P. Fallon, D. Howe, A.R. Mokhtar, J.F. Sharpey-Schafer, P. Walker, P. Chowdhury, B. Fabricius, G. Sletten, S. Frauendorf, and P. Walker, 1995, Nucl. Phys. A **587**, 111.
Kvasil, J., and R.G. Nazmitdinov, 1986, Sov. J. Part. Nucl. **17**, 265.
Landau, L.D., and E.M. Lifshitz, 1985, *Statistical Physics*, Third Edition (Pergamon, Oxford/New York/Toronto/Sydney/Paris/Frankfurt), p. 449.
Leander, G., S. Frauendorf, and F.R. May, 1983, in *High Angular Momentum Properties of Nuclei*, Nuclear Science Research Conference Series No. 4, edited by N.R. Johnson (Harwood, New York), p. 281.
Lee, I.Y., S. Asztalos, M.-A. Deleplanque, B. Cederwall, R.M. Diamond, P. Fallon, A.O. Macchiavelli, L. Phair, F.S. Stephens, G.J. Wozniak, S.G. Frauendorf, J.A. Becker, E.A. Henry, P.F. Hua, D.G. Sarantites, J.X. Saladin, and C.H. Yu, 1997, Phys. Rev. C **56**, 753.
Lieder, R.M., Ts. Venkova, S. Utzelmann, W. Gast, H. Schnare, K. Spohr, P. Hoernes, A. Georgiev, D. Bazzacco, R. Menegazzo, C. Rossi-Alvarez, G. de Angelis, R. Kaczarowski, T. Rząca-Urban, T. Morek, G.V. Marti, K.H. Maier, and S. Frauendorf, 1999, Nucl. Phys. A **645**, 465.
Lipoglavšek, M., D. Seweryniak, C.N. Davids, C. Fahlander, M. Górska, R.V.F. Janssens, J. Nyberg, J. Uusitalo, W.B. Walters, I. Ahmad, J. Blomqvist, M.P. Carpenter, J.A. Cizewski, S.M. Fischer, H. Grawe, G. Hackman, M. Huhta, C.J. Lister, D. Nisius, G. Poli, P. Reiter, J. Ressler, J. Schwartz, and A. Sonzogni, 1998, Phys. Lett. B **440**, 246.
Luo, W.D., A. Bouguettoucha, J. Dobaczewski, J. Dudek, and X. Li, 1995, Phys. Rev. C **52**, 2989.

Macchiavelli, A.O., R.M. Clark, M.A. Deleplanque, R.M. Diamond, P. Fallon, I.Y. Lee, F.S. Stephens, and K. Vetter, 1998a, Phys. Rev. C **58**, 3746.

Macchiavelli, A.O., R.M. Clark, M.A. Deleplanque, R.M. Diamond, P. Fallon, I.Y. Lee, F.S. Stephens, and K. Vetter, 1998b, Phys. Rev. C **58**, R621.

Macchiavelli, A.O., R.M. Clark, P. Fallon, M.A. Deleplanque, R.M. Diamond, R. Krücken, I.Y. Lee, F.S. Stephens, S.J. Asztalos, B. Busse, R.W. MacLeod, G.J. Schmid, K. Vetter, and D. Ward, 1998, Phys. Rev. C **57**, R1073.

Macchiavelli, A.O., P. Fallon, R.M. Clark, M. Cromaz, M.A. Deleplanque, R.M. Diamond, G.L. Lane, I.Y. Lee, F.S. Stephens, C.E. Svensson, K. Vetter, and D. Ward, 2000, Phys. Rev. C **61**, 041303(R).

Magierski, P., P.-H. Heenen, and W. Nazarewicz, 1995, Phys. Rev. C **51**, R2880.

Magierski, P., K. Burzynski, J. Dobaczewski, and W. Nazarewicz, 1995, Acta Phys. Pol. B **26**, 291.

March, J., 1992 *Advanced Organic Chemistry* (Wiley-Interscience, New York/Chichister/Brisbane/Toronto/Singapore), p. 94 ff.

Marshalek, E.R., 1979, Nucl. Phys. A **331**, 429.

Marshalek, E.R., 1982, Nucl. Phys. A **381**, 240.

Marshalek, E.R., 1987, Phys. Rev. C **35**, 1900; **36**, 2538.

Marshalek, E.R., 1991, in *Symposium on Contemporary Physics*, Drexel, edited by M. Vallieres, and D.H. Feng (World Scientific, Singapore), p. 191.

Marshalek, E.R., 1993, Nucl. Phys. A **557**, 301c.

Marshalek, E.R., and A. Goodman, 1978, Nucl. Phys. A **294**, 92.

Meng, J., K. Sugawara-Tanabe, S. Yamaji, P. Ring, and A. Arima, 1998, Phys. Rev. C **58**, R628.

Mikhailov, I.N., and P. Quentin, 1995, Phys. Rev. Lett. **74**, 3336.

Moore, E.F., M.P. Carpenter, Y. Liang, R.V.F. Janssens, I. Ahmad, I.G. Bearden, P.J. Daly, M.W. Drigert, B. Fornal, U. Garg, Z.W. Grabowski, H.L. Harrington, R.G. Henry, T.L. Khoo, T. Lauritsen, R.H. Mayer, D. Nisius, W. Reviol, and M. Sferrazza, 1995, Phys. Rev. C **51**, 115.

Mottelson, B., 1983, in *High Angular Momentum Properties of Nuclei*, Nuclear Science Research Conference Series, No. 4, edited by N.R. Johnson (Harwood, New York), p. 1.

Narimatsu, K., Y.R. Shimizu, and T. Shizuma, 1996, Nucl. Phys. A **601**, 69.

Nazarewicz, W., 1994, Nucl. Phys. A **574**, 27c.

Nazarewicz, W., P. Olanders, I. Ragnarsson, J. Dudek, and G. Leander, 1984, Phys. Rev. Lett. **52**, 1272; **53**, 2060(E).

Nazarewicz, W., and Z. Szymański, 1992, Phys. Rev. C **45**, 2771.

Neergard, K., V.V. Pashkevich, and S. Frauendorf, 1976, Nucl. Phys. A **262**, 61.

Neffgen, M., G. Baldsiefen, S. Frauendorf, H. Grawe, J. Heese, H. Hübel, H. Kluge, A. Korichi, W. Korten, K.H. Maier, D. Mehta, J. Meng, N. Nenoff, M. Piiparinen, M. Schönhofer, R. Schubart, U.J. van Severen, N. Singh, G. Sletten, B.V. Thirumala Rao, and P. Willsau, 1995, Nucl. Phys. A **595**, 499.

Nilsson, S.G., and I. Ragnarsson, 1995, *Shapes and Shells in Nuclear Structure* (Cambridge University Press, Cambridge, England).

Nolan, P.J., and P.J. Twin, 1988, Annu. Rev. Nucl. Sci. **38**, 533.

Novak, J.R., C.W. Beausang, N. Amzal, R.F. Casten, G. Cata Danil, J.F.C. Cocks, J.R. Cooper, P.T. Greenlees, F. Hannachi, K. Helariutta, P. Jones, R. Julin, S. Juutinen, H. Kankaanpää, H. Kettunen, R. Krücken, P. Kuusiniemi, M. Leino, B. Liu, M. Muikku, A. Savelius, T. Socci, J.T. Thomas, N.V. Zamfir, J.-y. Zhang, and S. Frauendorf, 1999, Phys. Rev. C **59**, R2989.

Ødegård, S. W., G.B. Magemann, D.R. Jensen, M. Bergström, B. Herskind, G. Sletten, S. Törmånen, J. N. Wilson, P.O. Tjøm, I. Mamamoto, K. Spohr, H. Hübel, A. Görgen, G. Schönwasser, A. Boacco, S. Leoni, A. Maj, C.M. Petrache, P. Bednarczyk, and D. Curien, 2001, Phys. Rev. Lett. in press.

Oi, M., N. Onishi, N. Tajima, and T. Horibata, 1998, Phys. Lett. B **418**, 1.

Oi, M., A. Ansari, T. Horibata, and N. Onishi, 2000, Phys. Lett. B **480**, 53.

Oliveira, J.R.B., S. Frauendorf, M.A. Deleplanque, B. Cederwall, R.M. Diamond, A.O. Macchiavelli, F.S. Stephens, J. Burde, J.E. Draper, C. Duyar, E. Rubel, J.A. Becker, E.A. Henry, M.J. Brinkman, A. Kuhnert, M.A. Stoyer, and T.F. Wang, 1994, Phys. Rev. C **50**, 1360.

Pavlichenkov, I.M., 1993, Phys. Rep. **226**, 175.

Pavlichenkov, I.M., 1997, Phys. Rev. C **55**, 1275.

Pavlichenkov, I.M., and S. Flibotte, 1995, Phys. Rev. C **51**, R460.

Pearson, C.J., P.M. Walker, C.S. Purry, G.D. Dracoulis, S. Bayer, A.P. Byrne, T. Kibédi, F.G. Kondev, T. Shizuma, R.A. Bark, G. Sletten, and S. Frauendorf, 1997, Phys. Rev. Lett. **79**, 605.

Persson, J., J. Cederkäll, M. Lipoglavšek, M. Palacz, A. Ataç, J. Blomqvist, C. Fahlander, H. Grawe, A. Johnson, A. Kerek, W. Klamra, J. Kownacki, A. Likar, L.-O. Norlin, J. Nyberg, H.A. Roth, R. Schubart, D. Seweryniak, G. de Angelis, P. Bednarczyk, Zs. Dombradi, D. Foltescu, D. Jerrestam, S. Juutinen, E. Mäkelä, G. Perez, M. de Poli, T. Shizuma, Ö. Skeppstedt, G. Sletten, S. Törmänen, T. Vass, 1997, Nucl. Phys. A **627**, 101.

Petrache, C.M., D. Bazzacco, S. Lunardi, C. Rossi Alvarez, G. de Angelis, M. De Poli, D. Bucurescu, C.A. Ur, P.B. Semmes, and R. Wyss, 1996, Nucl. Phys. A **597**, 106.

Piiparinen, M., R. Julin, S. Juutinen, A. Virtanen, P. Ahonen, C. Fahlander, J. Hattula, A. Lampinen, T. Lönnroth, A. Maj, S. Mitarai, D. Müller, J. Nyberg, A. Pakkanen, M. Sugawara, I. Thorslund, and S. Törmänen, 1993, Nucl. Phys. A **565**, 671.

Pohler, W., G. Baldsiefen, H. Hübel, W. Korten, E. Mergel, D. Roßbach, B. Aengenvoort, S. Chmel, A. Görgen, N. Nenoff, R. Julin, P. Jones, H. Kankaanpää, P.A. Butler, K.J. Cann, P.T. Greenlees, G.D. Jones, and J.F. Smith, 1999, Euro. Phys. J. A **5**, 257.

Porquet, M.-G., F. Hannachi, G. Bastin, V. Brindejonc, I. Deloncle, B. Gall, C. Schück, A.G. Smith, F. Azaiez, C. Bourgeois, J. Duprat, A. Korichi, N. Perrin, N. Poffé, H. Sergolle, A. Astier, Y. Le Coz, M. Meyer, N. Redon, J. Simpson, J.F. Sharpey-Schafer, M.J. Joyce, C.W. Beausang, R. Wadsworth, and R.M. Clark, 1994, J. Phys. G **20**, 765.

Ragnarsson, I., 1995, private communication.

Ragnarsson, I., 2000, in *Proceedings of the International Conference on The Nucleus: New Physics for the New Millenium*, NAC, Faure, South Africa, edited by F.D. Smit, R. Lindsay, and S.V. Förtsch (Kluwer Academic/Plenum, New York), p. 347.

Ragnarsson, I., V.P. Jansen, D.B. Fossan, N.C. Schmeing, and R. Wadsworth, 1995, Phys. Rev. Lett. **74**, 3935.

Ralph, D.C., C.T. Black, and M. Tinkham, 1997, Phys. Rev. Lett. **78**, 4087.

Ratna Raju, R.D., J.P. Draayer, and K.T. Hecht, 1973, Nucl. Phys. A **202**, 433.
Reimann, S., M. Koskinen, and M. Manninen, 1999, Phys. Rev. B **59**, 1613.
Reinhard, P.-G., and E.W. Otten, 1984, Nucl. Phys. A **420**, 173.
Reinhard, H., 1982, Nucl. Phys. A **381**, 217.
Reviol, W., H.-Q. Jin, and L.L. Riedinger, 1995, Phys. Rev. B **371**, 19.
Reviol, W., L.L. Riedinger, X.Z. Wang, J.-y. Zhang, H.J. Jensen, G.B. Hagemann, R.A. Bark, P.O. Tjom, S. Leoni, T. Lonnroth, H. Schnack-Petersen, T. Shizuma, J. Wrzesinski, and P. Semmes, 1999, Phys. Rev. C **59**, 1351.
Riemann, B., 1860, Abh. Akad. Wiss. Goettingen Math. Phys. Kl. **9**, 1.
Ring, P., R. Beck, and H.J. Mang, 1970, Z. Phys. **231**, 10.
Ring, P., and H.J. Mang, 1974, Phys. Rev. Lett. **33**, 1174.
Ring, P., and P. Schuck, 1980, *The Nuclear Many-Body Problem* (Springer, New York).
Röpke, H., and P.M. Endt, 1998, Nucl. Phys. A **632**, 173.
Röpke, H., 2000, Nucl. Phys. A **674**, 95.
Schiffer, J.P., 1971, Ann. Phys. (N.Y.) **66**, 798.
Schmid, K.W., 1992, in *Nuclear Structure Models*, edited by R. Bengtsson, J. Drayer, and W. Nazarewicz (World Scientific, Singapore), p. 333.
Schnare, H., R. Schwengner, S. Frauendorf, F. Dönau, L. Käubler, H. Prade, A. Jungclaus, K.P. Lieb, C. Lingk, S. Skoda, J. Eberth, G. de Angelis, A. Gadea, E. Farnea, D.R. Napoli, C.A. Ur, and G. LoBianco, 1999, Phys. Rev. Lett. **82**, 4408.
Semple, A.T., P.J. Nolan, C.W. Beausang, S.A. Forbes, E.S. Paul, J.N. Wilson, R. Wadsworth, K. Hauschild, I.M. Hibbert, R.M. Clark, J. Gizon, A. Gizon, D. Santos, and J. Simpson, 1996, Phys. Rev. Lett. **76**, 3671.
Sheikh, J.A., 1995, Phys. Rev. C **52**, 3061.
Sheikh, J.A., Y. Sun, and P.M. Walker, 1998, Phys. Rev. C **57**, R26.
Shimizu, Y.R., 1993, Nucl. Phys. A **520**, 490c.
Shimizu, Y.R., and M. Matsuzaki, 1995, Nucl. Phys. A **588**, 599.
Shimizu, Y.R., J.D. Garrett, R.A. Broglia, M. Gallardo, and E. Vigezzi, 1989, Rev. Mod. Phys. **61**, 131.
Simpson, J., M.A. Riley, J.R. Cresswell, P.D. Forsyth, D. Howe, B.M. Nyakó, J.F. Sharpey-Schafer, J. Bacelar, J.D. Garrett, G.B. Hagemann, B. Herskind, and A. Holm, 1984, Phys. Rev. Lett. **53**, 648.
Simpson, J., M.A. Riley, S.J. Gale, J.F. Sharpey-Schafer, M.A. Bentley, A.M. Bruce, R. Chapman, R.M. Clark, S. Clarke, J. Copnell, D.M. Cullen, P. Fallon, A. Fitzpatrick, P.D. Forsyth, J.F. Freeman, P.M. Jones, M.J. Joyce, F. Liden, J.C. Lisle, A.O. Macchiavelli, A.G. Smith, J.F. Smith, J. Sweeney, D.M. Thompson, S. Warburton, J.N. Wilson, T. Bengtsson, and I. Ragnarsson, 1994, Phys. Lett. B **327**, 187.
Stephens, F.S., 1975, Rev. Mod. Phys. **47**, 43.
Stephens, F.S., and R.S. Simon, 1972, Nucl. Phys. A **183**, 257.
Streitwieser, A., C.H. Heathcock, and E.M. Kosower, 1985, *Introduction to Organic Chemistry*, 3rd ed. (Macmillan, New York), p. 113.
Sun, Y., J.Y. Zhang, and M. Guidry, 1995, Phys. Rev. Lett. **75**, 3398.
Szymanski, Z., 1983, *Fast Nuclear Rotation* (Clarendon, Oxford).
Takami, S., K. Yabana, and M. Matsuo, 1998, Phys. Lett. B **431**, 242.
Terasaki, J., R. Wyss, and P. Heenen, 1998, Phys. Lett. B **437**, 1.
Thorslund, I., C. Fahlander, J. Nyberg, S. Juutinen, R. Julin, M. Piiparinen, R. Wyss, A. Lampinen, T. Lönnroth, D. Müller, S. Törmänen, and A. Virtanen, 1993, Nucl. Phys. A **564**, 285.
Thouless, D.J., and J.G. Valatin, 1962, Nucl. Phys. **31**, 211.
Tjøm, P.O., R.M. Diamond, J.C. Bacelar, E.M. Beck, M.A. Deleplanque, J.E. Draper, and F.S. Stephens, 1985, Phys. Rev. Lett. **55**, 2405.
Twin, P.J., B.M. Nyakó, A.H. Nelson, J. Simpson, M.A. Bentley, H.W. Cranmer-Gordon, P.D. Forsyth, D. Howe, A.R. Mokhtar, J.D. Morrison, J.F. Sharpey-Schafer, and G. Sletten, 1986, Phys. Rev. Lett. **57**, 811.
Vassanji, M.G., and M. Harvey, 1980, Nucl. Phys. A **344**, 61.
Veláquez, V., J.G. Hirsch, Y. Sun, and M.W. Guidry, 1999, Nucl. Phys. A **653**, 355.
Vigezzi, E., D.R. Bes, R.A. Broglia, S. Frauendorf, 1988, Phys. Rev. C **38**, 1448.
Vogel, P., 2000, Nucl. Phys. A **662**, 148.
Wadsworth, R., R.M. Clark, J.A. Cameron, D.B. Fossan, I.M. Hibbert, V.P. Janzen, R. Krücken, G.J. Lane, I.Y. Lee, A.O. Macchiavelli, C.M. Parry, J.M. Sears, J.F. Smith, A.V. Afanasjev, and I. Ragnarsson, 1998, Phys. Rev. Lett. **80**, 1174.
Walker, P.M., and G.D. Dracoulis, 1999, Nature (London) **399**, 35.
Walker, P.M., G.D. Dracoulis, A.P. Byrne, B. Fabricius, T. Kibédi, and A.E. Stuckbery, 1991, Phys. Rev. Lett. **67**, 433.
Walker, P.M., K.C. Yeung, G.D. Dracoulis, P.H. Regan, G.J. Lane, P.M. Davidson, and A.E. Stuchbery, 1993, Phys. Lett. B **309**, 17.
Walker, P.M., G.D. Dracoulis, A.P. Byrne, B. Fabricius, T. Kibédi, and A.E. Stuckbery, 1994, Nucl. Phys. A **568**, 397.
Wang, T.F., E.A. Henry, J.A. Becker, A. Kuhnert, M.A. Stoyer, S.W. Yates, M.J. Brinkman, J.A. Cizewski, A.O. Macchiavelli, F.S. Stephens, M.A. Deleplanque, R.M. Diamond, J.E. Draper, F.A. Azaiez, W.H. Kelly, W. Korten, E. Rubel, and Y.A. Akovali, 1992, Phys. Rev. Lett. **69**, 1737.
Werner, T.R., and J. Dudek, 1992, At. Data Nucl. Data Tables **50**, 179.
Werner, T.R., and J. Dudek, 1995, At. Data Nucl. Data Tables **59**, 1.
Wyss, R., 1999, personal communication, e-mail: wyss@msi.se
Wyss, R., A. Granderath, R. Bengtsson, P. von Brentano, A. Dewald, A. Gelberg, A. Gizon, J. Gizon, S. Harissopulos, A. Johnson, W. Lieberz, W. Nazarewicz, J. Nyberg, and K. Schiffer, 1989, Nucl. Phys. A **505**, 337.
Yamagami, M., and K. Matsuyanagi, 2000, Nucl. Phys. A **672**, 123.
Zelevinsky, V.G., 1980, Nucl. Phys. A **344**, 109.
Zhang, Jing-ye, J.D. Garrett, J.C. Bacelar, and S. Frauendorf, 1986, Nucl. Phys. A **543**, 104.